TIME LAPSE GRAVITY MONITORING AT COSO GEOTHERMAL FIELD

by

Rachel Vest Woolf

A thesis submitted to the Faculty and the Board of Trustees of the Colorado School of Mines in partial fulfillment of the requirements for the degree of Master of Science (Geophysics).

Golden, Colorado

Date _____

Signed: _____
Rachel Vest Woolf

Signed: _____
Dr. Yaoguo Li
Thesis Advisor

Golden, Colorado

Date _____

Signed: _____
Dr. Terence K. Young
Professor and Head
Department of Geophysics

ABSTRACT

An extensive time lapse gravity data set was acquired over the Coso geothermal field near Ridgecrest, California starting in 1987, with the latest data set acquired in 2013. In this thesis I use these gravity data to obtain a better understanding of mass changes occurring within the geothermal field.

Geothermal energy is produced by flashing naturally heated ground water into steam which is used to turn turbines. Brine and re-condensed steam are then re-injected into the reservoir. A percentage of the water removed from the system is lost to the process. The time lapse gravity method consists of gravity measurements taken at the same locations over time, capturing snap shots of the changing field. After careful processing, the final data are differenced to extract the change in gravity over time. This change in gravity can then be inverted to recover the change in density and therefore mass over time. The inversion process also produces information on the three dimensional locations of these mass changes.

Thirty five gravity data sets were processed and a subsection were inverted with two different starting times, a sixteen point data set collected continuously between 1991 and 2005, and a thirty-eight point data set collected between 1996 and 2005. The maximum change in gravity in the 1991 data group was -350μGal observed near station CSE2. For the 1996 data group the maximum gravity change observed over the nine year period was -248μGal.

The gravity data were then inverted using the surface inversion method. Three values of density contrast were used, -0.05g/cm^3, -0.10g/cm^3, and -0.20g/cm^3. The starting surface in 1991 was set to 2,500 ft above sea level. The changes in surfaces were then converted to mass changes. The largest total mass change recovered was -1.39x10^{11}kg. This mass value is of the same order of magnitude as published well production data for the field. Additionally, the gravity data produces a better understanding of the spatial distribution of mass loss. The mass loss is concentrated in one area of the field while others remain somewhat constant.

TABLE OF CONTENTS

LIST OF FIGURES

LIST OF TABLES

ACKNOWLEDGMENTS

This worked was funded in part by the National Renewable Energy Laboratory (contract: UGA-0-41025-42) under contract to the U.S. Navy Geothermal Program Office (GPO). It was also funded in part by the Gravity & Magnetics Research Consortium, whose current sponsors include Anadarko Petroleum Corporation, Bell Geospace, BG Group, BGP Inc., BP, CGG (Fugro) , Conoco Phillips, ExxonMobil, Gedex, Lockheed Martin, MicroG LaCoste, Marathon Oil Corporation, Petra Energia, BR Petrobras, Shell, and Vale. Additionally I'd like to acknowledge the GPO for supplying the existing gravity data set as well as assisting in the collection of the new field data set collected in January 2013, particularly Andy Sabin, Dave Mead, Kelly Blake, Mike Lazaro and also Allan Katzenstien, Charlie Rodgers, and Jeff Shoffner formerly of the GPO.

I'd like to thank and acknowledge my advisor Yaoguo Li who has been a great friend and support both during my Master's degree and my undergraduate degree eleven years ago. I'd also like to thank my remaining committee members, Mike Batzle, Masami Nakagawa who helped spark my interest in Geothermal, and Rich Krahenbuhl who provided a great deal of feedback and support on my data, figures and presentations. I'd also like to thank the entire geophysics department including Terry Young, department head, and Michelle Szobody, program assistant. Through both my degrees the entire department has been very understanding and supportive.

Lastly, I'd like to thank my family, my three children, Skyla, Arianna, and Declan and my husband of nine years Jeremy. I'd like to thank them for putting up with the long hours and the time spent away from them during these past few years and for the support and love they gave me in times of stress and frustration. I'd also like to thank my mother and father, Edwin and Susan Vest, for their support as well, and my sisters for the extra babysitting time they put in.

For my mother.

CHAPTER 1:
INTRODUCTION AND BACKGROUND

1.1 Introduction

An extensive time lapse gravity data set has been collected over the Coso Geothermal Field near Ridgecrest, CA. The purpose of this thesis is to use these data to gain a better understanding of the behavior of the geothermal field through careful processing, inversion and interpretation. Through the inversion, I plan to recover the shape and size of a density anomaly that would produce the observed time lapse gravity, as well as the total change in mass.

In this chapter, I will first present a brief background on of how hydrothermal fluids are used to produce electricity and summarize the exploration history and geology of the Coso Geothermal Field. I then will briefly discuss previous use of time lapse gravity and explain the basic theory behind it for monitoring. Last, I will introduce the Coso geothermal gravity data used for this project.

In Chapter 2, I will discuss the survey planning and data collection procedures involved in time lapse gravity surveys for geothermal reservoir characterization. I will then expand to describe how the data were collected at the Coso site in particular. Finally, I present the processing steps and considerations these surveys, first for the general case, and then focused on Coso specifics.

I present the time lapse gravity data collected from 1987 until 2005 in Chapter 3. The gravity data are inverted and the results presented in Chapter 4 along with interpretation of the changing Coso field.

Lastly, in Chapter 5, I provide a summary and some conclusions of this thesis project and the results produced from it as well as mentioned future work to be done at the field.

1.2 Geothermal Energy

Geothermal energy is energy derived from the natural heat of the earth. Naturally heated water is removed from a reservoir, and in the case of flash steam plants, such as those at Coso Field, the water is flashed to steam at the surface. The steam is used to power turbines and generate electricity while the remaining brine is used in the cooling towers. The steam is condensed and along with the remaining brine, both are re-injected into the reservoir in an attempt to maintain water levels (Ehresman, 2002). This type of power plant is shown in Figure 1.1.

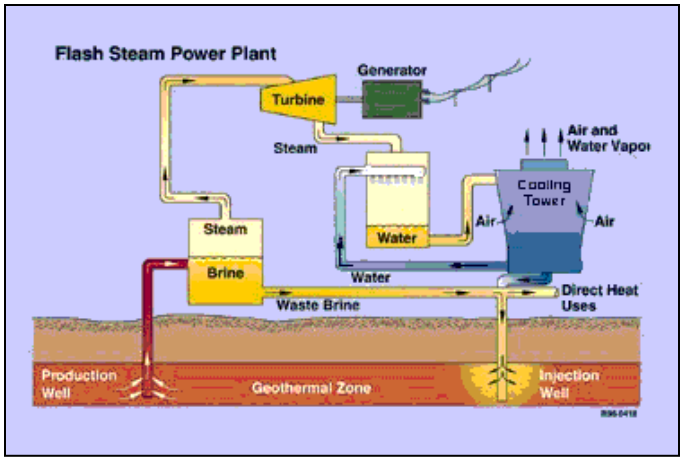

Figure 1.1: Diagram of a flash steam power plant. Naturally heated fluid is removed from the reservoir, flashed at the surface, where the steam is used to power turbines and generate electricity, while the brine is used in the cooling towers. The condensed steam and remaining brine are both re-injected into the reservoir. Image source: http://www.scs.sk.ca/vol-old/HTT/rr7/geothermal.id.doe.gov/what-is.html

1.3 Coso Geothermal Field

The Coso geothermal field is located on Naval Air Weapons Station China Lake in eastern California, shown in Figure 1.2.

Dr. Carl Austin first recognized the potential for energy development at the Coso geothermal field in the early 1960s. He begun the exploration project and by 1977 heat flow wells had been drilled and numerous geophysical surveys had been conducted. The first geothermal plant, Navy I came on line in 1987, with three additional plants, Navy II, BLM West, and BLM East following in 1991(Monastero F. C., 2002). A satellite image of the field is shown in Figure 1.3. Down hole temperatures of 320°C to 350°C have been measured in production wells (Monastero, et al., 2005).

The Coso geothermal field is located in the Southwest Basin and Range, east of the Sierra Nevada front (Monastero, et al., 2005). The field contains many rhyolite domes, pyroclastic deposits, active and formerly active fumaroles and mud pots, and a basalt flow to the south. Figure 1.4 shows the geothermal field on a geologic map, with the map units labeled in Table 1.1. Coso is located in a releasing step-over between two dextral faults, Figure 1.5 (Weaver & Hill, 1978). The Indian Wells Valley Fault lays to the southwest of the Coso field, with Wilde Horse Mesa to the northeast (Monastero, et al., 2005). Crustal thinning appears to be accommodating the dextral tension in the releasing bend as evident by earthquake epicenters. The brittle-ductile transition is elevated beneath the field to a depth of 3.5-4 km, deepening to 8-10km in all directions outside of the field (Monastero, et al., 2005).

Figure 1.2: The Coso Geothermal Field on China Lake Naval Weapons Station, located in the Northern Mohave dessert of Eastern California.

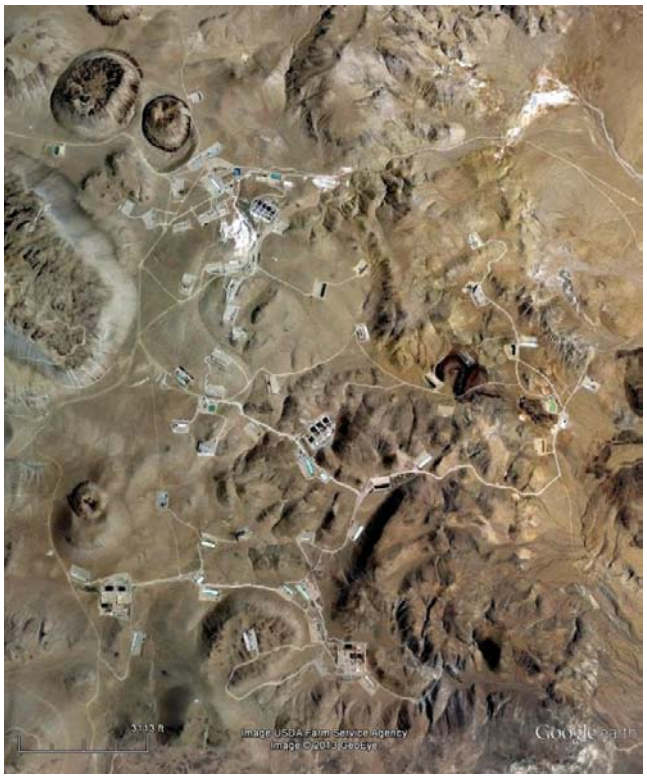

Figure 1.3: Satellite image obtained from Google Earth of Coso Geothermal Field. Rhyolite domes are seen to the north west, the Navy I plant to the north, the Navy II plant in the middle of the field, and the BLM West and BLM East plants to the south.

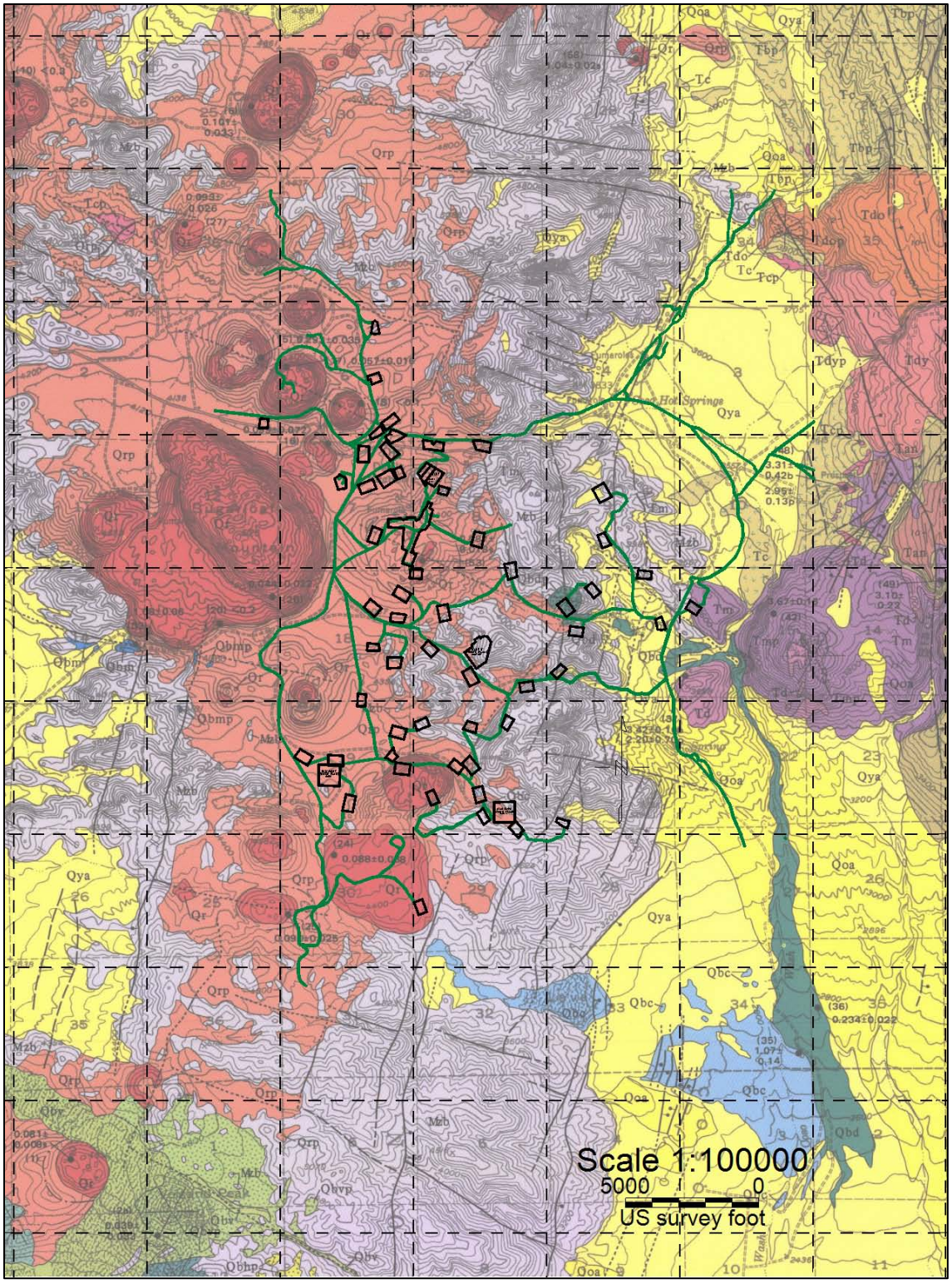

Figure 1.4: Geologic Map of Coso Geothermal field, derived from (Duffield & Bacon, 1981). Extensive vlcanic features are seen throughout and surrounding the geothermal field including extensive rhyolite domes, and large basalt flows to the south.

Table 1.1: Geologic unit descriptions as shown in Figure 1.4, derived from (Duffield & Bacon, 1981)

Terms "basalt", "andesite", and "dacite" refer to distinctions made in the field on basis of phenocryst species and abundances. These categories are generally substantiated by chemical analyses (unpub. data) when rocks are grouped as follows on basis of anhydrous SiO_2 content: basalt, <54 percent SiO_2; andesite, 54-60 percent SiO_2; dacite 60-65, percent SiO_2; rhyodacite, 65-70 percent SiO_2; rhyolite, >70 percent SiO_2. Moderately porphyritic rocks contain 5-20 percent phenocrysts; sparsely porphyritic rocks, <5 percent. All K-Ar ages from Duffield, Bacon, and Dalrymple (1980) unless otherwise noted. Numbers in parentheses are sample numbers in Lanphere, Dalrymple, and Smith (1975) and Duffield, Bacon, and Dalrymple (1980). Tertiary-Quaternary boundary is taken to be between 1.6 and 1.8 m.y. (Berggren and van Couvering, 1974).

Qya — YOUNGER ALLUVIUM – Alluvial fan deposits, stream deposits of gravel, sand, and silt, windblown sand, and deposits of silt and clay in closed depressions

BASALT OF VOLCANO PEAK – Moderately porphyritic basalt containing plagioclase, clinopyroxene, and olivine phenocrysts and rare quartz xenocrysts(?); probably youngest volcanic unit in map area. Divided into two parts:

Qbv — Flows, 2-6 m thick; K-Ar age, 0.039±0.033 m.y. (2a)

Qbvp — Pyroclastic deposits: cinder cone and adjacent cinder mantle

RHYOLITE WEST OF COSO HOT SPRINGS – Moderately porphyritic to aphyric rhyolite; most contains less than 1 percent phenocrysts, all smaller than 1 mm, of some or all of the phases quartz, sanidine, oligoclase, titanomagnetite, ilmenite, zircon, allanite, biotite, hornblende, clinopyroxene, orthopyroxene, and fayalite; inclusions of vesicular basalt present in some localities. Divided into two parts:

Qr — Steep-sided flows as long as 1 km and domes 40 to 350 m high, most covered by a carapace of sparsely vesicular perlite through which obsidian protrudes locally; K-Ar ages range from 1.04±0.02 m.y. (58) to 0.044±0.022 m.y. (26), but most emplaced since about 0.3 m.y. ago

Qrp — Pyroclastic deposits: well-bedded fragmental deposits of pumice, obsidian, and basement rocks, locally reworked from hillsides; forms explosion rings around some domes and generally mantles entire area of rhyolite field; includes minor playa deposits

BASALT SOUTHEAST OF DEVILS KITCHEN – Moderately porphyritic basalt containing plagioclase and olivine phenocrysts; xenoliths of granitic rocks common locally. Divided into two parts:

Qbd — Flow 2-7 m thick; K-Ar age, 0.234±0.022 m.y. (36)

Qbdp — Pyroclastic deposits: cinder cone

Qoa — OLDER ALLUVIUM – Alluvial fan and minor fluvial deposits; distinguished from younger alluvium by being partly dissected

Qbc — BASALT OF COSO WASH – Flows of moderately porphyritic basalt containing plagioclase, clinopyroxene, and olivine phenocrysts; xenoliths of granitic rocks common locally; intracanyon unit whose vent is probably buried by rhyolite west of Coso Hot Springs at upstream end of flow; 7-25 m thick; K-Ar age, 1.07±0.14 m.y. (35)

COSO FORMATION – Sedimentary and pyroclastic rocks. Age of Coso Formation in map area, previously considered to be Pliocene or Pleistocene (Hall and MacKevett, 1962; Evernden, and others 1964), is here considered to be Pliocene on basis of K-Ar dates on pyroclastic rocks near top of the Coso (given below), rhyodacite southeast of Haiwee Reservoir, and basalt of Upper Centennial Flat (Duffield and others, 1980). North of map area some beds assigned to the Coso Formation (Stinson, 1977) are intruded by rhyolite dated at 5.7±0.2 to 6.0±0.1 m.y. and are interbedded with rhyolite and basalt dated at 5.3±0.2 to 6.0±0.2 m.y. (Bacon, and others, 1979) and are thus probably Miocene in age. In this area the Coso Formation consists of:

Tc — Fanglomerate of basement rocks, arkosic sandstone, tuffaceous sandstone and siltstone, tuffaceous lacustrine beds, and silicic tuff; fanglomerate, coarse-grained arkose, and tuff predominate on high slopes southeast of Haiwee Reservoir and interfinger with finer grained rocks and lacustrine beds to north and west; northeast and east of Upper Cactus Flat and Coso Hot Springs fanglomerate predominates; weighted mean K-Ar age of biotite and sanidine in rhyolite pumice from pyroclastic flow interlayered with lacustrine beds, 3.14±0.15 m.y. (44). Evernden, Savage, Curtis, and James (1964) reported K-Ar age of 2.2 m.y. on altered(?) biotite from pumice in water-laid tuff north of map area. Recalculation using original analytical data, new decay constants, and isotopic composition of potassium gives age of 2.31 m.y., with a large analytical uncertainty. Contains Blancan mammalian fossils north of map area (Schultz, 1937)

YOUNGER DACITE EAST OF COSO HOT SPRINGS – Moderately porphyritic dacite containing plagioclase, quartz, orthopyroxene, hornblende, and subordinate biotite and clinopyroxene phenocrysts. Apparently overlain by fanglomerate and rhyodacite airfall pumice (48) of Coso Formation. Divided into two parts:

Tdy — Flow 10-60 m thick

Tdyp — Pyroclastic deposit

OLDER DACITE EAST OF COSO HOT SPRINGS – Moderately porphyritic dacite containing plagioclase, orthopyroxene, and quartz; subordinate hornblende, biotite, clinopyroxene, and opaque oxide phenocrysts; and rare olivine xenocrysts(?). Overlies fanglomerate containing rhyolite pumice deposit probably correlative with similar pumice within Coso Formation (44). Divided into two parts:

Tdo — Flow 5-50 m thick

Tdop — Pyroclastic deposit

BASALT OF PETROGLYPH CANYON – Sparsely porphyritic to moderately porphyritic basalt containing plagioclase and olivine phenocrysts, commonly in clots; also contains clinopyroxene phenocrysts and rare quartz xenocrysts(?) north of Haiwee Spring and Upper Cactus Flat. Divided into two parts:

Tbp — Flows typically 3-5 m thick; total thickness, from 3 to at least 150 m; south of Haiwee Spring and Silver Peak, typically displays vesicle cylinders and sheets, platy jointing near tops of flows, columnar jointing in flow interiors, and diktytaxitic texture; K-ar ages: 3.46±0.07 m.y. (59), 3.66±0.08 m.y. (41), 3.50±0.19 m.y. (46), 2.98±0.12 m.y. (50), 3.32±0.10 m.y. (3), and 3.53±0.17 m.y. (38) (dike)

Tbpp — Pyroclastic deposits

MAFIC ROCKS – Predominantly sparsely porphyritic to moderately porphyritic basalt containing plagioclase, olivine, and, commonly, clinopyroxene phenocrysts; quartz xenocrysts(?) and plagioclase crystals with sieved cores also common. Divided into two parts:

Tm — Flows 2 to 20 m thick; includes one or more andesite flows in Black Canyon; K-Ar ages, 3.67±0.16 m.y. (42) and 3.10±0.22 m.y. (49)

Tmp — Pyroclastic deposits

DACITE – Predominantly moderately porphyritic to porphyritic dacite containing plagioclase and various combinations of quartz, orthopyroxene, clinopyroxene, hornblende, biotite, opaque oxide, sphene, and zircon phenocrysts; minor olivine present locally. Divided into two parts:

Td — Flows and shallow intrusive bodies ranging in thickness from approximately 20 to at least 300 m; rounded inclusions of basalt or andesite a few millimeters to several meters in size form as much as 30 volum percent of some outcrops; K-Ar ages: 3.33±0.20 m.y. (54; biotite), 3.40±0.10 m.y. (37; weighted mean of biotite and plagioclase), and 3.50±0.15 m.y. (55; weighted mean of biotite and plagioclase)

Tdp — Pyroclastic deposits; commonly includes mafic cinders admixed with dacite cinders

Mzb — BASEMENT ROCKS – Principally granitic intrusive rocks of Mesozoic age; compositions range from granite to gabbro; mafic inclusions common, especially in southwestern part of map area; metamorphi pendants as long as 0.5 km present in eastern and northeastern parts of map area; generlly northwest trending Mesozoic(?) dikes of silici to mafic composition abundant locally

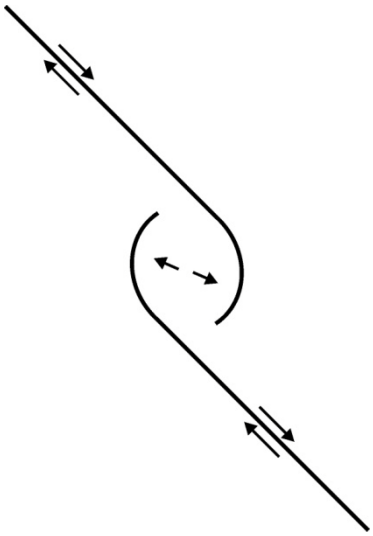

Figure 1.5: Simple model of a releasing bend between two transverse dextral faults. As the two sections of the faults to the north and the south move the area in the bend is pulled apart.

1.4 Time Lapse Gravity Method

The time lapse gravity method consists of several gravity recordings collected at various times at the same locations over a field. The data provide "snap shots" of the gravity field through time. The yearly data are difference to reveal the change in gravity over the time frame. The final time lapse gravity data provide information on changes in the subsurface mass.

1.4.1 Previous Use of the Time Lapse Gravity Method

The time lapse gravity method has been used for a variety of applications including caldera and water flood and artificial ground water storage monitoring. A large gravity network was established to monitor and detect changes in mass beneath the Yellowstone Caldera in 1977 and revealed a gravity increase associated with uplift from 1987 to 1993(Arnet, Hans-Gert, Klingele, Smith, & Meertens, 1997). More recently, time lapse gravity was successfully used to map a water injection into an oil and gas field at Prudhoe Bay, Alaska in harsh arctic conditions from 2003 to 2007 using absolute gravity meters(Fergunson, et al., 2008). Additionally in 2005 an artificial aquifer water storage program was also monitored using time-lapse gravity(Davis, Li, & Batzle, 2008).

Within the geothermal industry, time lapse gravity has been used extensively. The first use was by Dr. Trevor Hunt at the Wariaki field in New Zealand where twelve surveys were collected between 1961 and 1991 (Hunt T. M., 1995). Additionally, a sixty-station grid was set up in Cerro Preito in 1980

(Grannell, et al., 1980). Also, the effects of reinjection were tracked at the Rotokawa field, again in New Zealand from 1997 until 2004 (Hunt & Bowyer, 2007). In yet another example of the use of time lapse gravity, data were collected from 1980 until 1999 over the Bulalo field in the Philipines and used to calibrate numerical models on mass movement (Nordquist, Protacio, & Acuna, 2004). The time lapse gravity method is well established and understood.

1.4.2 Time Lapse Gravity Theory

The integral equation for time lapse gravity calculation is

$$\Delta g(x,y,z,\Delta t) = \mathrm{G}\int_0^{\infty}\int_{-\infty}^{\infty}\int_{-\infty}^{\infty}\frac{\Delta\rho(x',y',z',\Delta t)(z-z')}{[(x-x\prime)^2+(y-y\prime)^2+(z-z\prime)^2]^{3/2}}dx'dy'dz' \tag{1.1}$$

where the position of the gravity observation point is given by (x,y,z), the location of each point source of gravity is at (x',y',z'), the gravitational constant G is equal to $6.67398 \times 10^{-11}\ m^3/kg\ s^2$ and $\Delta\rho$ is the change in density. Time lapse gravity is most often described using the unit microGal (μGal) which is equivalent to 10^{-8} m/s^2.

In the subsurface, mass changes are most often driven by subsurface fluid movement, accomplished through porosity and faults (Biegert, Fergunson, & Li, 2008). The change in density as driven by porosity and saturation of one fluid and one gas is

$$\Delta\rho = \phi_2\left[S_2\rho_f + (1-S_2)\rho_g\right] - \phi_1\left[S_1\rho_f + (1-S_1)\rho_g\right] \tag{1.2}$$

where ϕ is the porosity and S is the saturation at two varying times, ρ_f is the density of the pore fluid, and ρ_g is the density of the gas (Sarkowi, Wawan, & Santoso, 2005). If the porosity does not change over time, the density of the fluid is equal to 1 g/cm^3, the density of the gas is 0 g/cm^3, the saturation at time one is 100% and the saturation at time two is 0%, the change in density is equivalent to the negative porosity.

1.4.3 Sources of Noise

In additional to instrument noise there are a variety of other sources that can create noise in time lapse gravity data. These can include changes in elevation, atmospheric pressure, water table fluctuations, rain fall, and activities within the field such as above surface construction. If these sources cannot be

corrected for during the data processing stage, such as through modeling, then they must be included in the error levels of the data.

1.5 Coso Geothermal Time Lapse Gravity Data

I obtained an extensive set of time lapse gravity data collected over the Coso geothermal field. The data span from eleven stations in 1987, prior to energy production to 139 stations collected between 1996 and 2005. However not all stations were collected on a continuous basis. The data were primarily collected by Allan Katzenstein of the Navy Geothermal Program Office (GPO), the organization that oversees the operations at the Coso Geothermal field. Dr. Katzenstein collected the gravity data in the years prior to his retirement in 2003. Charlie Rodgers, also with the GPO, collected the data from 2004 and 2005. Included, are 23 separate data collections collected. The gravity surveys included numerous stations inside and surrounding the geothermal field as well as stations in the surrounding valleys and mountains. These data were in various stages of processing when received.

In addition to the pre-existing data, I performed an additional gravity survey January of 2013. With the new gravity data, there are now gravity data spanning 26 years at Coso.

CHAPTER 2:
DATA COLLECTION AND PROCESSING

In this chapter I first discuss the general considerations that should be taken when planning and conducting a time lapse gravity survey. I then move on to the specific methods used and complications encountered during the Coso data collections. Last, I will discuss time lapse gravity data processing in a general sense before discussing the specifics of the processing of the Coso data.

2.1 Time Lapse Gravity Survey Planning and Data Collection

There are several aspects of time lapse gravity survey planning and data collection that are important including the reference station, base station, individual gravity stations, and the corresponding elevation surveys.

2.1.1 Reference Station

Most time lapse gravity surveys require the use of a reference station. A reference station is a location outside of the field where zero gravity change over time is assumed. This condition is vital in that it allows relative gravity meters to be used. Conversely a reference station is not needed when absolute meters are available such as was done in Prudhoe Bay Alaska (Fergunson, et al., 2008). Relative gravity meters measure the change in gravity from one point to the next rather than the absolute value of gravity. In order to tie the readings from one year to the others or from one meter to another, all readings must be made relative to the same point, the reference station. The gravity at the reference station is set to zero for each data collection with all other data points adjusted accordingly. In order for this reference leveling to be successful, the zero gravity assumption must also be valid. This assumption requires that the station be outside of the area influenced by the mass changes to be observed. Forward modeling can be used to ensure that the reference station selected is indeed outside this area of influence. Additionally, it is useful if more than one reference station is established. This ensures that if the original station is lost, another reference station exists (Davis, Li, & Batzle, 2008).

2.1.2 Base Station

Relative gravity meters are also subject to instrument drift and gravity changes produced by the tides. As with all gravity surveys, these effects need to be corrected for. This is generally done by

reoccupying the same base station every two to three hours and assuming a linear drift between base station reoccupation. If due to a large survey extent, the same base station cannot be reoccupied in the required time, data collection loops are necessary utilizing a number of base stations that are tied together (Blakely, 1995).

2.1.3 Time Lapse Station Repeatability and Reading Accuracy

An additional requirement for time lapse gravity surveys is the ability to reoccupy the same stations every year. A common approach is to survey the locations of the stations using real-time-kinematic Global Positioning Systems (GPS) and marking the stations with a stake or flag. Ideally to improve relocation, and leveling, permanent concrete platforms may be established at each location.

Foresight into future operations at a site could prove beneficial when planning and conducting a time lapse gravity survey. If the survey is to be conducted over, for example, an active geothermal field, or near an active gravel quarry, it is preferred to select station locations as far away from activity as possible as this activity can generate unwanted changes in gravity.

The signal observed in most time lapse surveys is generally small, within 100s of μGals, making accuracy important to minimize noise as much as possible. Gravity meters need to be handled with care to avoid creating excess drift or tares in the data. The leveling of the gravity meters should be performed accurately. Additionally, it is beneficial to re-collect approximate 20% of all gravity stations during each survey to quantify error levels and repeatability.

2.1.4 Elevation Surveys

The strongest source of gravity signal in any survey is the mass of the Earth as a whole. A small change in the distance from this mass will produce a measurable anomaly in the gravity. For this reason, any changes in elevation over time need to be corrected for in the time lapse gravity data. The signal produced by changing elevation is the free air correction of -308.6 μGal/m. (Blakely, 1995). Real time kinematic elevation surveys need to be collected within the same time periods as the time lapse gravity data in order to perform this correction.

2.1.5 Coso Geothermal Time Lapse Gravity Data Collection

Gravity data were acquired at the Coso Geothermal field by the Navy Geothermal Program Office (or the organization that became the GPO) starting with a few stations in 1987. Data were then collected on a semi-regular basis from 1991 until 2005. I collected an additional data set in January 2013. A Locoste and Romberg Model G was used from 1987 until the 1994. A Scintrex CG-3 was used from 1994 until 2005. The 2013 data were acquired using two Scintrex CG-5s. The various time lapse stations collected are shown on Figure 2.1 and Figure 2.2, with the exception of some stations from 1987. The easting and northing of these stations are unknown at this time. Both figures are presented in a modified California NAD 1927 State Plane, US Survey Feet.

Station CGB (Figure 2.1) was used as the reference station in 1987. From 1991 until 1996 station J-4 was the reference station. In 1996 several gravity stations were added and the reference station was moved to B-14. The data surveys were collected using data loops. Only four of the stations collected in 1987 were repeated again, and could be located. These stations were CGB, DOR68, CER1, and CER15.

During the last data collection in 2013, it was observed that an active geothermal field presents additional difficulties to a time lapse gravity survey. Four of the gravity stations on the field were either damaged or could not be located due to construction activities. Additionally when new structures are built near a station the data will be influenced. This equivalently occurs when the ponds near wells are filled or emptied. Lastly the activities of the wells, such as venting to the atmosphere, can create noise in the readings due to the small vibrations generated.

Elevation surveys were conducted by outside contractors using real-time kinematic global positioning systems. These surveys were collected yearly to every three years beginning in 1987 up to 2009. An elevation survey corresponding with the 2013 data was collected in the summer of 2013 at which point it was not able to be used for data processing. Consequently the 2013 gravity data are not included in the results and inversions presented here.

2.2 Time Lapse Gravity Data Processing

There are some general steps that must be taken when processing time lapse gravity data. I next discuss these, followed by the specific processing performed on the Coso geothermal gravity data.

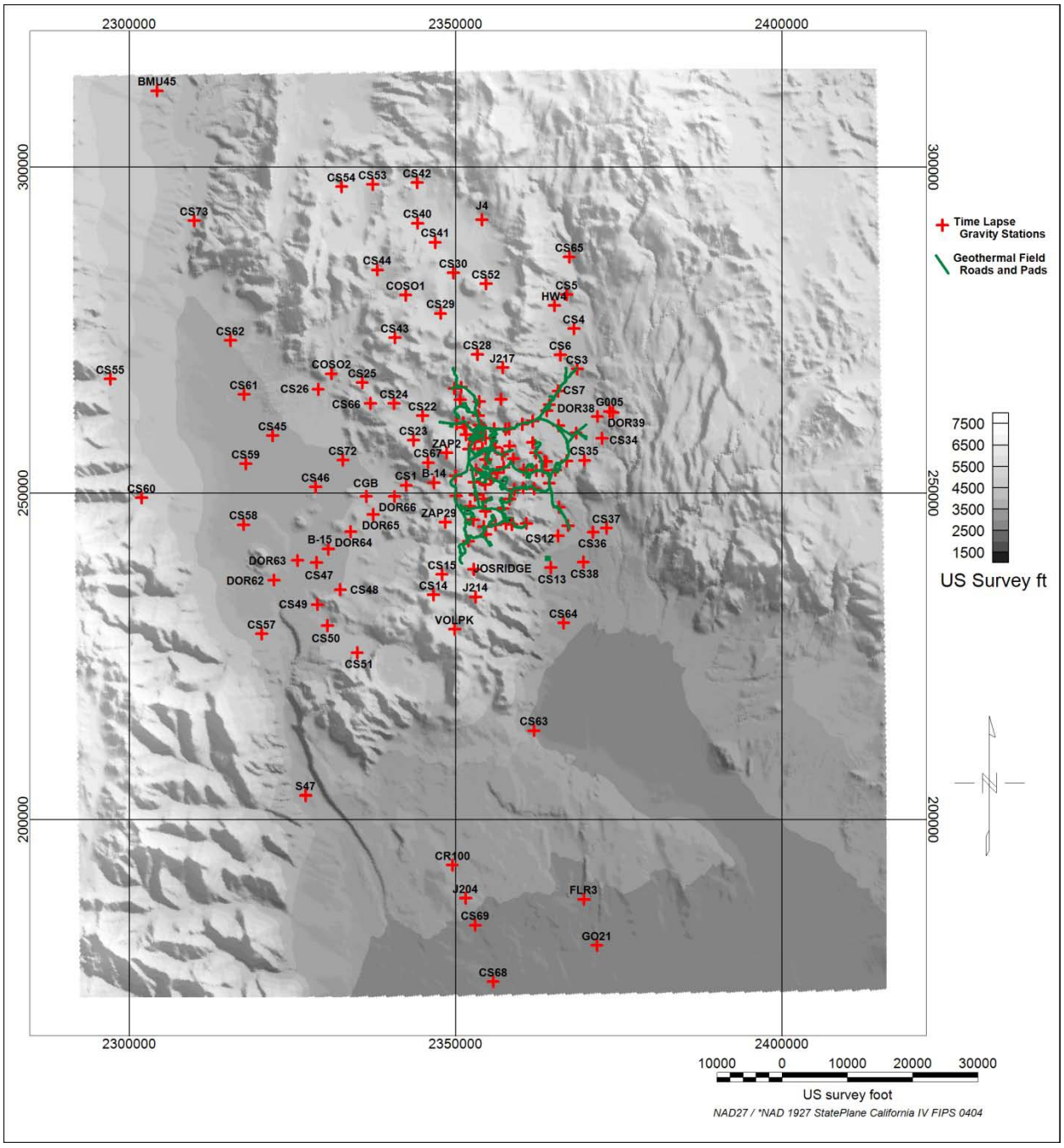

Figure 2.1: Time lapse gravity stations outside geothermal field, collected between 1987 and 2013. Not all stations were occupied during every survey. Some stations from 1987 are not shown.

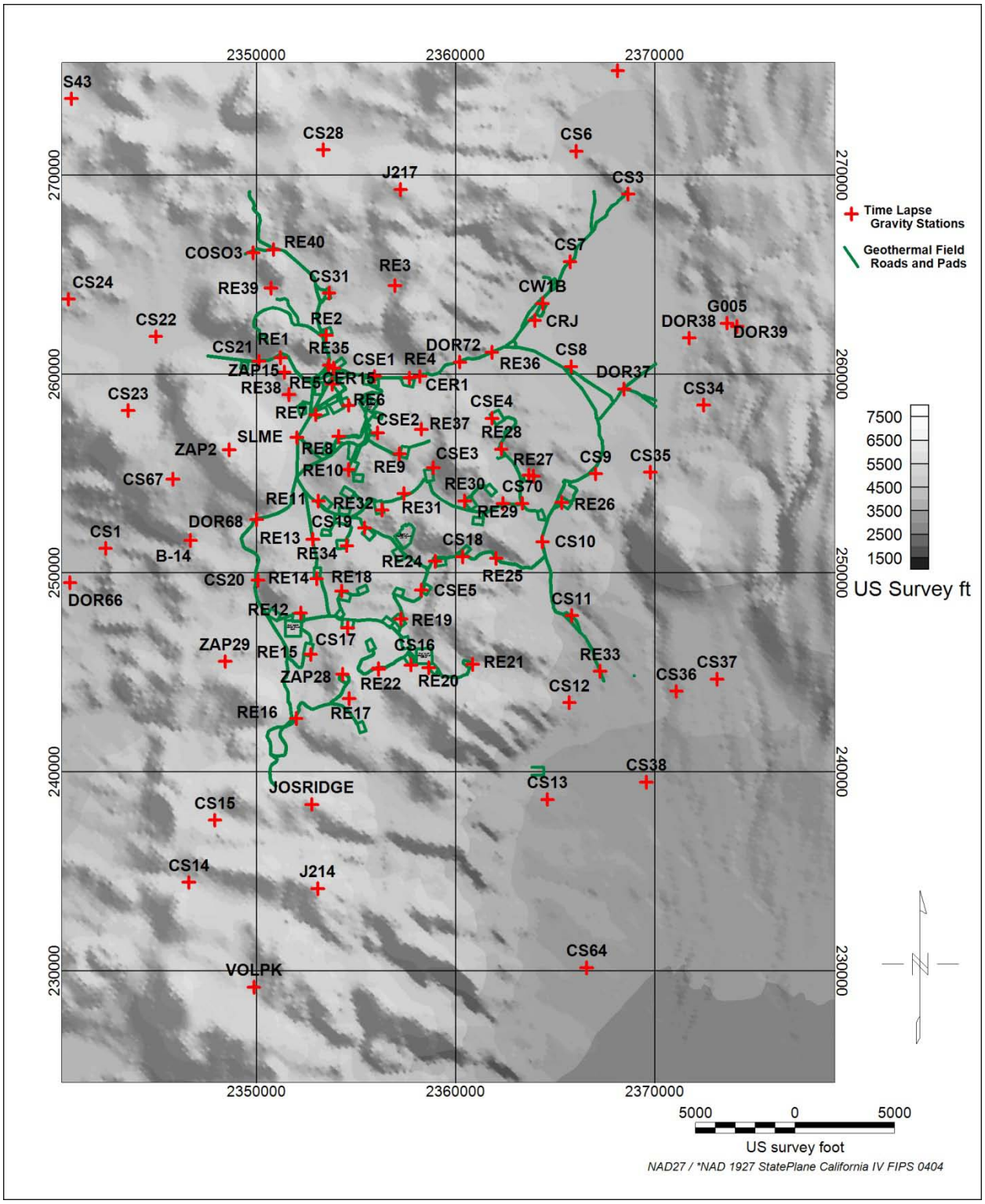

Figure 2.2: Time lapse gravity stations inside and surrounding geothermal field, collected between 1987 and 2013. Not all stations were occupied during every survey. Some stations from 1987 are not shown.

2.2.1 General Time Lapse Data Processing Steps

Observed relative gravity data require a number of processing steps to isolate the gravity anomaly. A drift and tidal correction, free air correction, and Bouguer and terrain corrections are generally applied (Blakely, 1995). However for time lapse gravity surveys, with the exception of the drift and tidal correction, the effects that these processing techniques correct for are removed during the differencing of the data sets (Davis, Li, & Batzle, 2008).

The processing steps that are performed on time lapse gravity data include drift corrections, reference station leveling, and elevation change corrections. Instrument drift and the effects of the tides are removed by re-occupying a base station ever one to two hours and performing traditional drift correction (Blakely, 1995). The time lapse gravity data cannot be generated through subtraction unless they contained a shared quiet point. This is why the reference station is vital. This station is set to zero and the value recorded at this station is subtracted from all other stations. As mentioned, any changes in elevation over time need to be recorded and corrected for. This is done by applying the free air correction of 308.6 μGal/m for the elevation change observed at each location.

Additional sources of gravity signal over time that are not due to the desired signal are not desired and therefore should be corrected for if possible. These can include shallow water table changes, changes in atmospheric pressure, and the addition or removal of mass above the surface.

Once the data are corrected for instrument drift, tidal variations, the reference station, elevation changes and unwanted signal source, these data can then be compared and subtracted to produce the final time lapse gravity data.

2.2.2 Coso Geothermal Time Lapse Gravity Data Processing

The time lapse gravity data set collected at the Coso geothermal field was provided in various states of data processing. The data from 1987, 2004 and 2005 were uncorrected and in the form of scanned form. These data required complete processing. These three data sets were corrected for daily drift and tidal changes first. The data from 1991 to 1996 were reference leveled to a different station than the data from 1996 to 2003, requiring the earlier data to be re-leveled to the second reference station B-14 station.

The data were also corrected for elevation changes using real time kinematic elevation data. The maximum elevation change occurred at station CSE2, where a subsidence of 1.35 ft was recorded between 1991 and 2005. This corresponds to a gravity signal of 130 μGal. Seven stations, shown in Figure 2.3, experienced an elevation changes greater than -0.6 ft, or -56 μGal. Two stations, CS1, and CS22, well outside the field experienced small positive changes in elevation. This observed change in elevation indicates that the assumption of no change in porosity mentioned in Section 1.4.2 is invalid. The subsidence indicates a collapse of porosity, most likely within the density anomaly. If the anomaly is 1000 ft in thickness, and the subsidence is 1.35ft, each foot of reservoir compacted by 0.00135ft, so the change the maximum change in porosity would be 0.135%, which is well within the error of the porosity estimate.

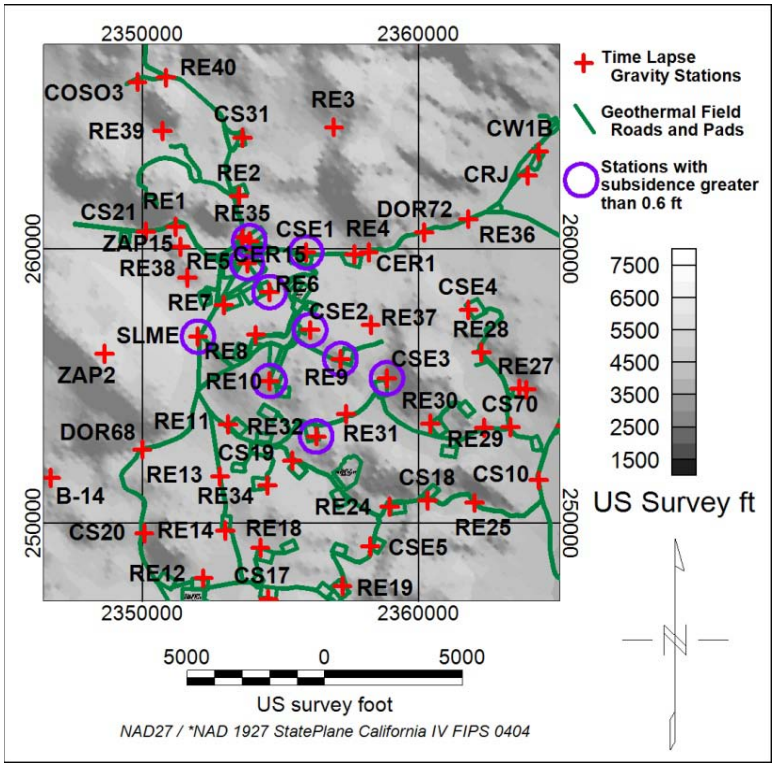

Figure 2.3: Gravity Stations where elevation changes greater than -0.6ft between 1987 or 1991 and 2005 were recorded are circled in purple. This elevation change will produce a gravity signal of 56 μGal or greater, which is on the order of the expected gravity change produced by changes in the reservoir.

Additional sources of signal during these surveys needed to be considered. First, change in rainfall or shallow ground water tables can create time lapse anomalies. However, the field is located in the Mohave Desert and receives very little rainfall. Furthermore, geochemical data indicates there is currently no low salinity ground water in the system (Adams, Moore, Bjornstad, & Norman, 2000). A

second source of signal is changes in above surface mass. Little is recorded on when or how these changes occurred making it impossible to correct for. Changes in barometric pressure can also produced changes in the gravity, however this effects all stations including the reference station and is therefore removed during the data subtraction (Davis, Li, & Batzle, 2008).

Station B-14 is located approximately 5,300ft (1.6 km) from the nearest well pad. The exact location of the edge of the reservoir is unknown as is the depth and porosity of the reservoir. Figure 2.4 shows the time lapse gravity response of a 1000ft deep reservoir with varying change in surface level and density contrasts value of -0.05g/cm^3, 3,000ft and 5,000 ft off the edge of the reservoir. The reservoir would need to be 1000ft deep and experience a change in to surface of more than 1000ft at a distance of 3,000ft from the reference station for the zero gravity assumption to be invalid. As will be shown in Section 4.1.1 the maximum inverted thickness of the anomaly 3,000ft from station B-14 was approximately 60ft. Stations CS1 and CS22 were considered for replacement base stations as they are located at a greater distance to the field; however their elevations varied more than B-14.

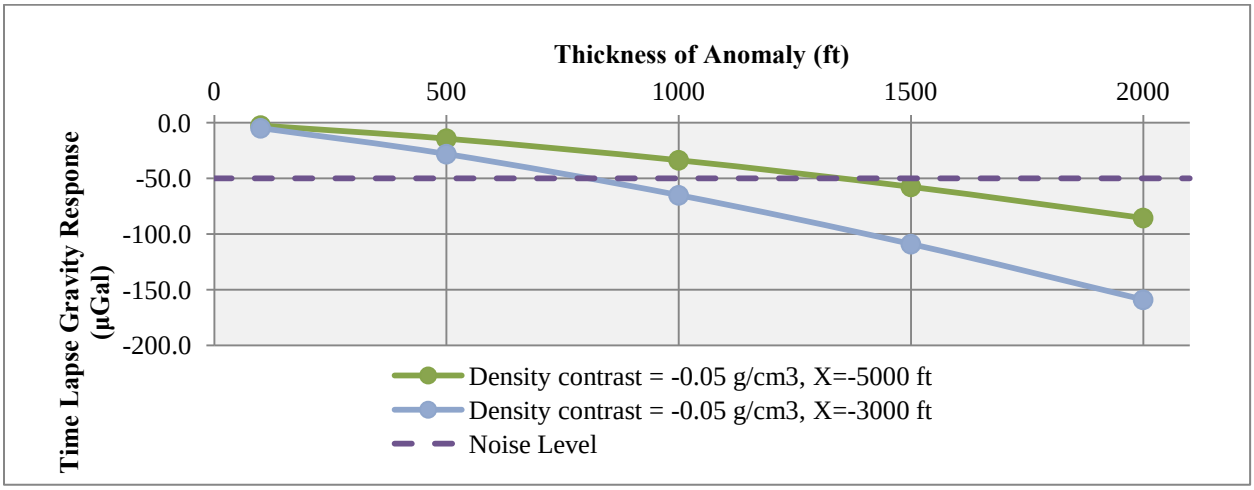

Figure 2.4: The time lapse gravity response 5,000ft and 3000ft off the edge of a 16,000ft by 20,000ft density anomaly, with a depth of 1000ft. The noise level, 50 µGal is shown in purple

2.3 Summary

In this chapter I presented the general data collection considerations taken for time lapse gravity surveys including the establishment of a reference station, the use of a base station for drift corrections, the accuracy and repeatability needed, and the corresponding elevation surveys required. I also discussed the data collection that has occurred at the Coso Geothermal site, starting in 1987 and continuing with the latest data collection in 2013. The data processing steps necessary were discussed next. The Coso data

were introduced as was the processing status of the data when received. The procedures used for processing and reprocessing the data were also discussed.

CHAPTER 3:
FINAL TIME LAPSE GRAVITY DATA AT COSO

In this chapter final time-lapse gravity data recovered for the Coso geothermal field will be presented. In later chapters, inversion results and interpretations are provided.

3.1 Change in Gravity from 1987 until 2005

Figure 3.1 shows the change in gravity at the three stations collected continuously from 1987 to 2005. Station CER1 appears to have an increase in gravity from 1987 to 1991. It appears relatively flat from 1992 until 1994 then declines. The gravity at CER15 declines steadily with a slight increase 1999 and 2002. Station DOR72 also sees a period of relatively consistent gravity from 1999 until 2002.

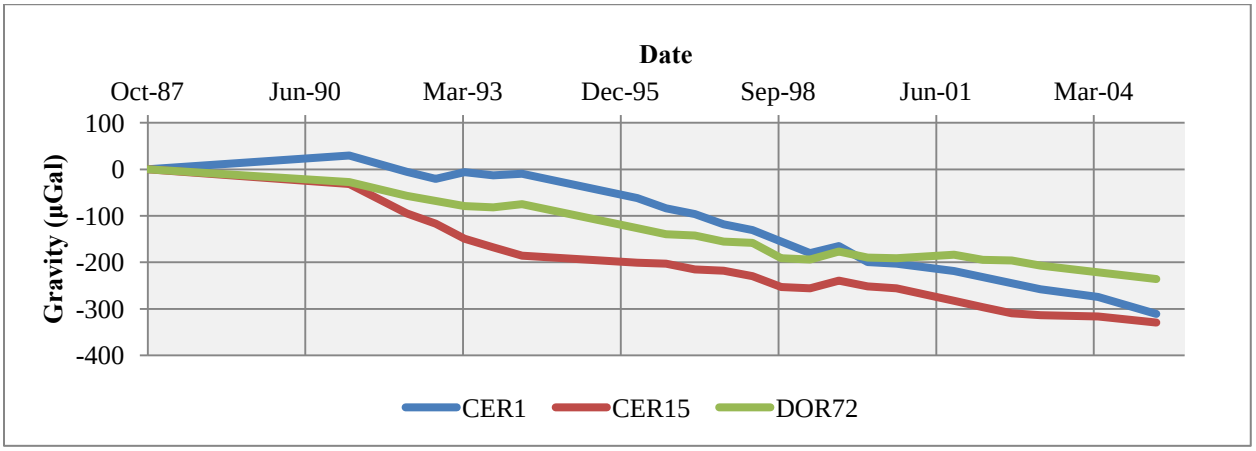

Figure 3.1: Change in gravity from fall of 1987 of the three stations collected that year, CER1, CER15 and DOR72.

3.2 Change in Gravity from 1991 until 2005

There are eighteen stations (not including the reference station, B-14) with gravity and elevation data in 1991. Sixteen of those were collected continuously until 2005. The changes in gravity of the north-central stations around the Navy I power plant are shown in Figure 3.2. All six stations in that area show a decline in gravity ranging from -200µGal to -350µGal. Figure 3.3 shows the gravity change in that same time period at the stations on the east and south-east edges of the field. These stations have small change in gravity ranging from -25µGal to -225µGal. The stations, Figure 3.4, show the least

amount of gravity change with some appearing to have a relatively constant gravity value. The maximum gravity change seen in these stations is -84μGal.

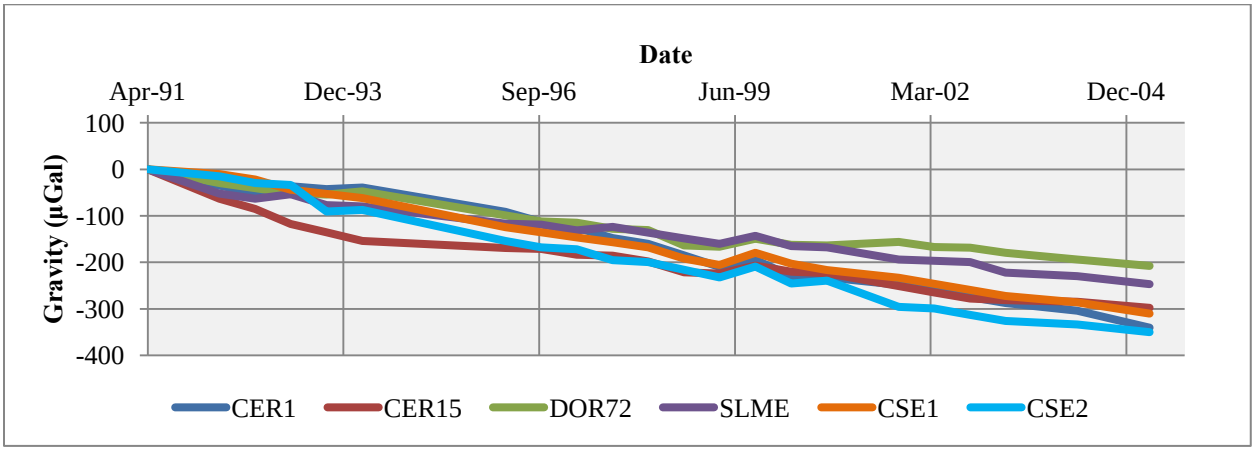

Figure 3.2: Change in gravity in the north-central stations from 1991 until 2005, using 1991 as a starting point and B-14 as a reference station

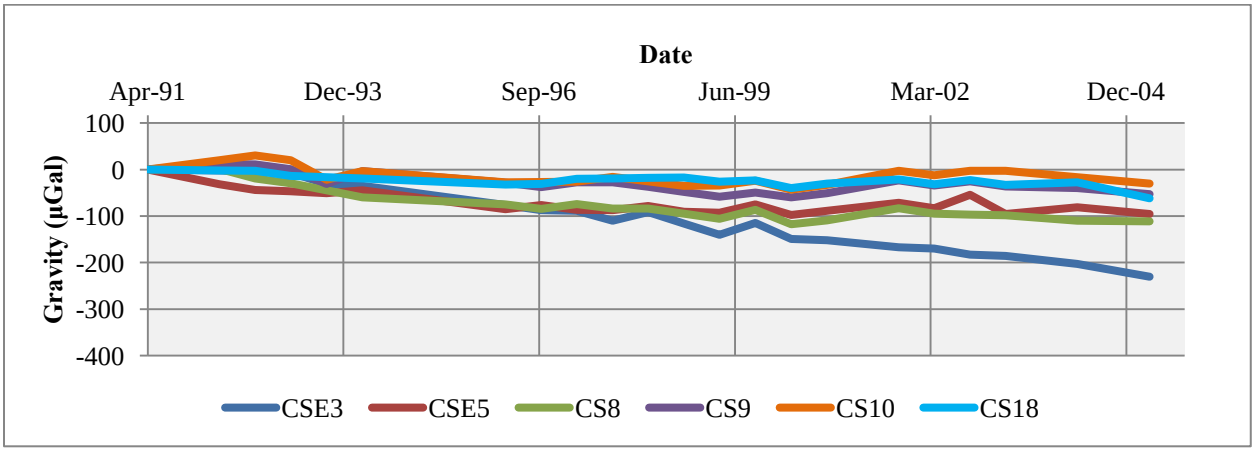

Figure 3.3: Change in gravity in the eastern stations from 1991 until 2005, using 1991 as a starting point and B-14 as a reference station

Next, I present the gravity changes throughout the field from 1991 to 2005 in surface contour form, Figure 3.5 to Figure 3.10 . The stations at which both gravity and elevation data were collected continuously from 1991 until 2005 are shown. Only the spring changes are plotted for simplicity and to minimize signal from seasonal changes in water levels.

Figure 3.5 displays the two year gravity change from spring 1991 until 1993. The largest change in gravity, -117μGal was recorded at station CER15 in the center of the field. Station CS10 to the southeast of the field saw in increase in gravity of 20μGals. The average gravity change seen across all sixteen stations was -30μGal.

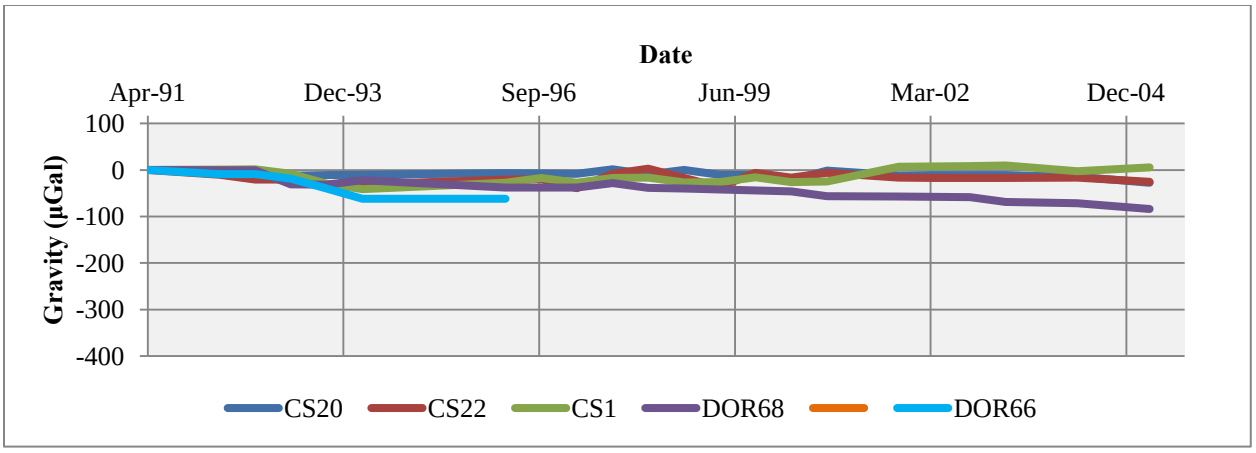

Figure 3.4: Change in gravity in the western stations from 1991 until 2005, using 1991 as a starting point and B-14 as a reference station

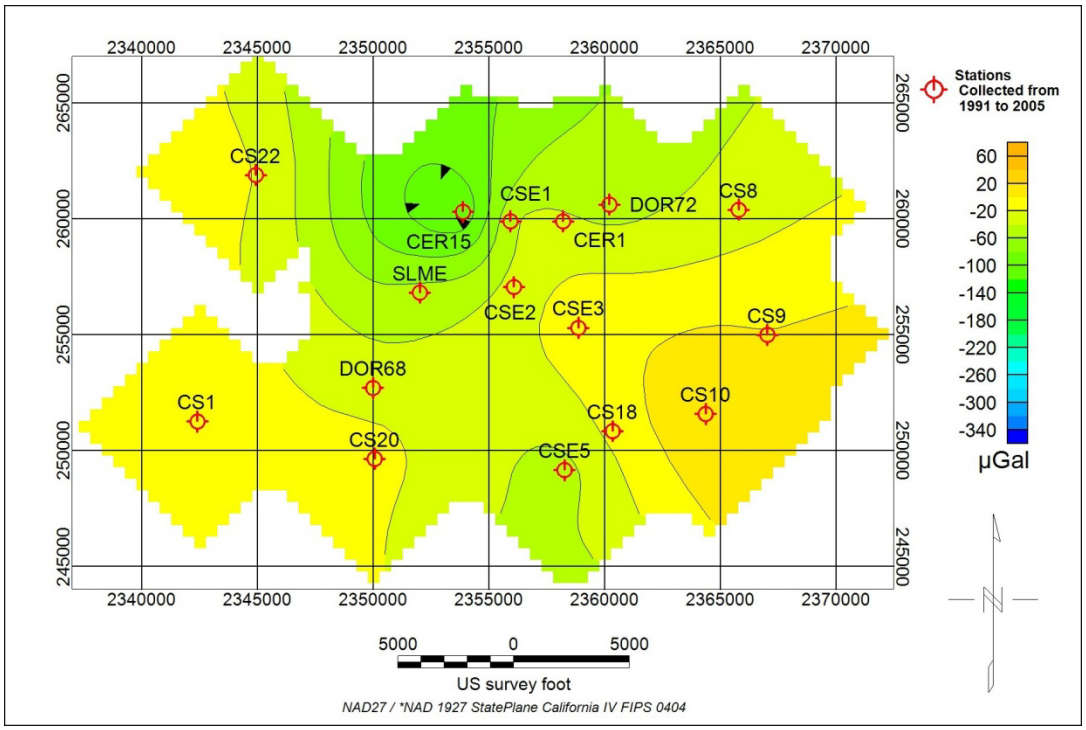

Figure 3.5: Change in gravity from spring 1991 until spring 1993. Sixteen stations have both elevation and gravity data for this time period, marked with red symbols. Station CER15, shows the strongest gravity change, -117µGal. CS10 shows a positive change of 20 µGal.

Again station CER15 shows the greatest change in Figure 3.6 which displays the five year change in gravity from spring 1991 until spring 1996. There are no positive gravity changes for this time period. The smallest negative gravity change was seen at station CS20 to the south of the field at -7µGal. The average gravity change was -76µGal over this period.

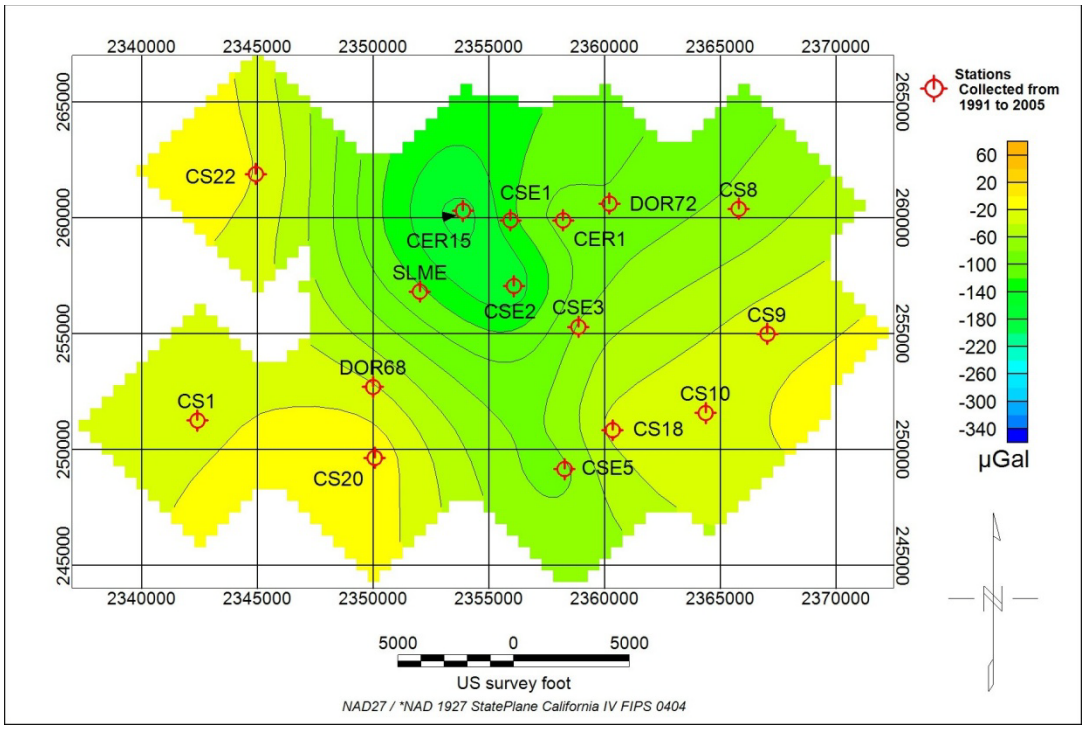

Figure 3.6: Change in gravity from spring 1991 until spring 1996. Station CER15 shows the strongest gravity change, -169µGal. CS20 shows the least amount of change with -7µGal.

The gravity changes from spring 1991 until spring 1998 are shown next in Figure 3.7. CS22, to the northwest shows a positive gravity change of 3µGal. This station is outside of the field and the variations in gravity seen there are discussed in further detail in Section 3.4. The average gravity change is -87µGal. The change of greatest magnitude is seen at station CSE2, with -199µGal. This station is just to the south of CER15 which shows a change -198µGal for this time period. These are both stations in the north central section of the field which show the most change overall as was seen in Figure 3.2. A change of -87µGal was seen on average during this seven year period.

The time lapse gravity data for the nine years span from 1991 until 2000 is shown in Figure 3.8. The negative anomaly in the north central section of the field decreases to less than -200µGal. CSE2 shows a gravity change of -246µGal, CER1 shows -230µGal, and CER15 shows -220µGal. A change in gravity of -16µGal was recorded at station CS22, with -26µGal at the nearby CS1. CS20 also shows a change of only 22µGal. The average change over the sixteen stations recorded was -115µGal.

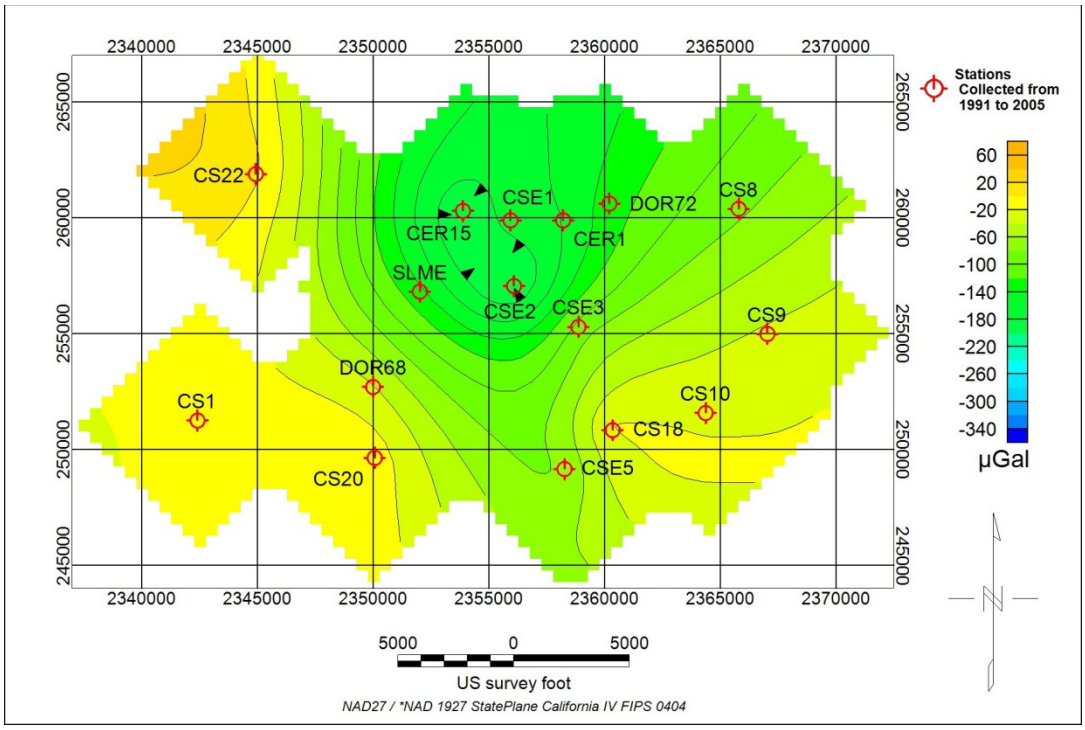

Figure 3.7: Change in gravity from spring 1991 until spring 1998. Station CSE2 shows the strongest gravity change, -199µGal. CS22 shows the least amount of change with a positive 3µGal.

The steep changes from the edges of the field to the north central negative anomaly become more evident in Figure 3.9 which shows the gravity change from spring 1991 until spring 2003. The gravity at station CSE2 decreased by 326µGal during this time period. The gravity decreased at near-by stations CER1 and CER15 by 288µGal and 282µGal respectively. CSE1 and SLME saw gravity changes of -273µGal and -222µGal. However station CS1, to the northwest shows an increase in gravity from spring 1999 to spring 2003 of 9µGal. CS20 to the south shows a decrease in gravity of only 11µGal. The average gravity change observed at the stations for this 12 year span was -132µGal.

Figure 3.10 shows the final time lapse gravity signal from spring 1991 until spring 2005. Station CSE2 shows a decrease in gravity of 350µGal, and station CER1 340µGal. The gravity at station CER15 decreased by 298µGal in the 14 years shown. CS1 shows a positive gravity change of 6µGal. The average gravity change was -154µGal. The stations on the edges of the field show much less change than those in the center.

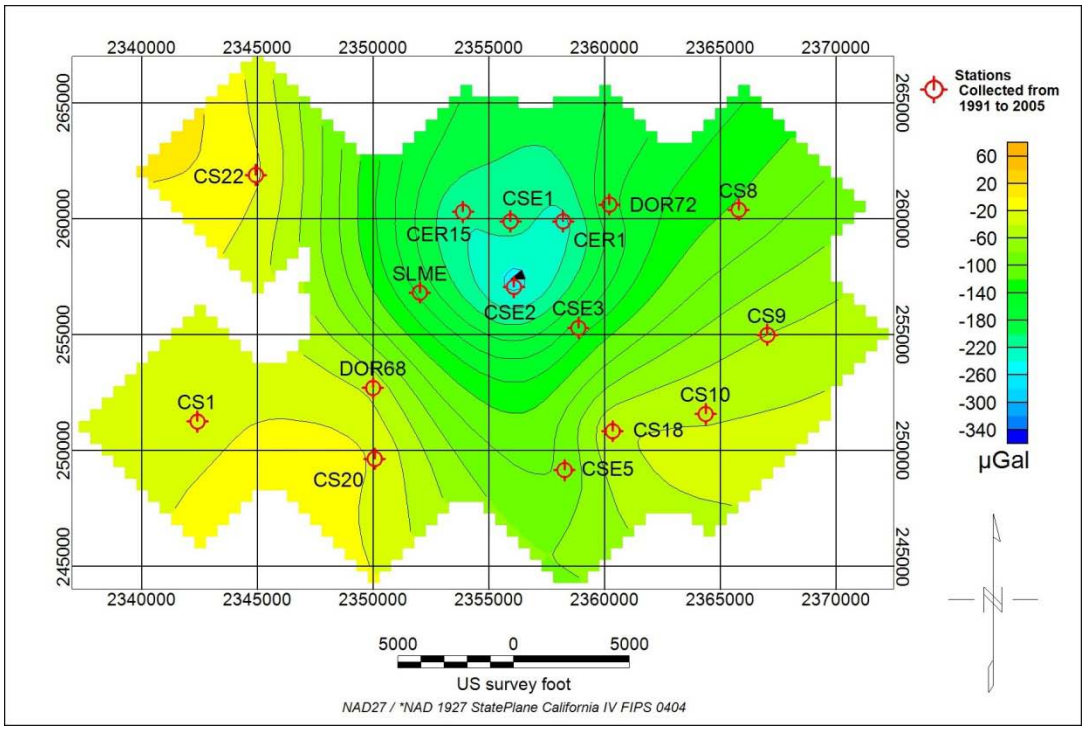

Figure 3.8: Change in gravity from spring 1991 until spring 2000. Station CER15 shows the strongest gravity change, -246µGal. CS22 shows the least amount of change, -16 µGal.

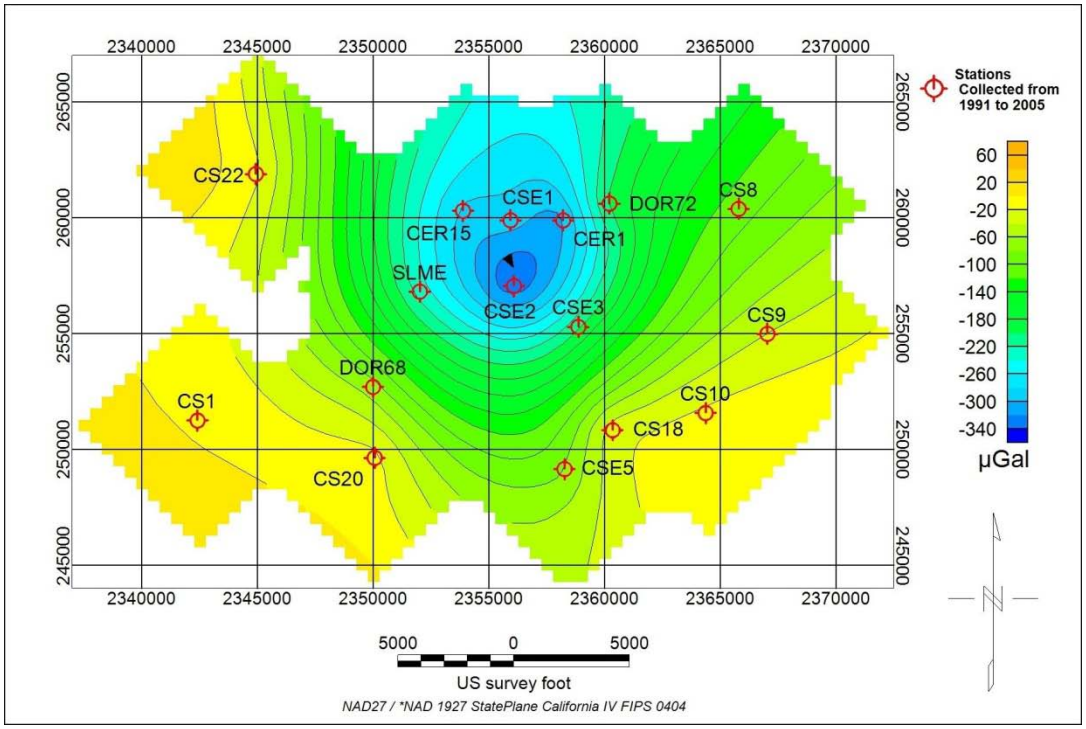

Figure 3.9: Change in gravity from spring 1991 until spring 2003. Station CSE2 shows the strongest gravity change, -326µGal. CS1 shows a positive 9µGal change in gravity

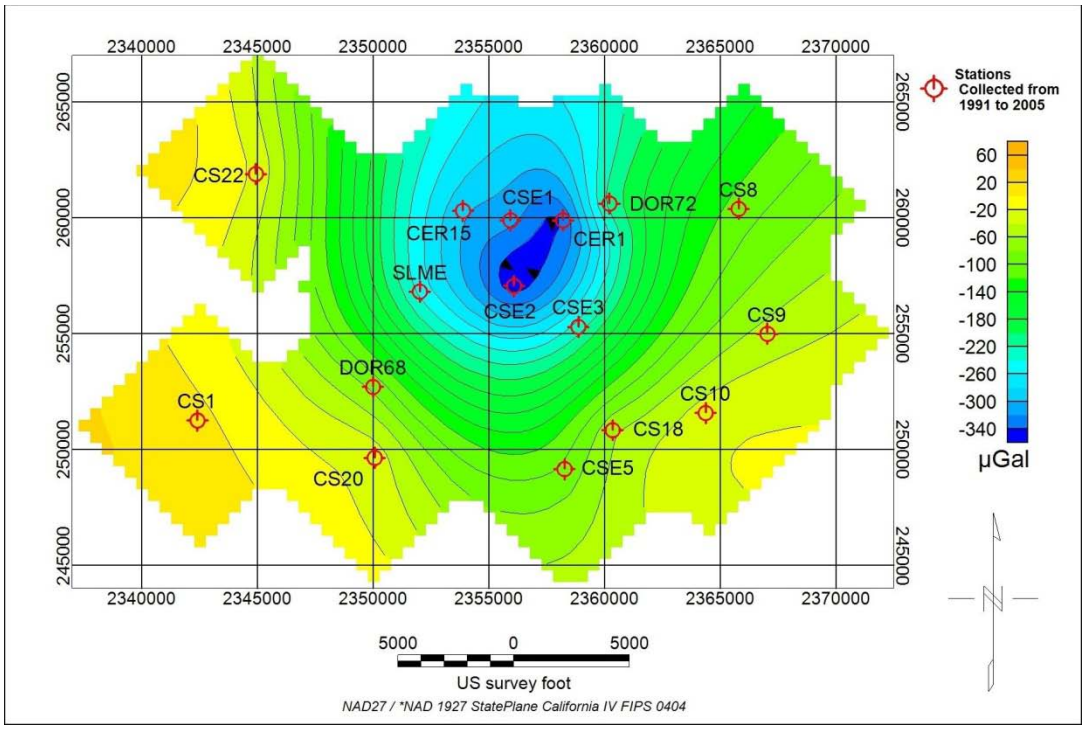

Figure 3.10: Change in gravity from spring 1991 until spring 2005. Station CSE2 shows the strongest gravity change, -350µGal. CS1 shows the least amount of change, a positive 6µGal.

When examining the change in gravity from 1991 until 2005, the gravity decreases greatly in the north central area of the field around stations CER1, CER15, and CSE3. The gravity changes are smaller on the edges of the field, at stations CS22, CS20, CS10. However, station CSE5 to the south does seem to change slightly more than the other edge stations. CS1 is the only station with a net positive change for the fourteen years shown.

3.3 Change in Gravity from 1996 until 2005

There are thirty-eight stations with gravity and elevation data from spring 1996 to spring 2005. The changes in gravity of the north-central stations around the Navy I power plant are shown in Figure 3.11 and Figure 3.12. The six stations in that area show a decrease in gravity from -50µGal to -250µGal. Figure 3.13 and Figure 3.14 show the gravity changes on the eastern flank of the field. Stations CSE3 and CSE4 experience the greatest change with decreases of approximately 150µGal. The gravity at most of the stations on the eastern flank changes by less than 50µGal. The southern stations and western stations, shown in Figure 3.15 and Figure 3.16, show the least amount of change, less than +/- 50µGal.

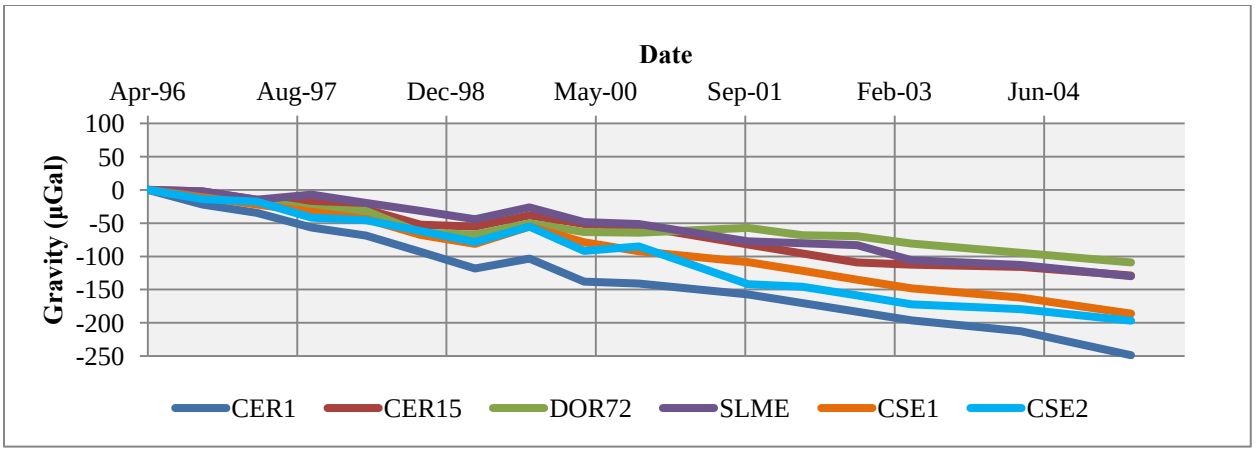

Figure 3.11: Gravity changes for six of the north-central stations, CER1, CER15, DOR72, SLME, CSE1, and CSE2, from spring 1996 until spring 2005.

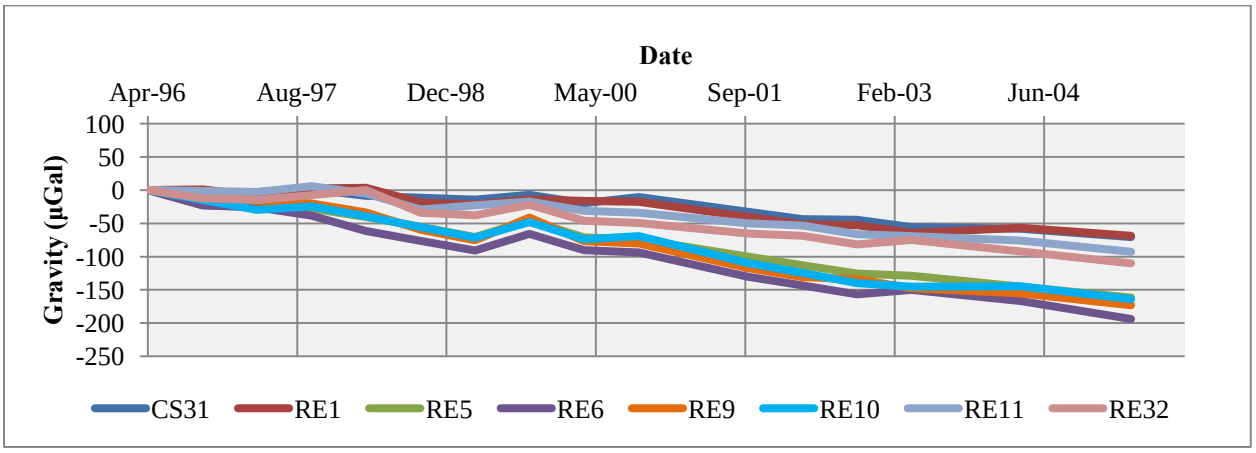

Figure 3.12: Gravity changes for seven of the north-central stations, CS32. RE1, RE5, RE6, RE9, RE10, RE11, and RE32, from spring 1996 until spring 2005.

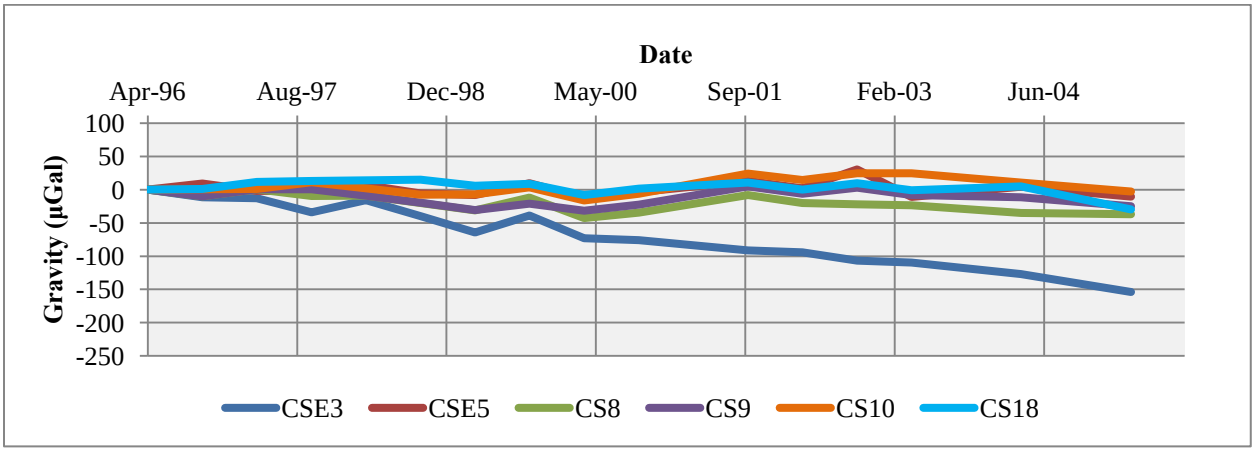

Figure 3.13: Gravity changes for six of the eastern stations, CSE3, CSE5, CS8, CS9, CS10, and CS18, from spring 1996 until spring 2005.

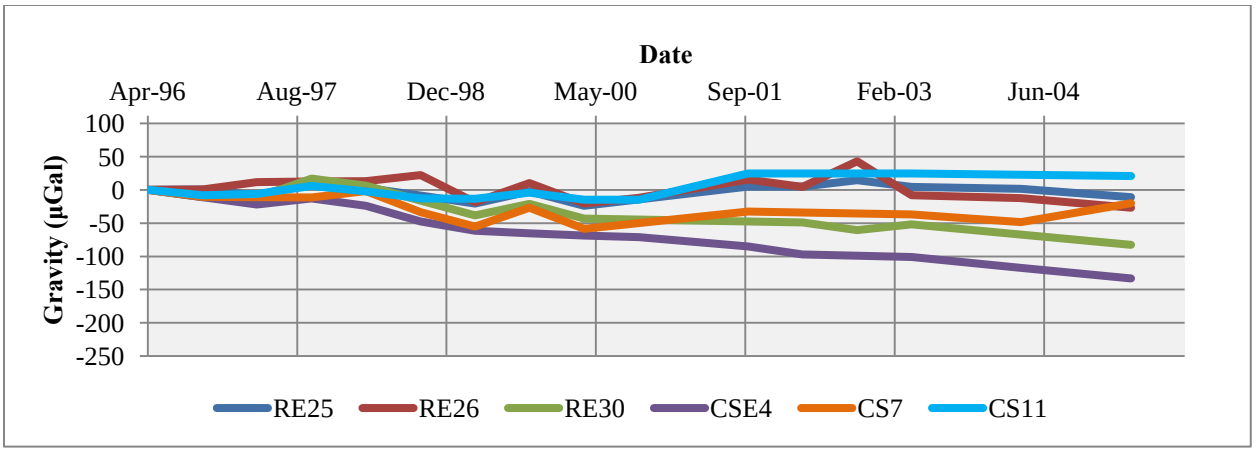

Figure 3.14: Gravity changes for six of the eastern stations, RE25, RE26, RE30, CSE4, CS7, and CS11, from spring 1996 until spring 2005.

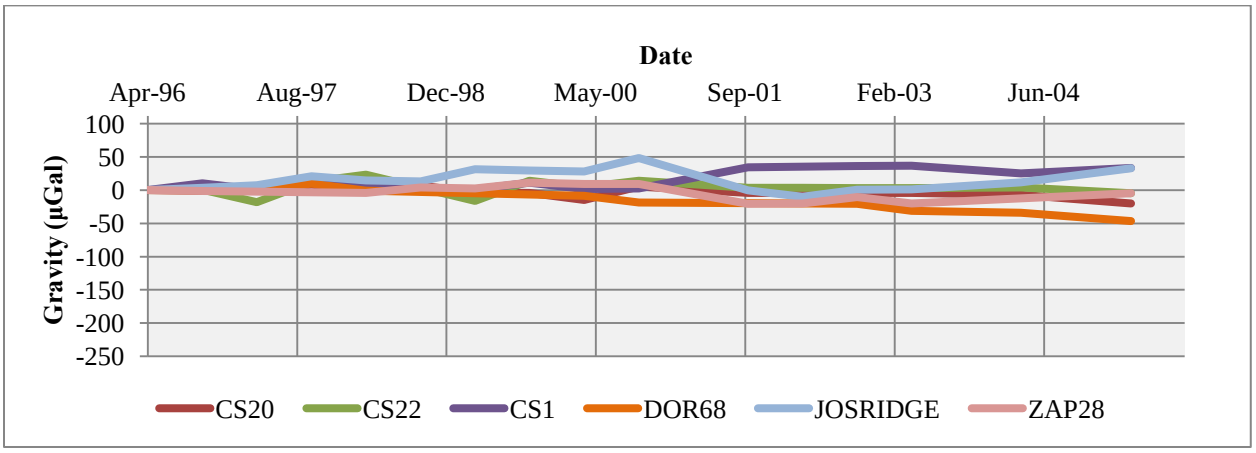

Figure 3.15: Gravity changes for size of the southern and western stations, CS20, CS22, CS1, DOR 68, JOSRIDGE, and ZAP28, from spring 1996 until spring 2005.

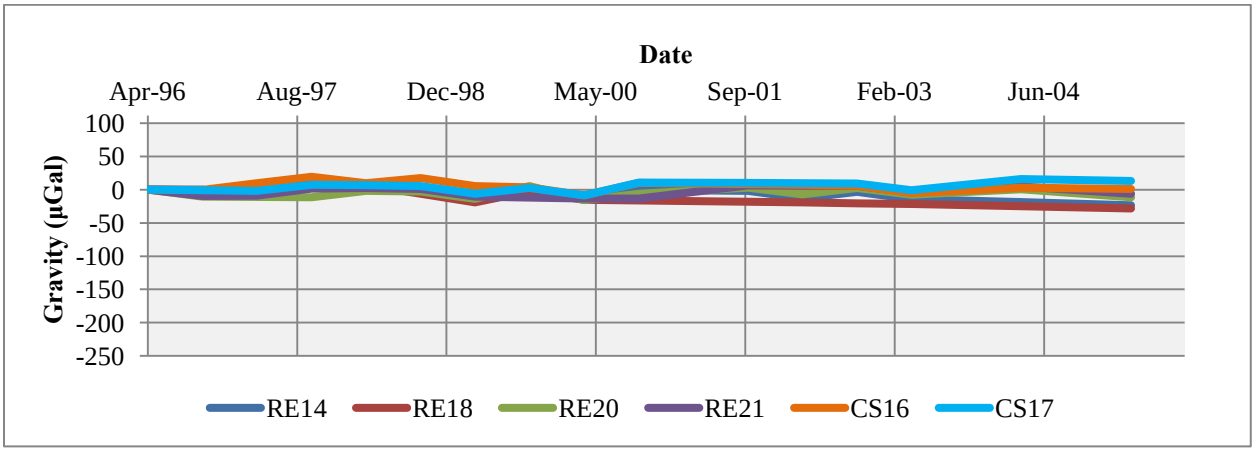

Figure 3.16: Gravity changes for six of the southern stations, RE14, RE18, RE20, RE21, CS16 and CS17, from spring 1996 and spring 2005.

Figure 3.17 displays the gravity changes from 1996 until 1998. The area showing the biggest changes is still the north-central. The greatest negative change was seen at station CER1, -69μGal. Sixteen stations shown positive gravity changes for this two year period, with the greatest positive change at station CS22, 23μGal.

The gravity changes from 1996 until 2000 are shown in Figure 3.18. The negative anomaly in the north central area intensified, and spread to the east slightly. CER1 shows the greatest negative change at -138μGal. Four stations appear to have experienced a positive change over this four year span, including the JOSRIDGE station at 28μGal.

Figure 3.19 shows the change in gravity from 1996 until 2000. Station CER1 experienced a change of -196μGal during this time period, with stations RE6, and RE9 changing by -150μGal, and -147μGal respectively. The gravity change at station CS1, one of six with a positive change, was 37μGal for this time period.

The time lapse gravity response between 1996 and 2005 is shown in Figure 3.20. There is a negative anomaly centered on CER1. The gravity steeply increases toward the western, southern and to a lesser extent the eastern edges of the field. CER experienced a change in gravity of –249μGal. The gravity at station CSE5, to the south but still within the field, only changed by -11μGal. CS1, to the west, saw a change in gravity of 33μGal.

The data from 1996 to 2005 contains more data points and more information. Similar to the data from 1991 to 2005 the area of greatest and most consistent change is the north central part of the field. This change in gravity is approximately -250μGal The stations to the south that are still within the geothermal field and near active well pads show a much smaller change than those to the north. The stations on the far edges of the field show increases in gravity which might be attributed to noise or water influx from the outside the area of gravity coverage.

3.4 Error Levels

As discussed previously, there are several sources of error in a time lapse gravity data. An estimate of the error level is essential for the reliable inversion.

First, I examined repeated data stations as a first step to estimate the error in the data. A number of stations had gravity data collected several times in the spring of 2004. Five of these stations were

collected on three different dates. Of those five stations, station RE20 (collected 8 times on 3 dates), had the largest standard deviation of 7.5µGal.

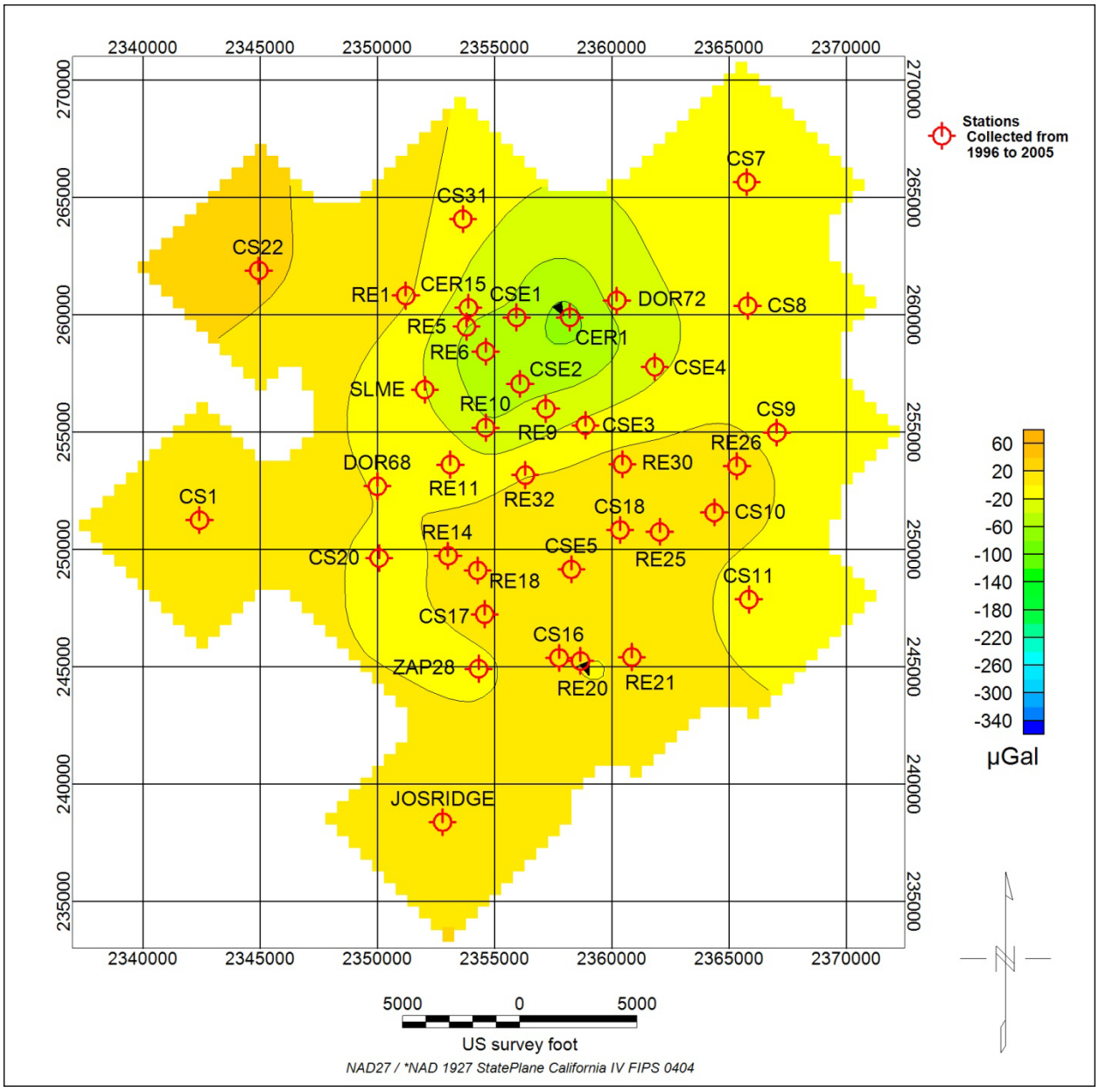

Figure 3.17: Gravity changes from spring 1996 until spring 1998. Thirty-eight stations have both elevation and gravity data for this time period, marked with red symbols. CER1 shows the strongest gravity change, -69µGal. CS22 shows the largest positive change of 23µGal.

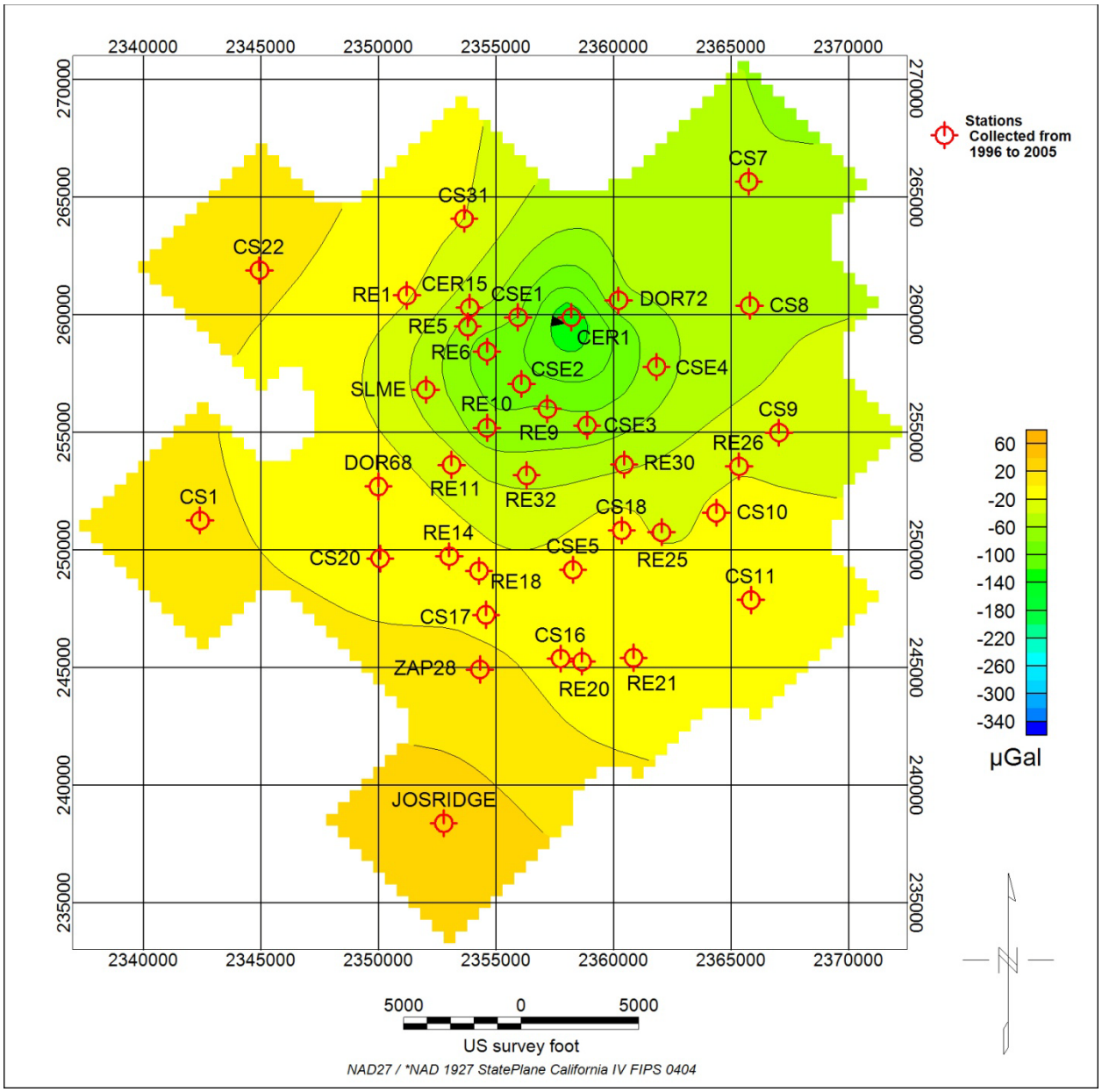

Figure 3.18: Gravity changes from spring 1996 until spring 2000. Station CER1 shows the strongest gravity change, -138µGal. JOSRIDGE shows the largest positive change of 23µGal.

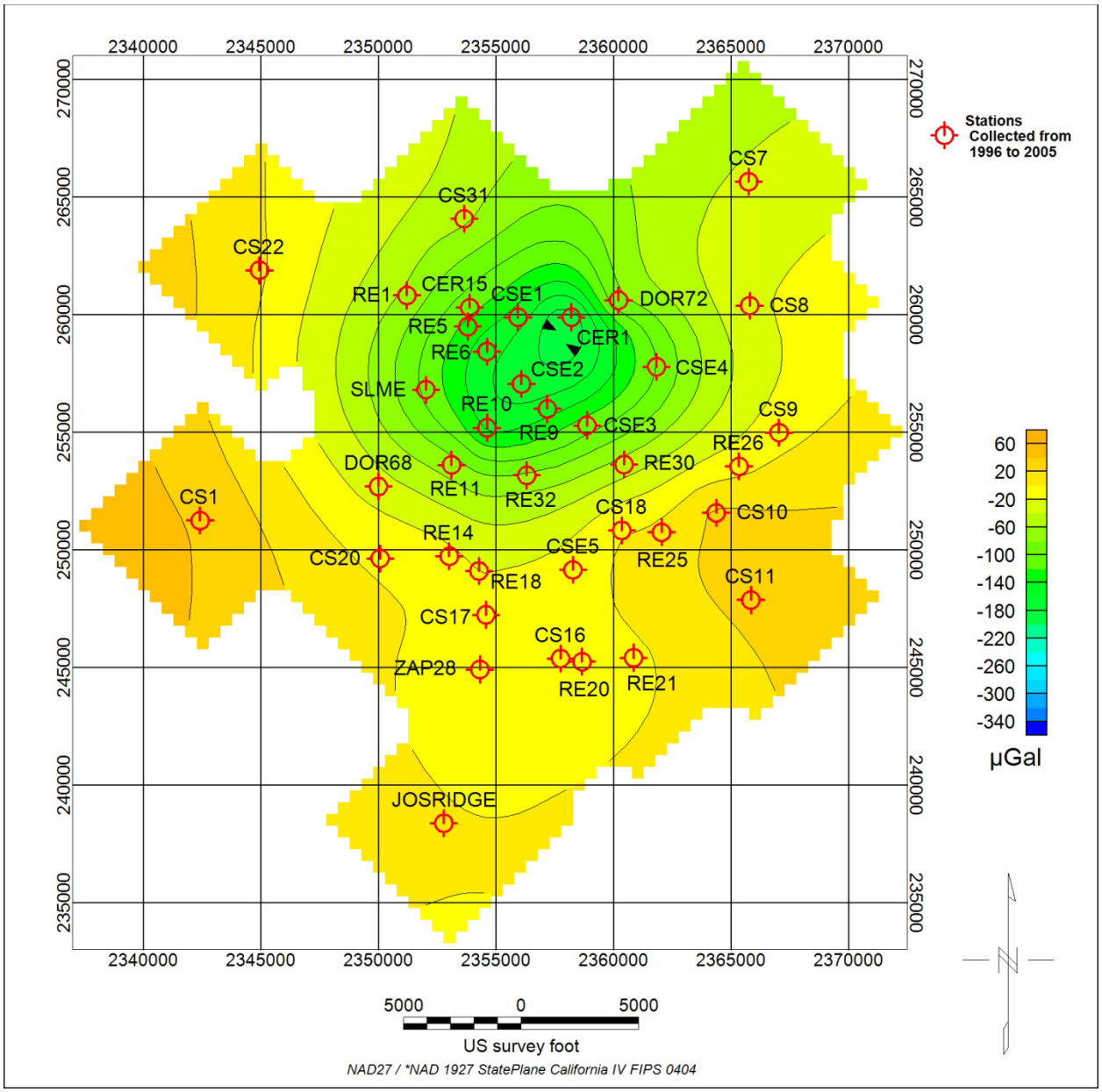

Figure 3.19: Gravity changes from spring 1996 until spring 2003. Station CER1 shows the strongest gravity change, -196µGal. CS1 shows the largest positive change of 37µGal.

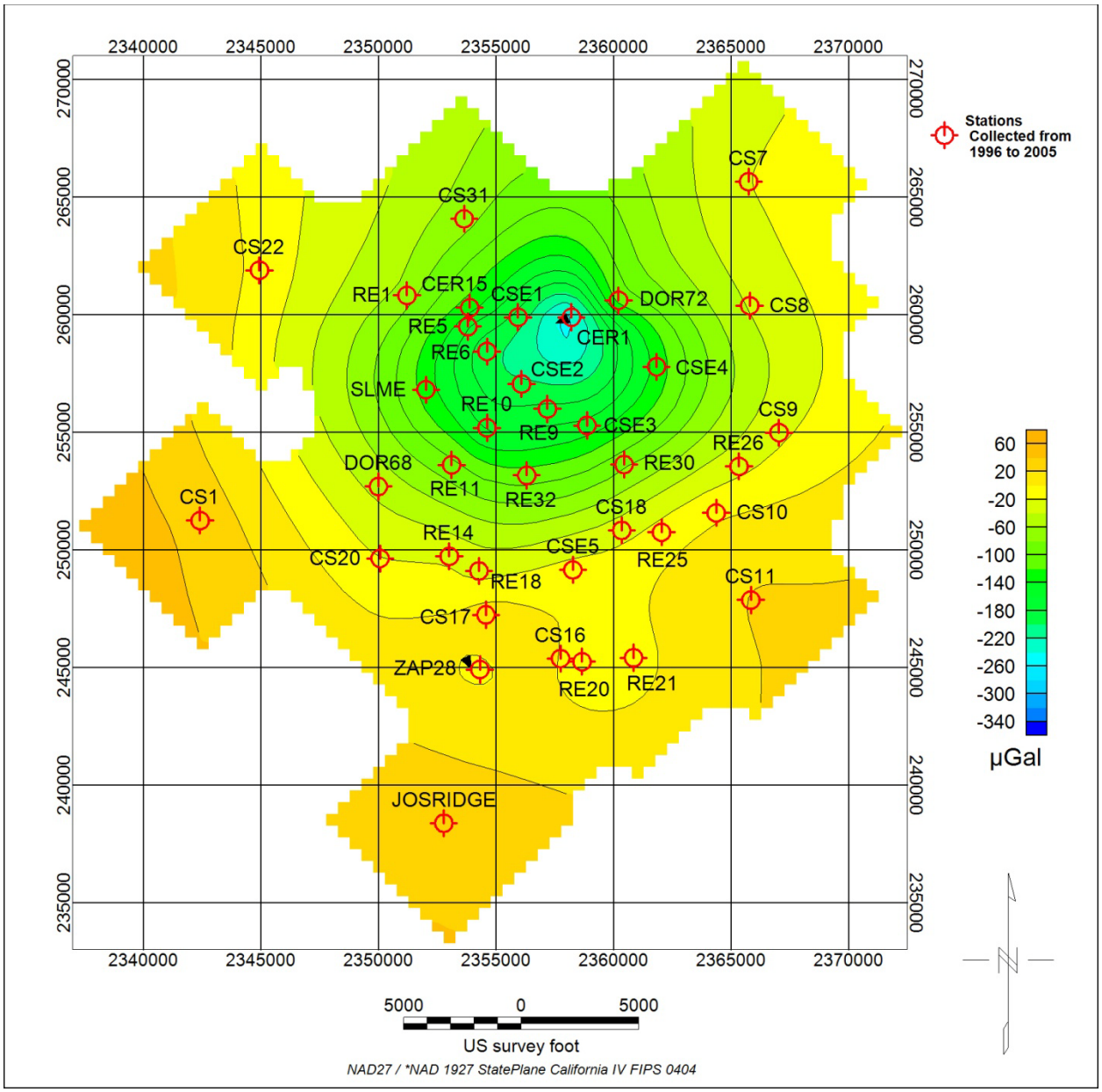

Figure 3.20: Gravity changes from spring 1996 until spring 2005. Station CER1 shows the strongest gravity change, -249µGal. CS1 shows the largest positive change of 33µGal.

Next, I examined the signal from two stations outside of the field, Stations CS1 and CS22. These stations should be outside the area of influence of the changes in reservoir as they are both located at distances greater than B-14 from the field, and therefore their time lapse gravity signal should be zero. Figure 3.21 shows the time varying gravity recorded at these stations. The changes seen at these stations should not be due to mass changes under the geothermal field. The mean of the signal seen at station CS1 is -31.6µGal, and -18.9µGal at station CS22. The standard deviations are 16.5µGal at CS1 and

11.85μGal. The change seen in these stations might be the response to ground water changes near these stations that are not being removed by the reference leveling, or that the reference station zero gravity assumption is invalid. It is not possible to move the reference station so these variations must be taken into consideration as errors for all other data points.

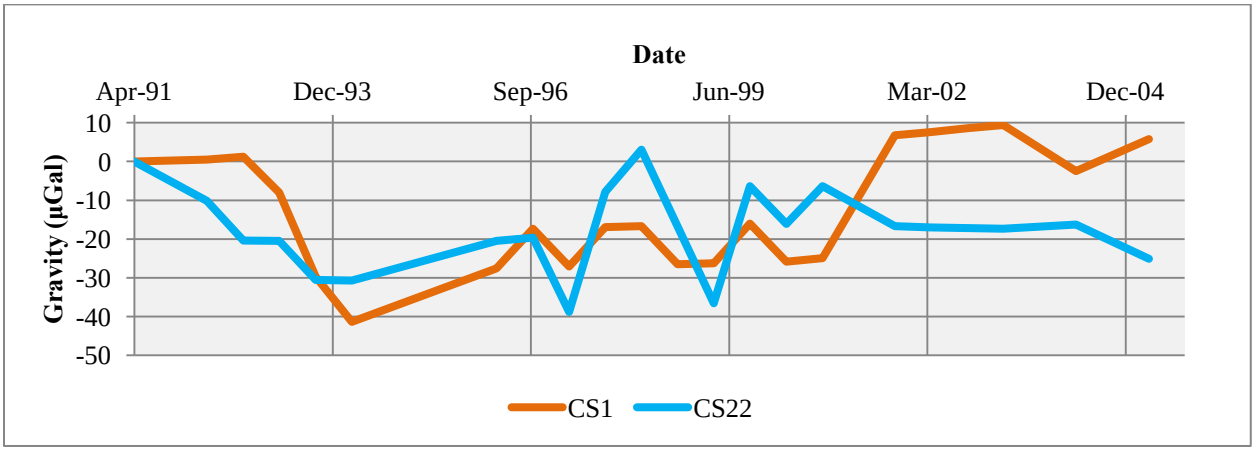

Figure 3.21: Time lapse gravity profiles for stations CS1 and CS22, both located outside the geothermal field give an indication of the noise levels of the Coso Geothermal data set.

Lastly, to estimate the effect surface changes would have on the data forward modeling was performed. The first structure modeled represents a fluid pond that can be empty during one data collection and full during another. The modeled pond was 10ft wide and deep and 30ft long. A response of 5.61μGal was calculated at a point 10ft from the edge of the middle of the pond. Next, a mound of dirt of the same dimensions added at the surface was model. A density of 1.2g/cm^3 was used for this structure, and it produced a response at the middle of the mound, 10ft away of -6.73μGal. The surface construction at the field was estimate to contribute approximately +/-7μGal of error to the stations.

With the collective sources of noise and data error, an estimated standard deviation of the total data error in the final time lapse gravity data is 17.04μGal.

3.5 Summary

The time lapse gravity data were presented in this chapter, starting with the three data points collected continuously from 1987 to 2005, continuing with the data from 1991 to 2005 and ending with the data collected from 1996 to 2005. These data show a large negative anomaly in one section of the field near stations CSE2 and CER1. The maximum magnitude change in gravity observed was at CSE2

from 1991 to 2005 of -350μGal. The error levels of the data were discussed resulting in a final estimated standard deviation of 17μGal.

CHAPTER 4:
INVERSION AND INTERPRETATION

In order to gather further information from the time lapse data set, I applied inversion as I will be describing in this chapter.

The inversion algorithm chosen for the Coso time lapse gravity data was surface inversion, a nonlinear inversion where one fixed surface and a density contrast are entered. The program inverts for the height of the density contrast column for each model cell, using a smoothest model approach.

For the time lapse gravity anomalies observed at the Coso Geothermal field it is expected that a negative density contrast volume is being created at the top of the reservoir. It is the height of this volume that is being inverted for. The depth to the top of the reservoir at the first time used to generate the time lapse gravity data serves as the top of the anomaly. The bottom of the anomaly, the result of the inversion, is the top of the reservoir at the second time.

An estimate of 5-10% "bulk porosity" was supplied by Navy personnel (Lazaro, 2013). Assuming a near constant porosity during the time frame analyzed, and that the pores were 100% saturated at time one, and 0% saturated at time two, the density contrast within the anomaly is equivalent to the negative porosity. The density contrast is the controlling factor in the inversion. A smaller density contrast will result in a larger column of density change, while a larger contrast will results in a smaller column. Since the exact value of density is unknown, density contrast estimates of 5%, 10% and 20% were used.

Due to the sparseness of the data from 1987, it was not used during inversion.

4.1 1991 until 2005 Data Inversion

Surface inversion was applied to the time lapse gravity data that were collected continuously at the sixteen stations between 1991 and 2005.

To estimate the initial top surface of the reservoir, a memorandum was obtained from the Coso Operating Company describing free water levels at the field. The free water level is generated using well pressure data and it is the surface at which the water would be if it were unconfined. It is an imaginary surface; however it provides insight into the true water levels in the reservoir. Prior to geothermal power production the free water level in the reservoir was estimated at 3500ft above sea level. Between the

years of 1989 and 1991 when the geothermal plants began, operation the free water level dropped to 3000ft near Navy I, 2500ft near Navy II and 2000ft near BLM. Some areas of the field predicted an increase in free water level to 4500ft due to injection. This 4500ft imaginary free water level is above the ground surface in many areas (Spielman, 2002). Due to the uncertainly of the relationship between the free water level and the true water level, an estimate of 2500ft was used as the starting water level in 1991 for inversion. The water level may not have been flat in 1991 however without additional prior information on the water levels it is a reasonable assumption for a starting surface. Beginning with this initial water surface, the inversion then seeks a final water level for each time period based on the change gravity field.

4.1.1 Density Contrast of -0.05g/cm^3

The results of the surface inversion performed on the difference in gravity between that collected in spring of 2005 and spring 1991, using a density contrast of -0.05g/cm^3 and a starting top surface of 2500ft above sea level is shown in Figure 4.1. A three dimensional image is shown in Figure 4.3, with a vertical exaggeration of 5 for visualization. The maximum thickness of the inverted density anomaly is 998ft in the area surrounding station CSE2. The total recovered mass change from the inversion is -1.39x10^{11} kg. The predicted data are a good match with to the observed data (Figure 4.4). The stations with the greatest difference between the two data sets are CSE2 and CER1, which are the areas with the largest change in gravity.

The inverted surfaces for the smaller time intervals between 1991 and 2005 are show in Figure 4.9, along the profile in Figure 4.1, and gives insight into the evolution of the changing water levels of the field over time.

In order to demonstrate the influence of the initial top surface of the reservoir I ran another surface inversion using a starting top of 3000ft above sea level, shown in Figure 4.2. The maximum thickness of the density anomaly recovered was 885ft and the total mass change was -1.11x10^{11}kg. The thickness is less than that of the results produced by the deeper top surface as is the magnitude of the total change in mass. The predicted data are compared to the observed data in Figure 4.8, and they likewise compare well.

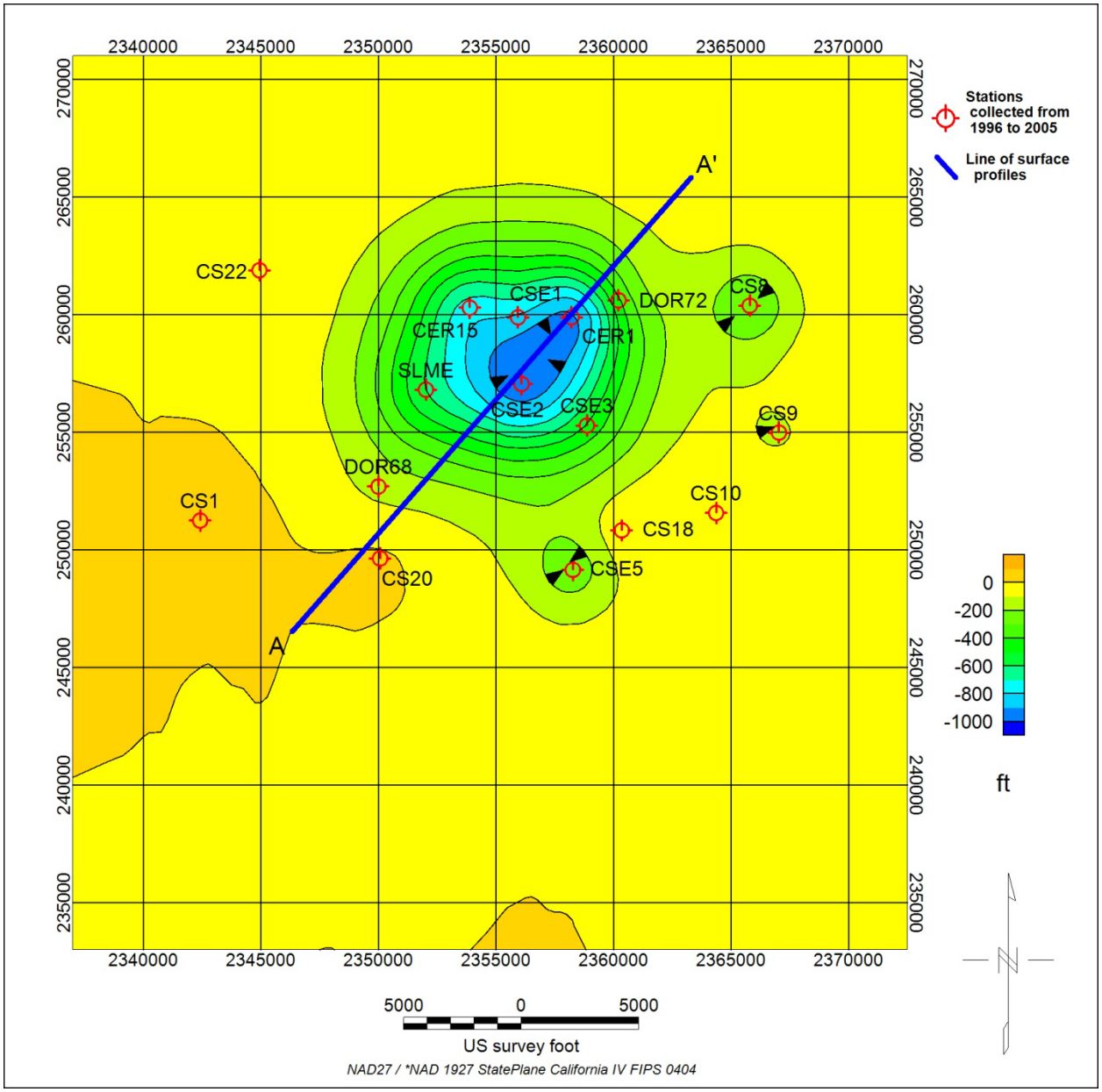

Figure 4.1: Difference between starting top surface and bottom surface produced by the surface inversion using gravity data between spring 1991 and spring 2005, an assumed density contrast of -0.05g/cm^3 and a top surface of 2500ft above sea level. The maximum thickness of the density anomaly is 999ft and the total mass change -1.39x10^{11}kg. Shown is the A to A' profile used to display the surfaces in Figure 4.10 and subsequent figures.

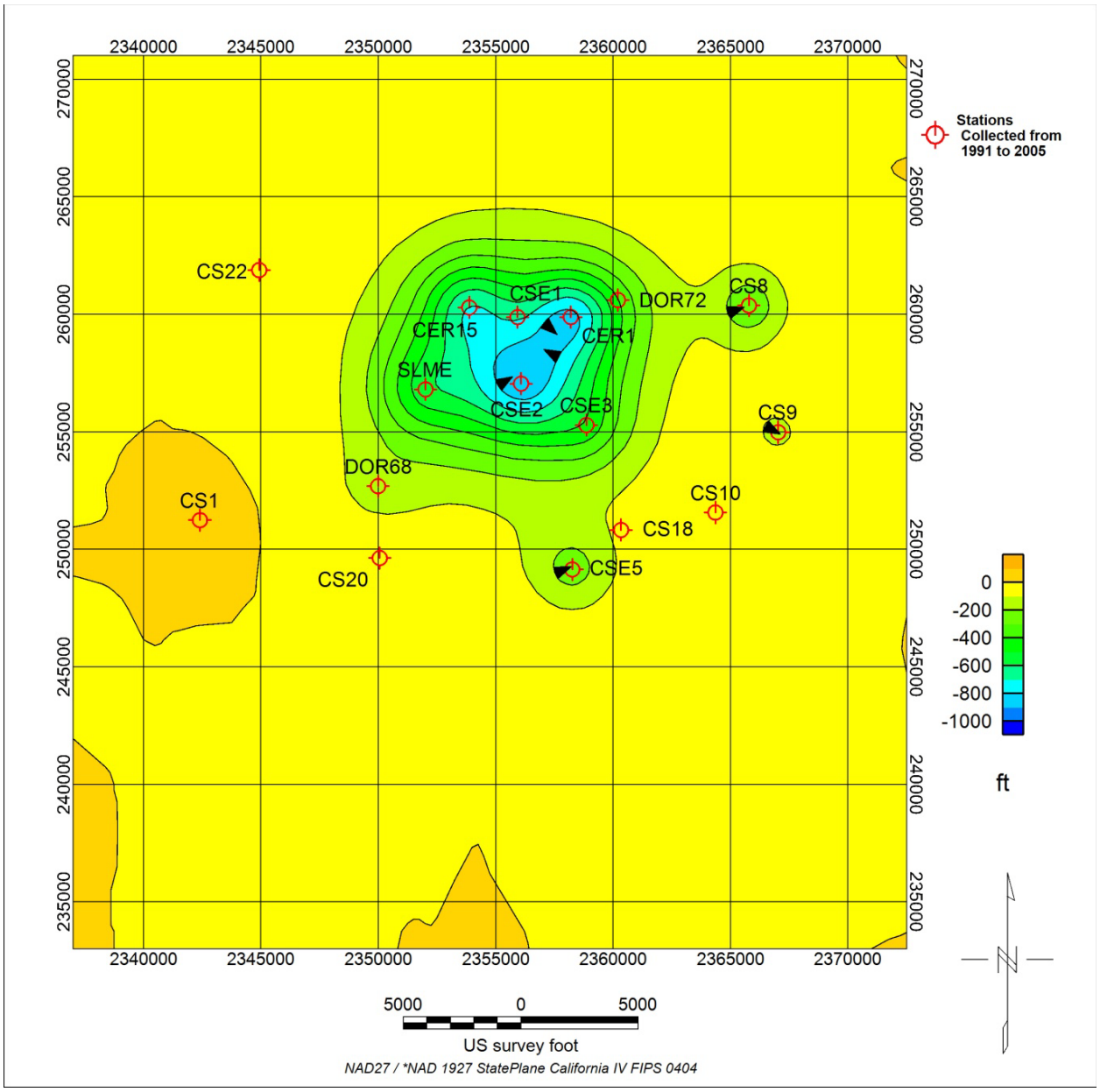

Figure 4.2: Difference between starting top surface and bottom surface produced by the surface inversion using gravity data between spring 1991 and spring 2005, an assumed density contrast of -0.05g/cm^3 and a top surface of 3000ft above sea level. The maximum thickness of the density anomaly is 885ft and the total mass change -1.11x10^{11}kg.

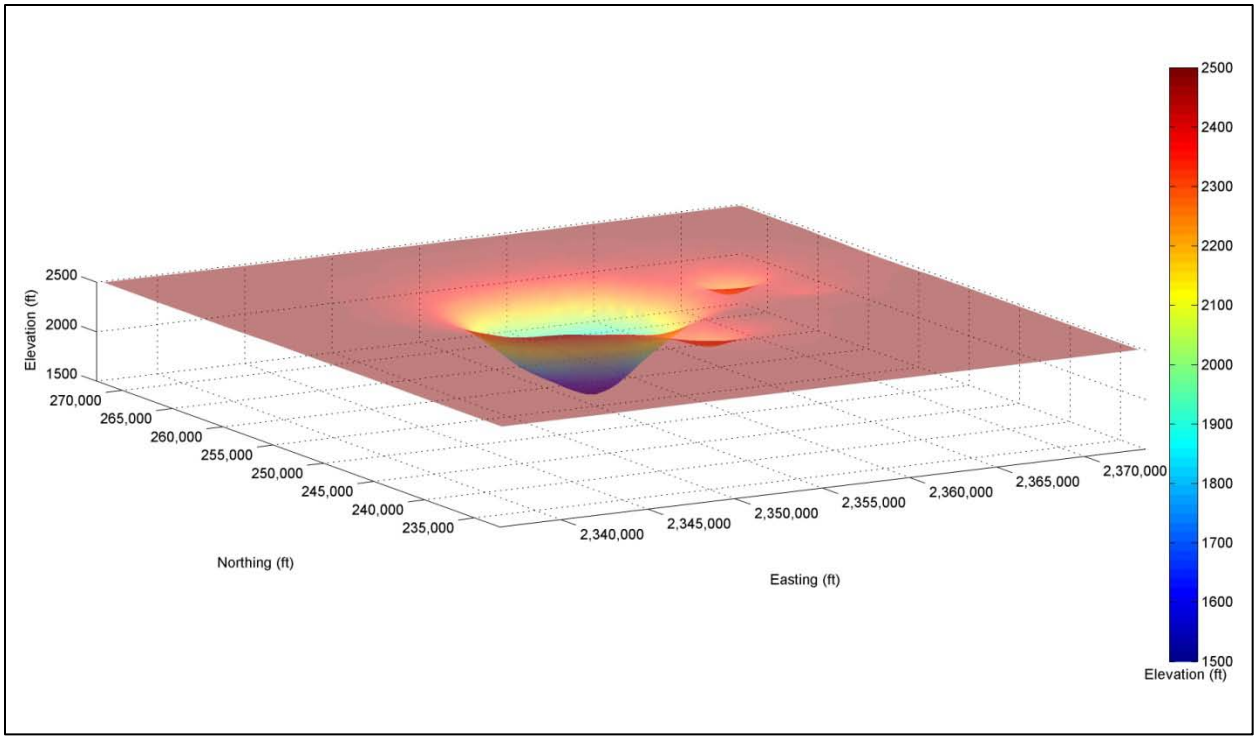

Figure 4.3: Inverted density contrast anomaly produced using gravity data from 1991 to 2005 and a density contrast of -0.05g/cm^3 shown in three dimensions with height above sea level as Z axis. The vertical scale has been increased by a factor of 5.

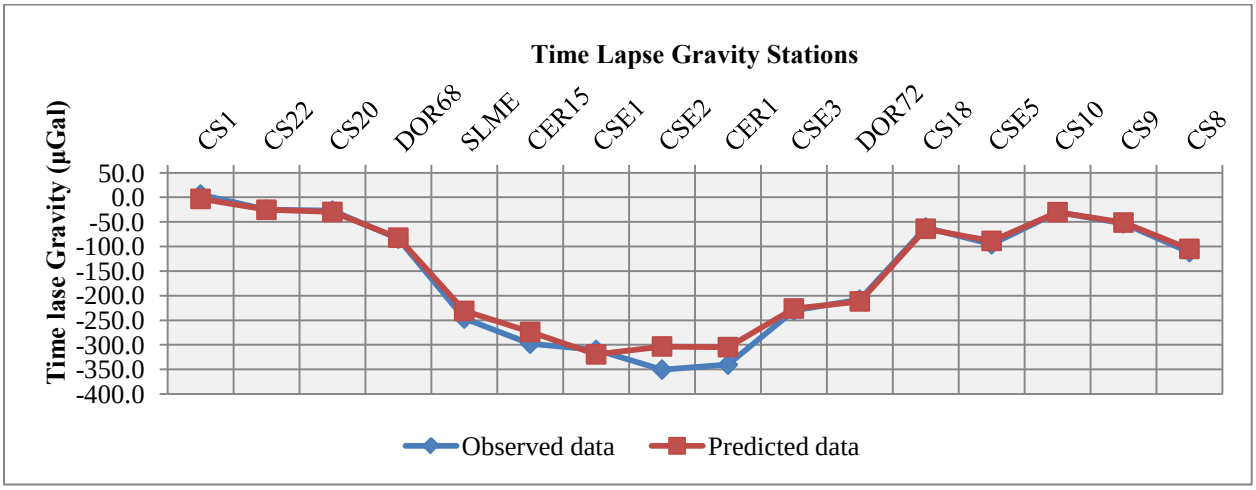

Figure 4.4: The predicted data produced by the surface inversion algorithm using the time lapse gravity data between 1991 and 2005, a density contrast of -0.05g/cm3, and top surface of 2500ft above sea level.

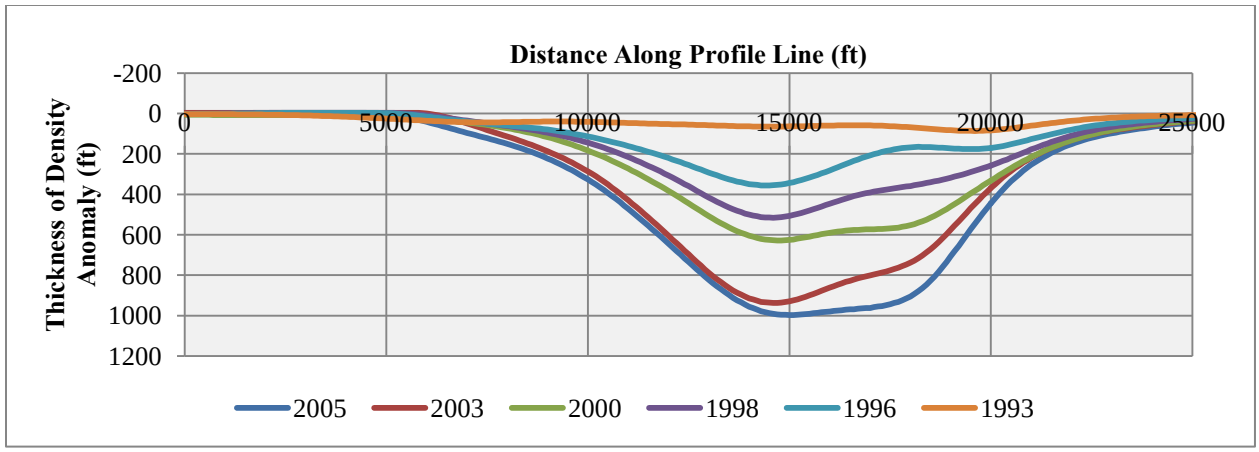

Figure 4.5: Thickness of density anomaly recovered using the surface inversion algorithm, the time lapse gravity data collected between 1991 and 2005, a top surface of 2500ft above sea level, and a density contrast value of -0.05g/cm^3, with smaller time increments shown.

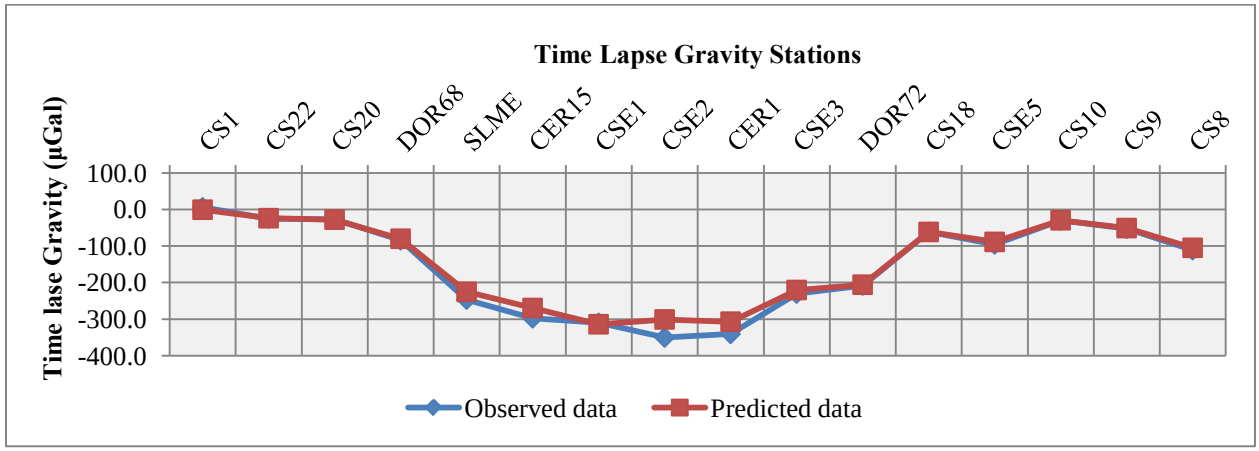

Figure 4.6: The predicted data produced by the surface inversion algorithm using the time lapse gravity data between 1991 and 2005, a density contrast of -0.05g/cm3, and top surface of 3000ft above sea level.

4.1.1 Density Contrast of -0.10g/cm3

The data predicted data by the surface inversion using a density contrast of -0.10g/cm^3 are are compared with the observed data in Figure 4.7. The contour map of the recovered model shown in Figure 4.9. A three dimensional representation is shown in Figure 4.8. The maximum thickness of the density anomaly recovered was 480ft, approximately half of the thickness recovered using a density contrast of -0.05g/cm^3, again with the thickest anomaly under station CSE2. The total mass change produced was 1.3x10^{11}kg, 9x10^{9}kg less than that produced using the lower density contrast. Similar to what was seen with the lower density; the stations with the lowest gravity signal have the poorest data fit.

Figure 4.10 shows the bottom inverted surfaces of the incremental time periods along the profile show in Figure 4.1, using a density contrast of -0.10g/cm3. The shapes of the bottom surfaces are very similar to what was shown in Figure 4.10 however the thicknesses are approximately one half.

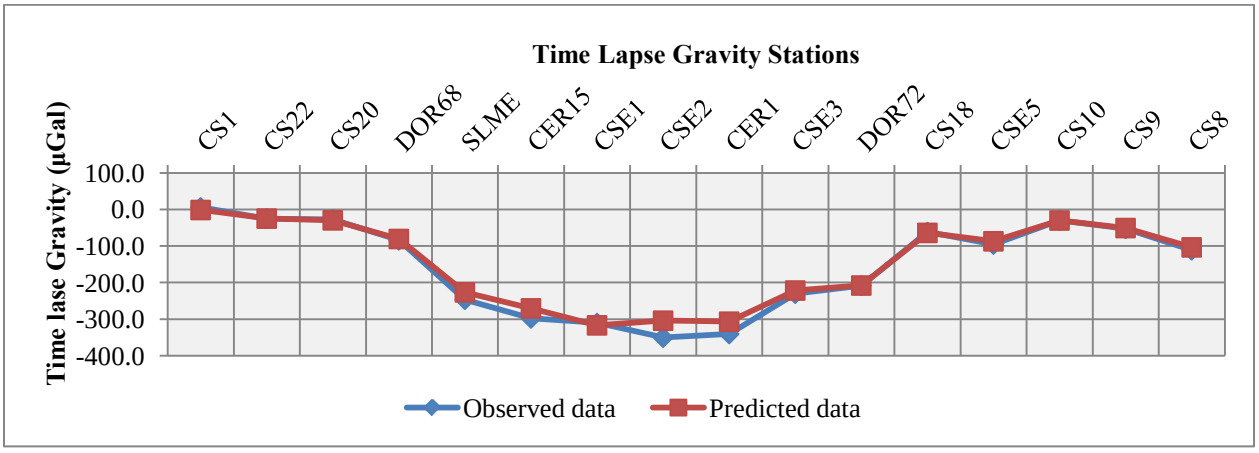

Figure 4.7: The predicted data produced by the surface inversion algorithm using the time lapse gravity data between 1991 and 2005, a density contrast of -0.10g/cm3, and top surface of 2500ft above sea level.

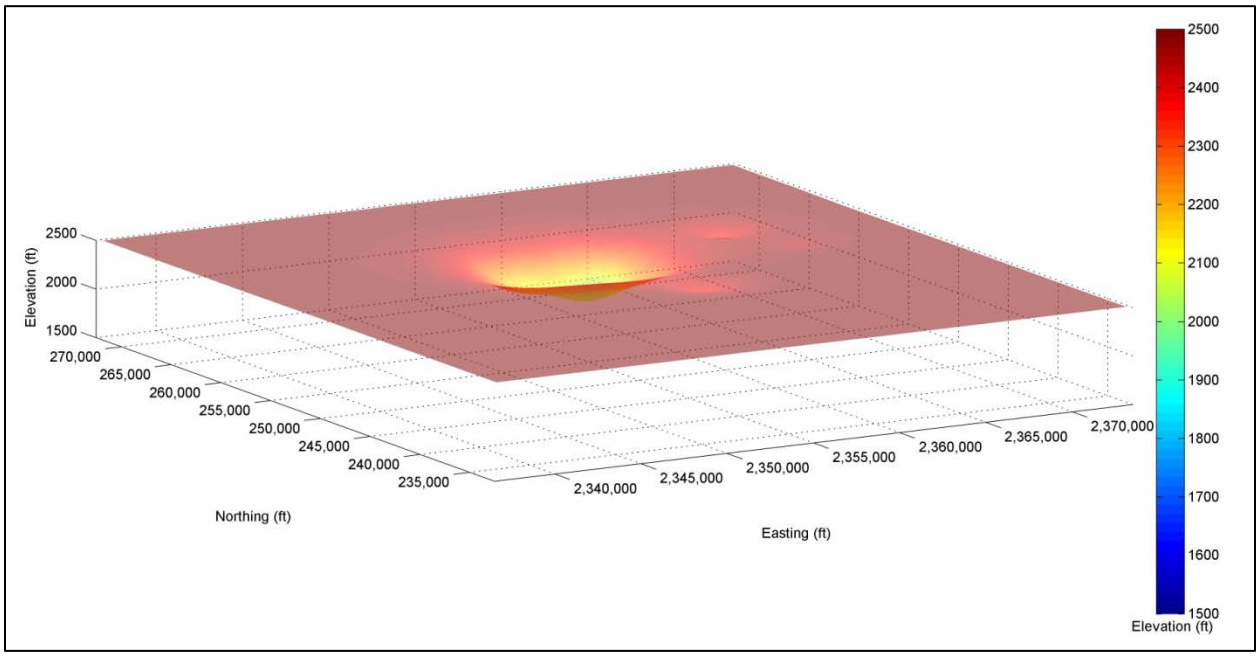

Figure 4.8: Inverted density contrast anomaly produced using gravity data from 1991 to 2005 and a density contrast of -0.10g/cm^3 shown in three dimensions with height above sea level as Z axis. The vertical scale has been increased by a factor of 5.

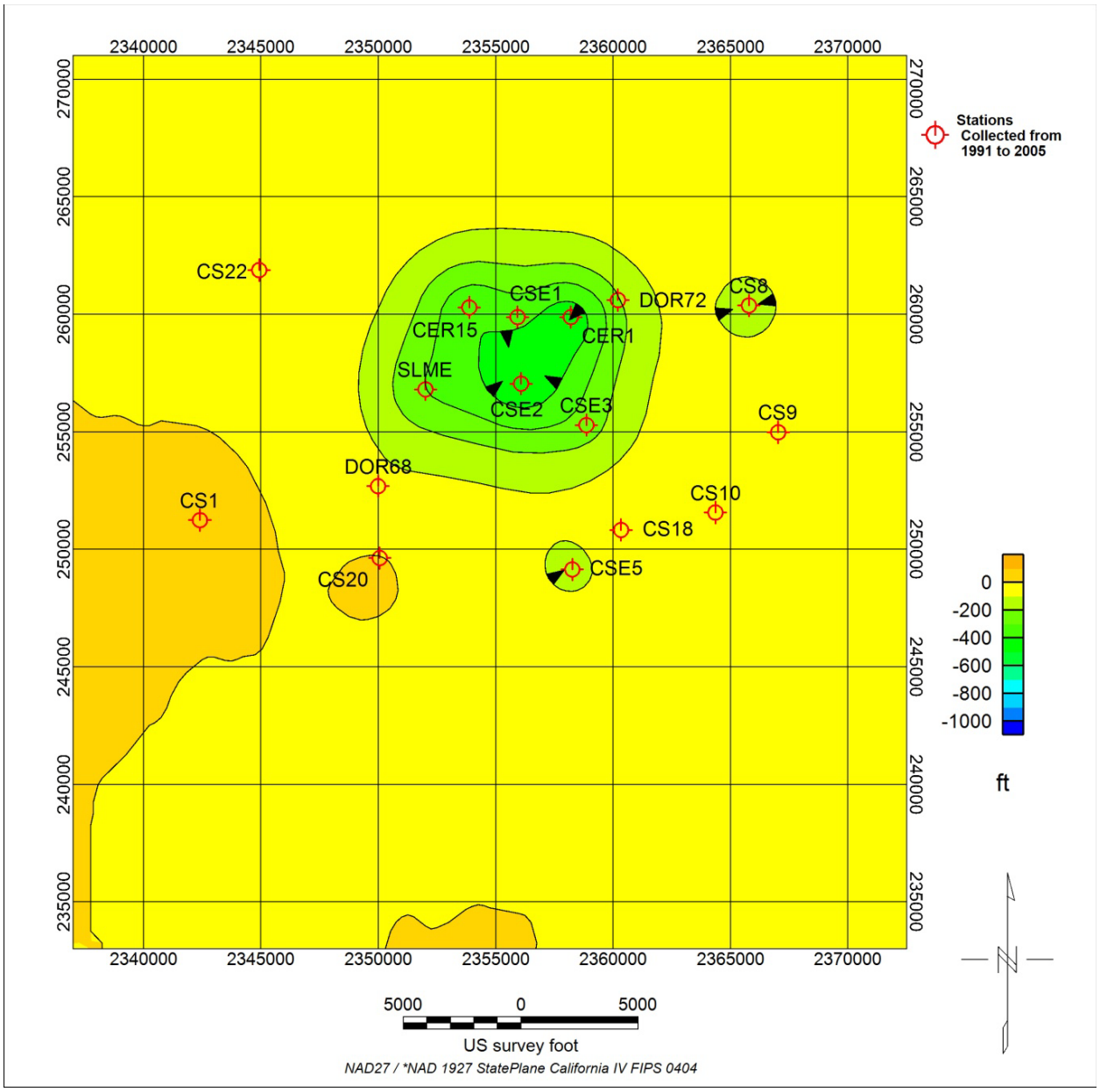

Figure 4.9: Difference between starting top surface and bottom surface produced by the surface inversion using gravity data between spring 1991 and spring 2005, an assumed density contrast of -0.10g/cm^3 and a top surface of 2500ft above sea level. The maximum thickness of the density anomaly is 480ft and the total mass change -1.30x10^{11}kg.

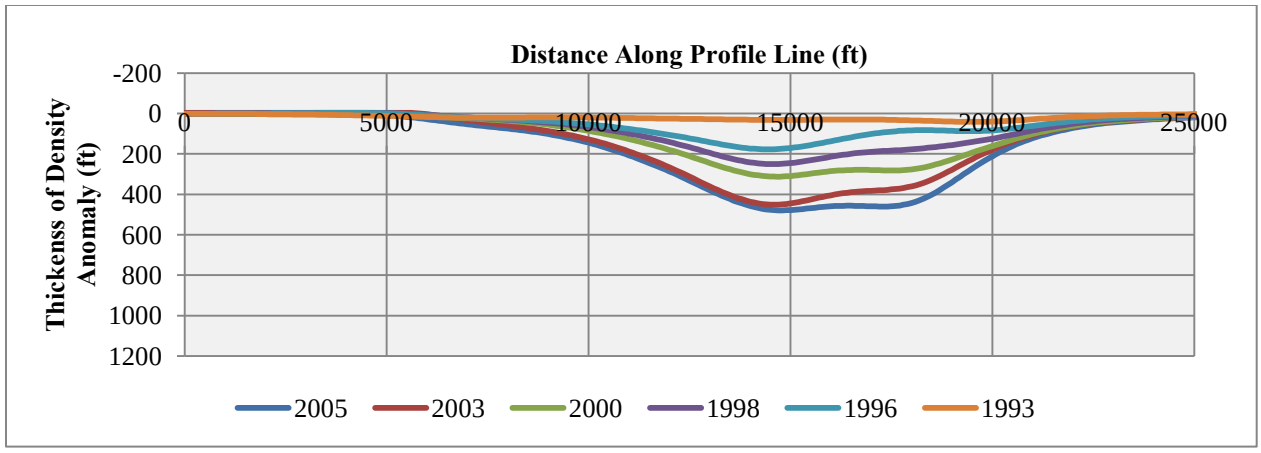

Figure 4.10: Thickness of density anomaly recovered using the surface inversion algorithm, the time lapse gravity data collected between 1991 and 2005, a top surface of 2500ft above sea level, and a density contrast value of -0.10g/cm^3, with smaller time increments shown.

4.1.1 Density Contrast of -0.20g/cm^3

Figure 4.12 displays the surface inversion results using a density contrast of -0.20g/cm^3 and a starting top surface of 2500ft above sea level, Figure 4.13 shows a three dimensional view, and Figure 4.11, the difference between the observed and predicted data. The maximum thickness of the density anomaly inverted was 236ft, approximately a fourth that of the thickness recovered using a density of -0.5g/cm3 as expected, with a total mass change of -1.26x10^{11}kg, . The mass change is less than it had been using the smaller density contrast values. Figure 4.14 shows the incremental surface inversion results.

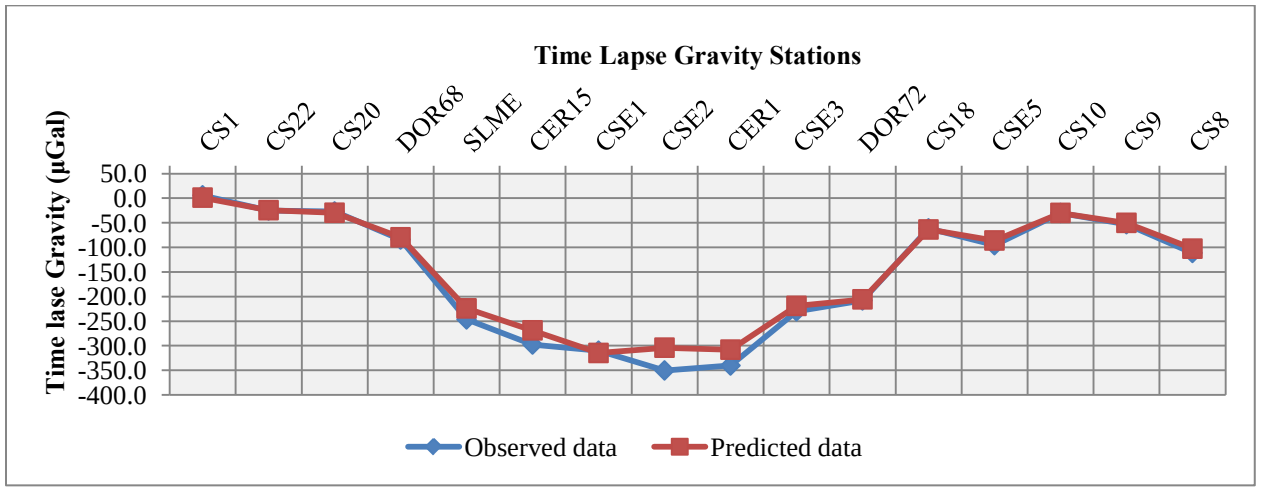

Figure 4.11: The predicted data produced by the surface inversion algorithm using the time lapse gravity data between 1991 and 2005, a density contrast of -0.20g/cm3, and top surface of 2500ft above sea level.

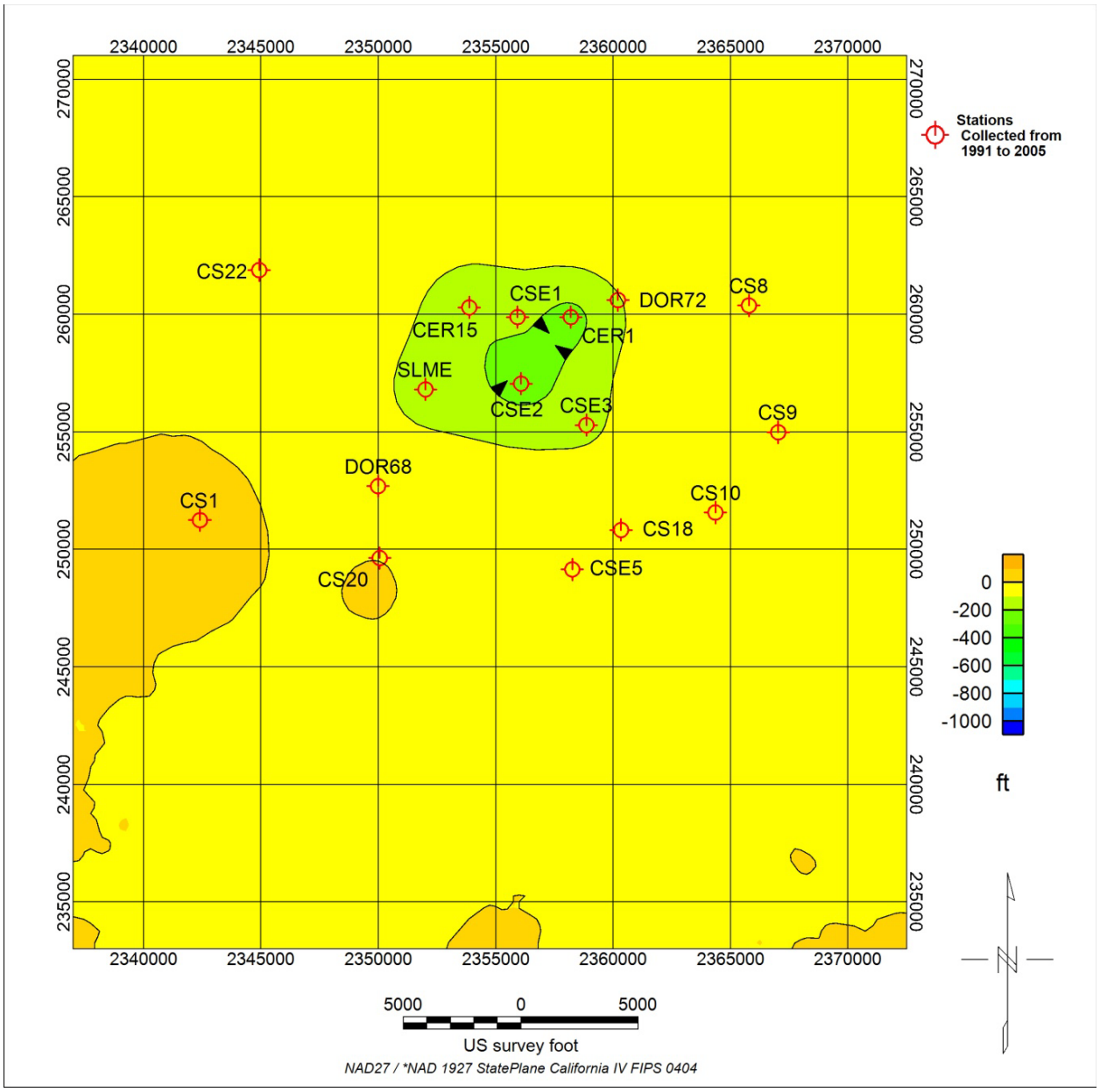

Figure 4.12: Difference between starting top surface and bottom surface produced by the surface inversion using gravity data between spring 1991 and spring 2005, an assumed density contrast of -0.20g/cm^3 and a top surface of 2500ft above sea level. The maximum thickness of the density anomaly is 236ft and the total mass change -1.26x10^{11}kg.

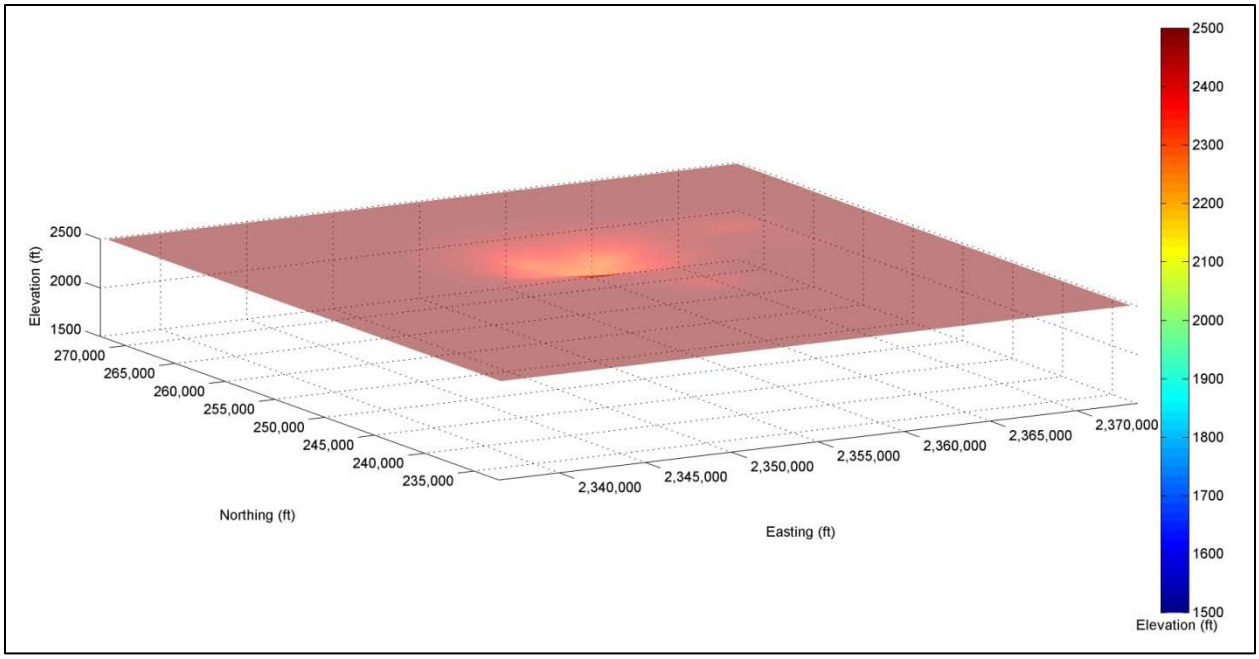

Figure 4.13: Inverted density contrast anomaly produced using gravity data from 1991 to 2005 and a density contrast of -0.20g/cm^3 shown in three dimensions with height above sea level as Z axis. The vertical scale has been increased by a factor of 5.

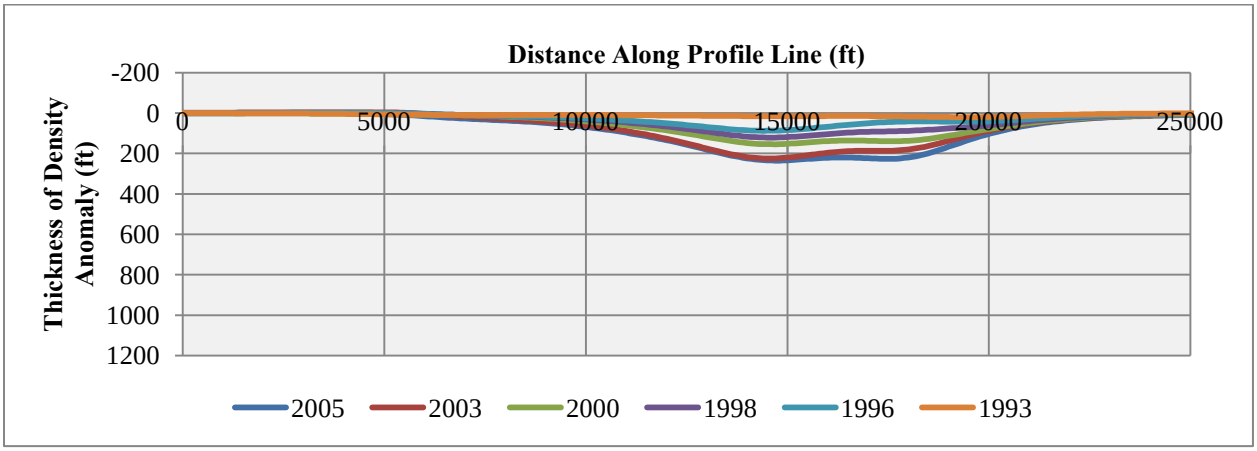

Figure 4.14: Thickness of density anomaly recovered using the surface inversion algorithm, the time lapse gravity data collected between 1991 and 2005, a top surface of 2500ft above sea level, and a density contrast value of -0.20g/cm^3, with smaller time increments shown.

4.1.2 Summary of Results from 1991 until 2005

The final results of the surface inversions performed on the gravity data collected from 1991 until 2005 are show in Table 4.1. Figure 4.15 displays the results of the surface inversions of the time lapse gravity data from 1991 until 2005 using all three density values and a starting surface of 2500ft above sea

level, shown along the profile seen in Figure 4.1. The shapes of the bottom surface are similar. The mass changes for each time increment and density contrast inverted are shown in Figure 4.16. The mass changes are slightly lower for the larger amplitude density estimates corresponding to the more shallow depth as the deeper surfaces. It can be seen that the period with the most mass change was from 1993 until 1996.

Table 4.1: Results of all surface inversions from 1991 to 2005

Assumed Density Contrast (g/cm^3)	Assumed Top Surface (ft above sea level)	Maximum Thickness of Density Anomaly(ft)	Total Change in Mass (kg)
-0.05	2500	998	-1.39E+11
-0.05	3000	885	-1.11E+11
-0.10	2500	480	-1.30E+11
-0.20	2500	236	-1.26E+11

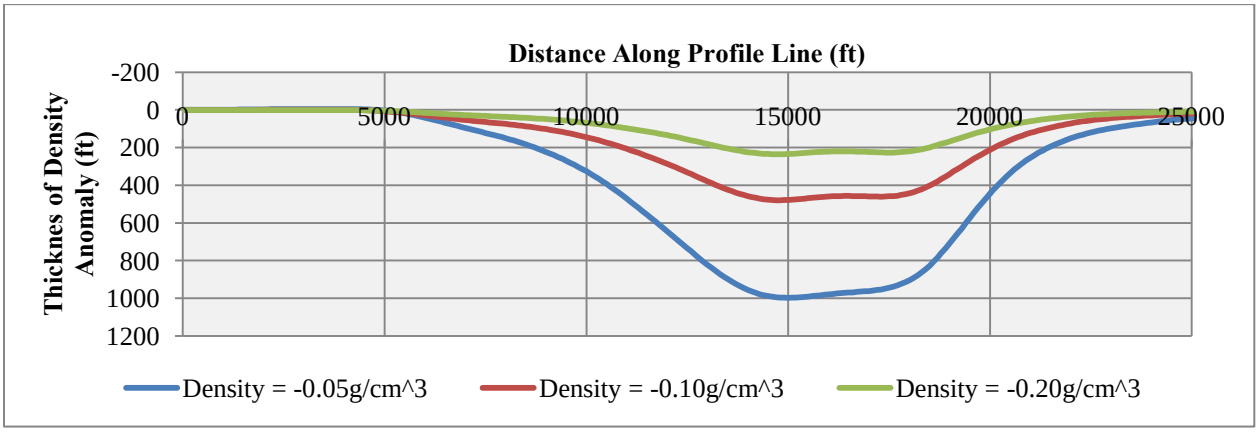

Figure 4.15: Thickness of density anomaly recovered using the surface inversion algorithm, the time lapse gravity data collected between 1991 and 2005, a top surface of 2500ft above sea level, and density contrast values of -0.05g/cm^3, -0.10g/cm^3 and -0.20g/cm^3.

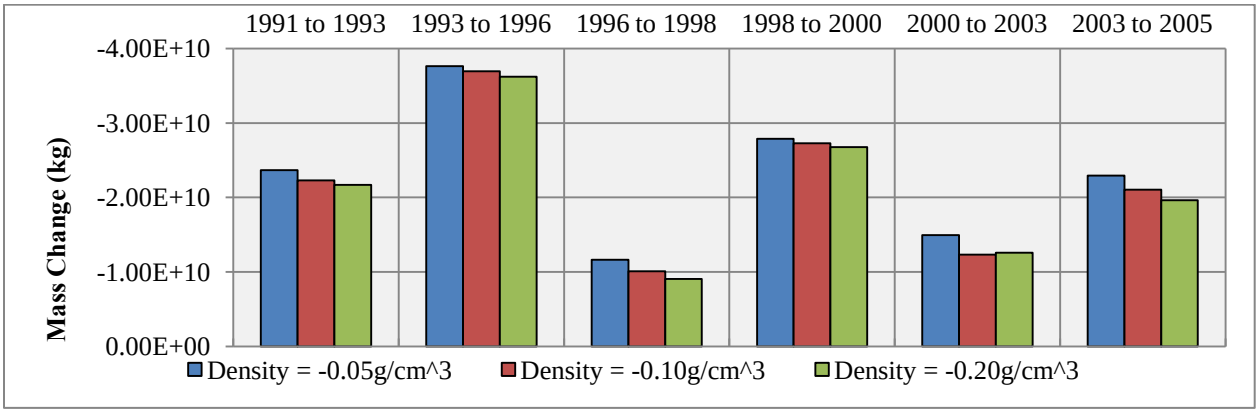

Figure 4.16: Mass change produced by surface inversion for each time period between 1991 and 2005, density values of -0.05g/cm^3, -0.10g/cm^3, and -0.20g/cm^3, starting top surface of 2500ft above sea level.

4.2 1996 until 2005 Results

As described previously twenty-two additional gravity stations were added to the survey in 1996. The time lapse gravity data for these stations combined with the sixteen from 1991 are next inverted surface inversion using the surface obtained by the inversion of the data from 1991 until 1996 as the starting top surface. The discrepancy principle was once again used to determine the proper regularization parameter, with the desired data misfit around 38, the new number of data points.

4.2.1 Density Contrast of -0.05g/cm^3

Figure 4.18 shows the results of the surface gravity inversion using this new larger data set collected from 1996 until 2005. The results of the inversion using the sixteen data stations from 1991 until 1996 were used as the starting top surface for this new inversion. The total thickness and mass were calculated from the original starting surface of 2500ft above sea level. A three dimensional view of the surface is shown in Figure 4.17. The predicted data for the original sixteen data stations are compared to the predicted data in Figure 4.19. The data fit inside the area with the greatest change is the poorest. The newly added data stations are shown in Figure 4.20. Figure 4.23 shows a profile of the inverted surfaces through the various time increments.

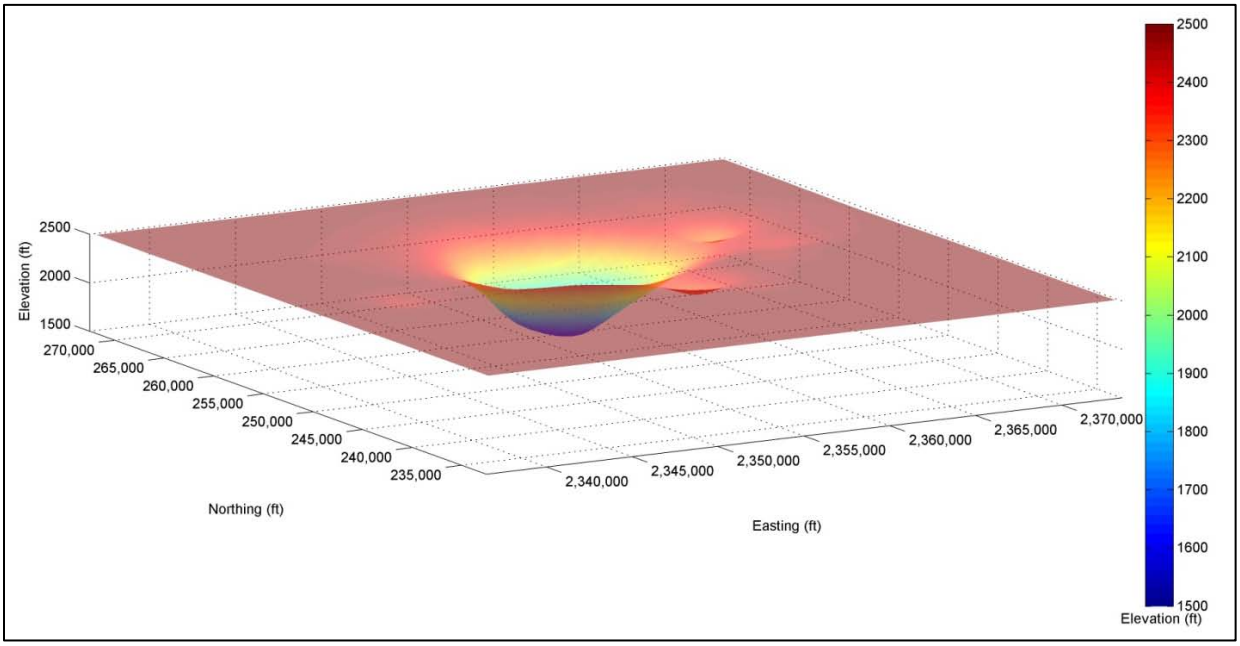

Figure 4.17: Inverted density contrast anomaly produced using gravity data from 1996 to 2005 and a density contrast of -0.05g/cm^3 shown in three dimensions with height above sea level as Z axis. The vertical scale has been increased by a factor of 5.

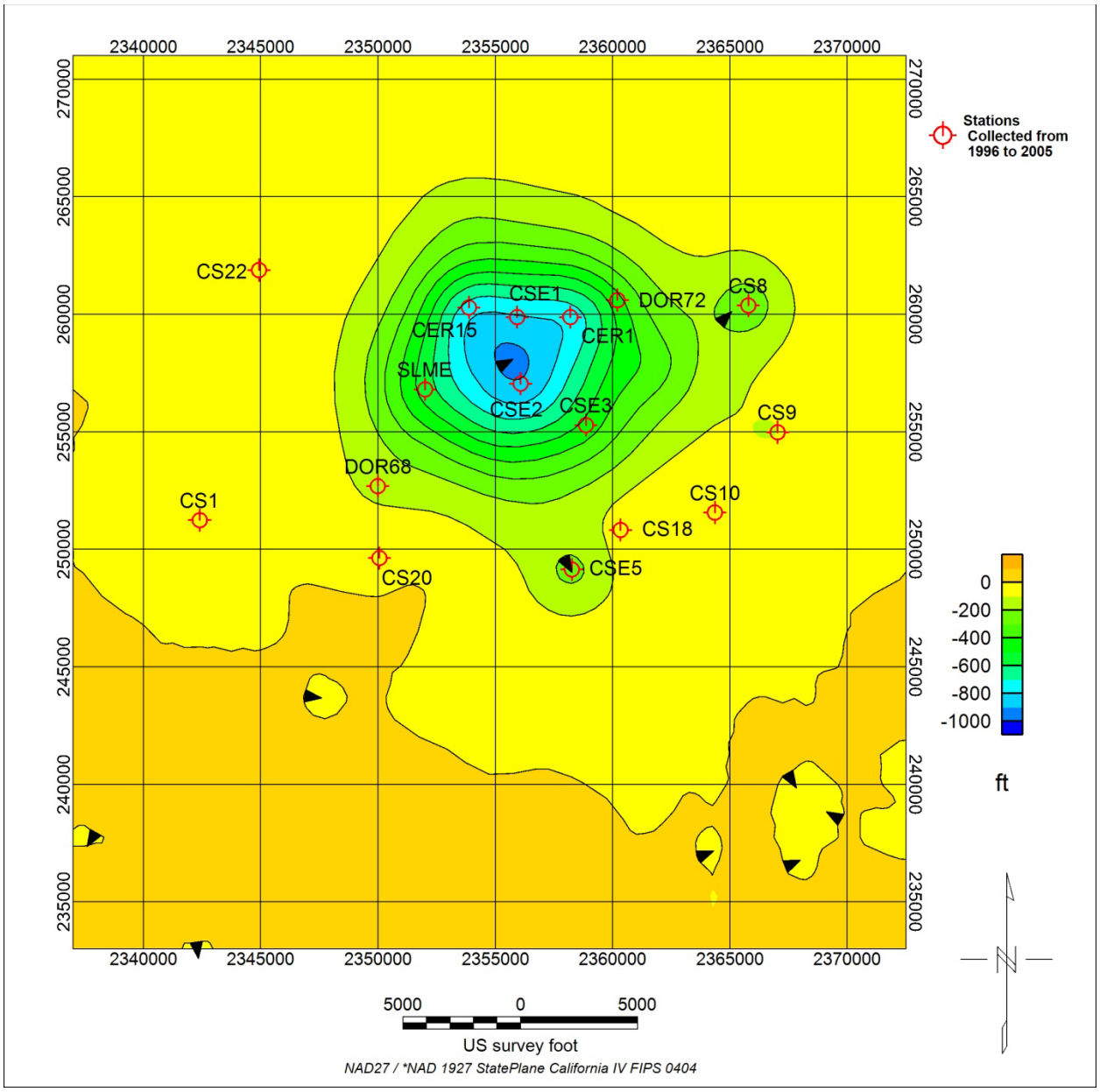

Figure 4.18: Difference between starting top surface and bottom surface produced by the surface inversion using gravity data between spring 1996 and spring 2005, an assumed density contrast of -0.05g/cm^3. The results from the inversion performed using the gravity data from 1991 until 1996 were used as the top surface. The maximum thickness of the total density anomaly from 1991 until 2005 is 918ft and the total mass change -1.30x10^{11}kg.

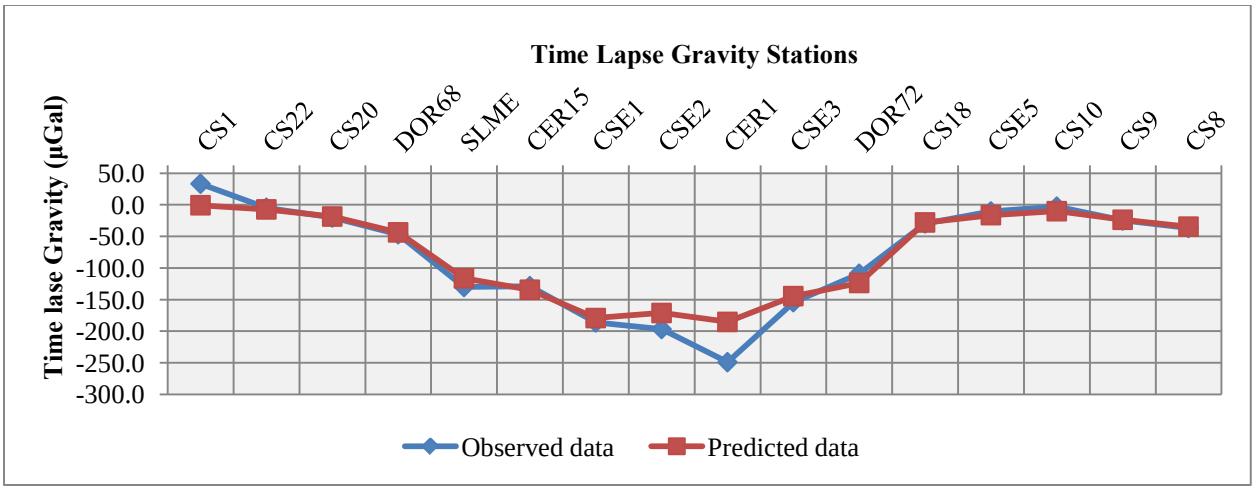

Figure 4.19: The predicted data at the original data points produced by the surface inversion algorithm using the time lapse gravity data between 1996 and 2005, a density contrast of -0.05g/cm3, and the top surface from the 1991 until 1996 inversion results.

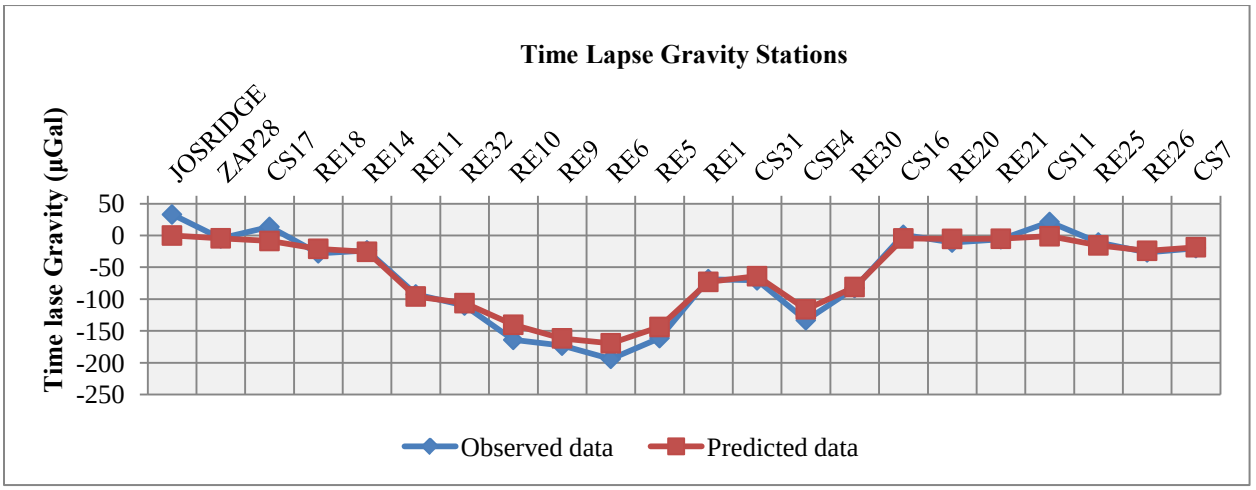

Figure 4.20: The predicted data at the added data points produced by the surface inversion algorithm using the time lapse gravity data between 1996 and 2005, a density contrast of -0.05g/cm3, and the top surface from the 1991 until 1996 inversion results.

4.2.2 Density Contrast of -0.10g/cm3

When an assumed density contrast of -0.10g/cm3 is used the results of the surface inversion algorithm are as shown in Figure 4.21 and Figure 4.22. As previously, the recovered thickness of the density anomaly is approximately half that recovered using the lower density estimate. That thickness was 431ft. The total mass anomaly was -1.23×10^{11}kg. The predicted data are compared with the observed data in Figure 4.24 and Figure 4.25. Once again, the area of poorest fit is within the area of

most change in gravity. The profiles of the inversion results for the smaller time increments are shown in Figure 4.26.

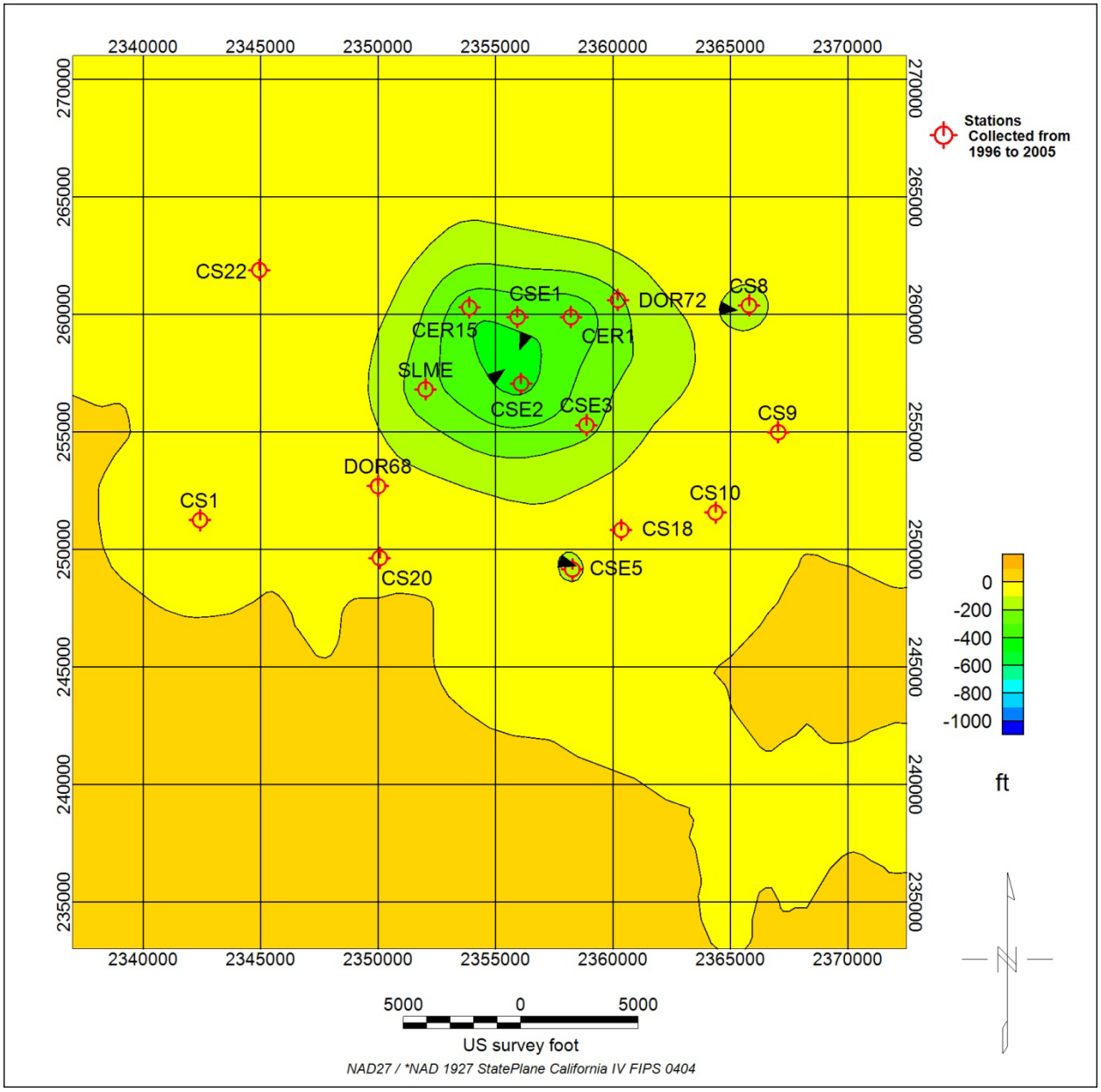

Figure 4.21: Difference between starting top surface and bottom surface produced by the surface inversion using gravity data between spring 1996 and spring 2005, an assumed density contrast of -0.10g/cm^3. The results from the inversion performed using the gravity data from 1991 until 1996 were used as the top surface. The maximum thickness of the total density anomaly from 1991 until 2005 is 431ft and the total mass change -1.23x10^{11}kg.

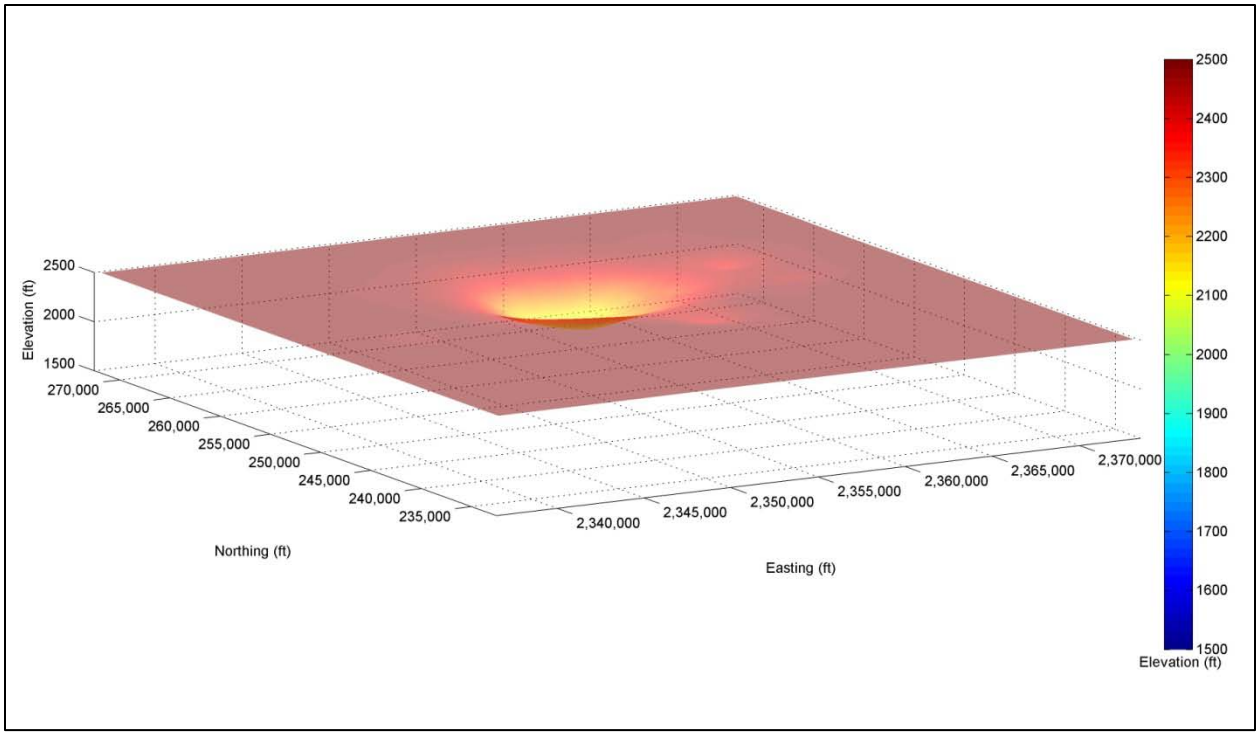

Figure 4.22: Inverted density contrast anomaly produced using gravity data from 1996 to 2005 and a density contrast of -0.10g/cm^3 shown in three dimensions with height above sea level as Z axis. The vertical scale has been increased by a factor of 5.

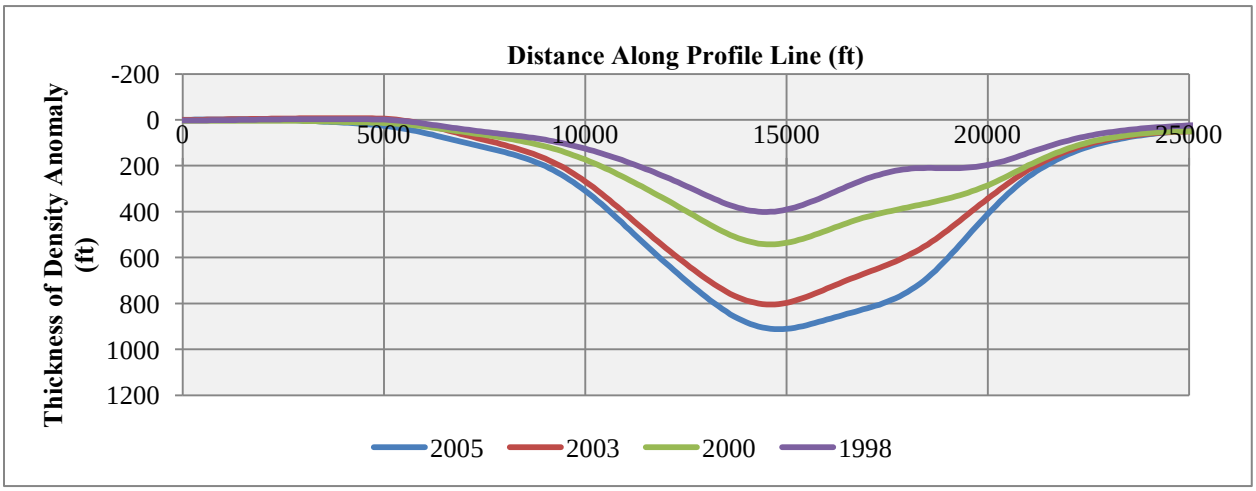

Figure 4.23: Thickness of density anomaly recovered using the surface inversion algorithm, the time lapse gravity data collected between 1996and 2005, a density contrast value of -0.05g/cm^3, and the top surface from the 1991 until 1996 inversion results, with smaller time increments shown.

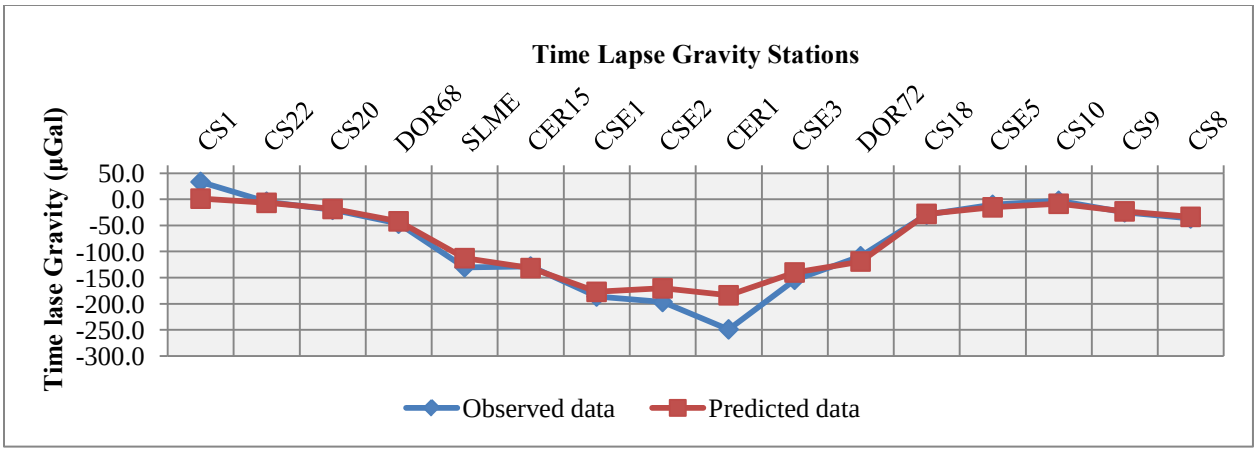

Figure 4.24: The predicted data at the original data points using the time lapse gravity data between 1996 and 2005, a density contrast of -0.10g/cm3, and the top surface from the 1991 until 1996 inversion results.

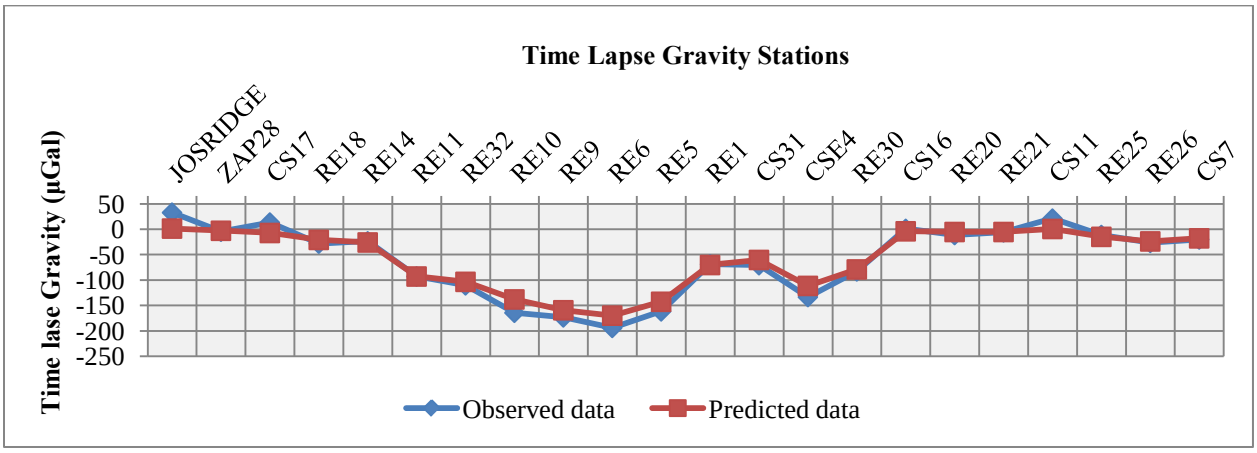

Figure 4.25: The predicted data at the added data points using the time lapse gravity data between 1996 and 2005, a density contrast of -0.10g/cm3, and the top surface from the 1991 until 1996 inversion results.

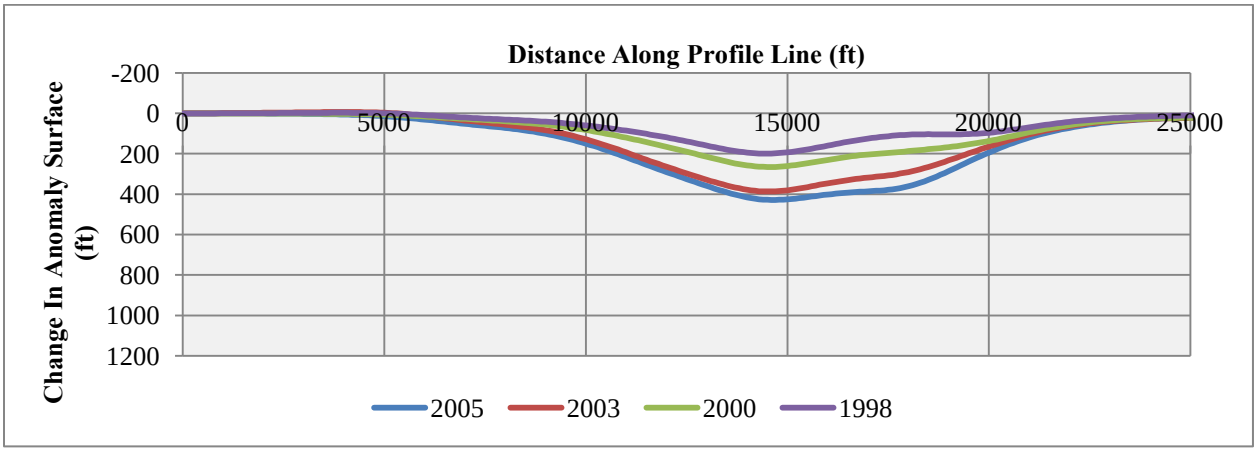

Figure 4.26: Thickness of density anomaly recovered using the time lapse gravity data collected between 1996and 2005, a density contrast value of -0.10g/cm^3, and the top surface from the 1991 until 1996 inversion results, with smaller time increments shown.

4.2.3 Density Contrast of -0.20g/cm^3

The results of the surface inversion using a density contrast estimate of -0.20g/cm^3 are shown in Figure 4.29. The maximum thickness of the density anomaly recovered was 209ft and the total mass change was -1.19x10^{11}kg. A three dimensional view of the surface is shown in Figure 4.30. The predicted data are compared with the observed data in Figure 4.27 and Figure 4.28. The profiles of the surfaces produced by inverting the smaller time increments are shown in Figure 4.31.

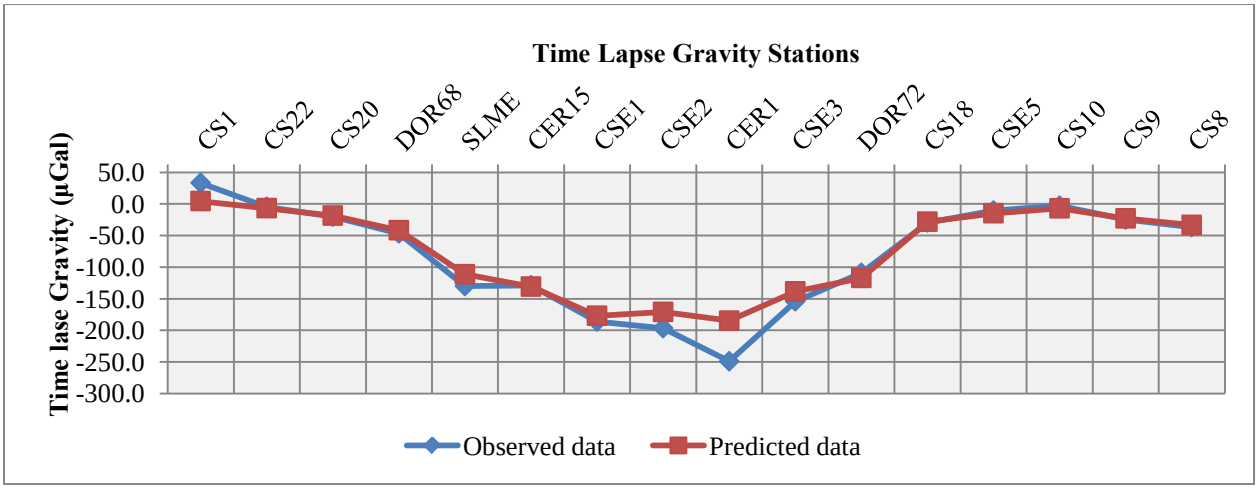

Figure 4.27: The predicted data at the original data points produced by the surface inversion algorithm using the time lapse gravity data between 1996 and 2005, a density contrast of -0.20g/cm3, and the top surface from the 1991 until 1996 inversion results.

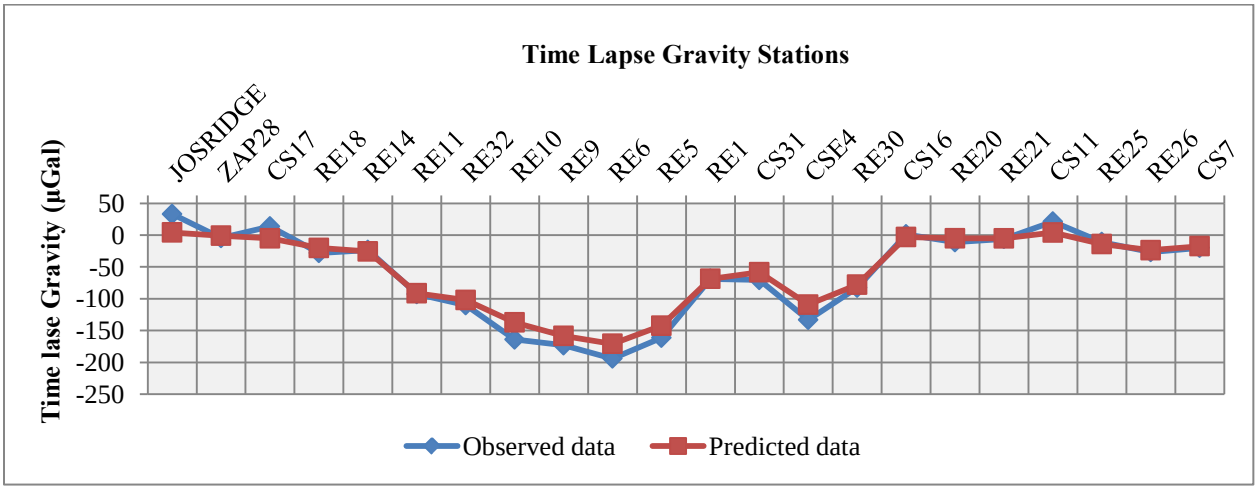

Figure 4.28: The predicted data at the added data points produced by the surface inversion algorithm using the time lapse gravity data between 1996 and 2005, a density contrast of -0.20g/cm3, and the top surface from the 1991 until 1996 inversion results.

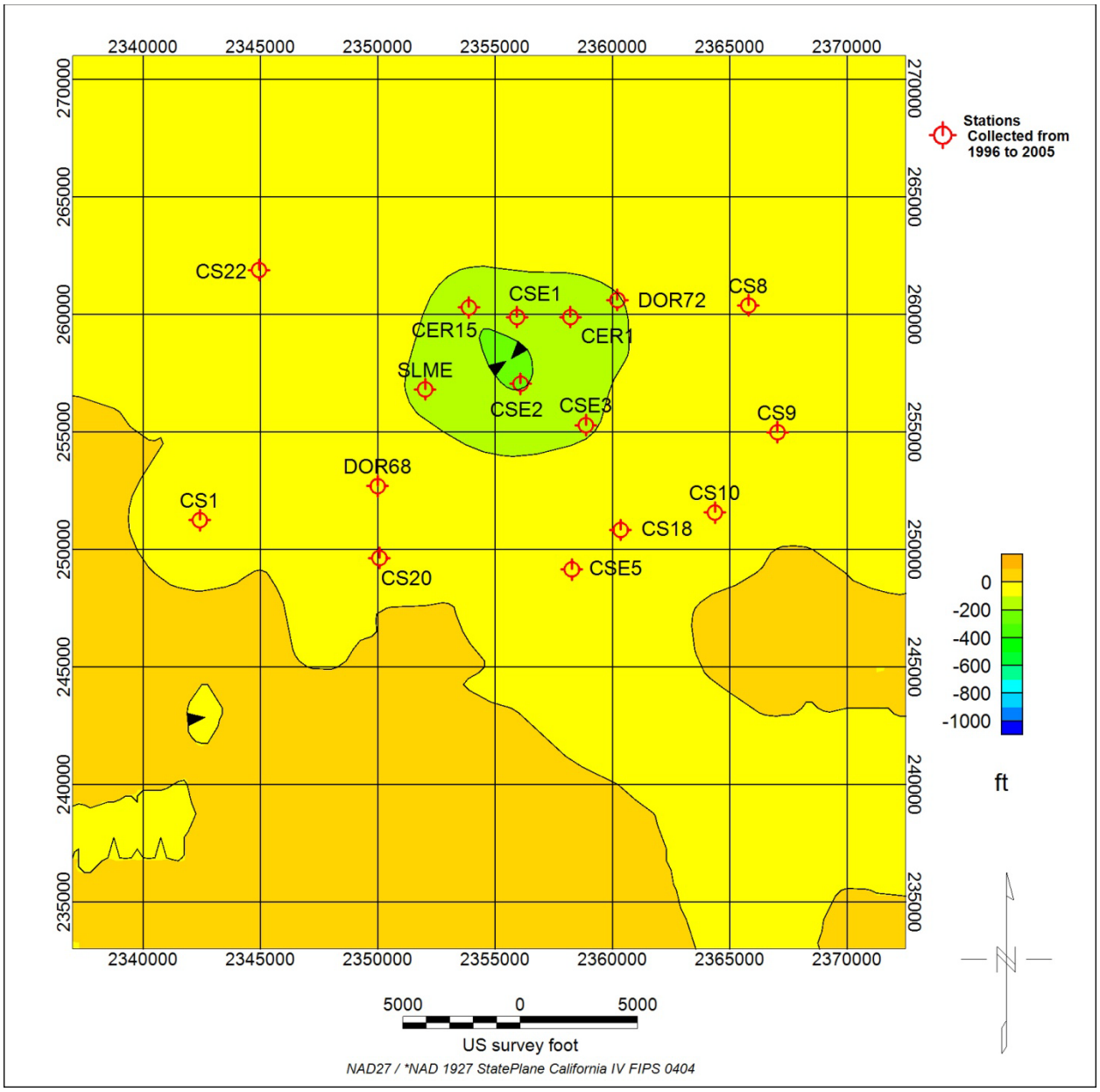

Figure 4.29: Difference between starting top surface and bottom surface produced by the surface inversion using gravity data between spring 1996 and spring 2005, an assumed density contrast of -0.20g/cm^3. The results from the inversion performed using the gravity data from 1991 until 1996 were used as the top surface. The maximum thickness of the total density anomaly from 1991 until 2005 is 209ft and the total mass change -1.19x10^{11}kg.

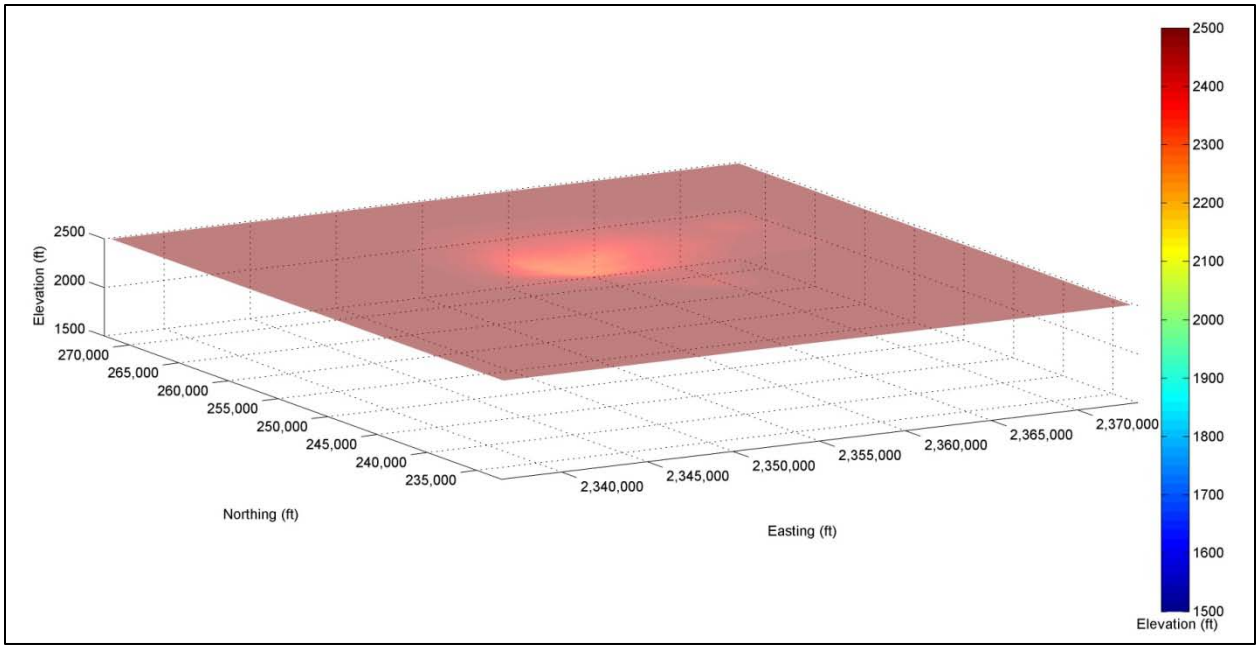

Figure 4.30: Inverted density contrast anomaly produced using gravity data from 1996 to 2005 and a density contrast of -0.20g/cm^3 shown in three dimensions with height above sea level as Z axis. The vertical scale has been increased by a factor of 5.

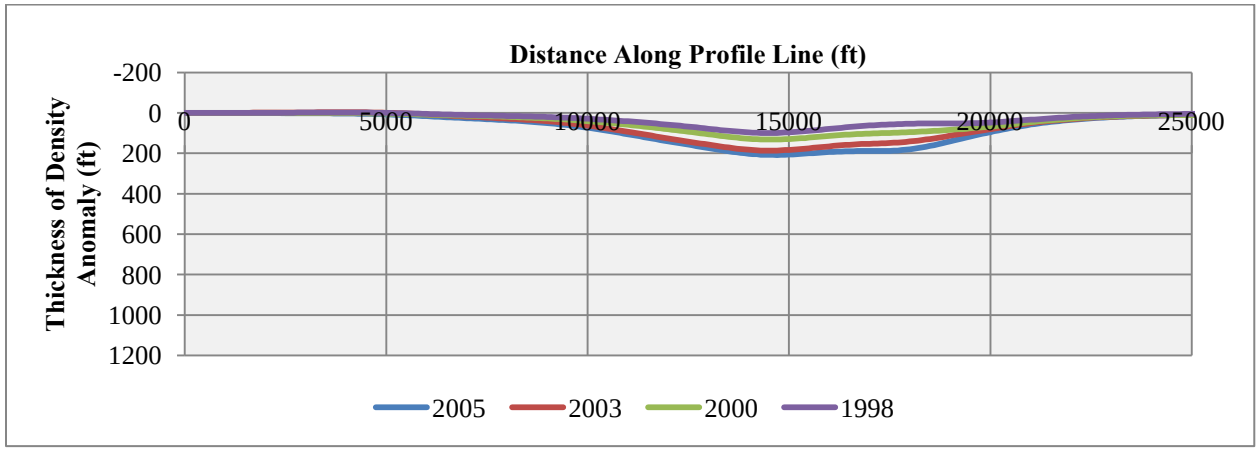

Figure 4.31: Thickness of density anomaly recovered using the surface inversion algorithm, the time lapse gravity data collected between 1996and 2005, a density contrast value of -0.20g/cm^3, and the top surface from the 1991 until 1996 inversion results, with smaller time increments shown.

4.2.4 Summary of Results from 1996 until 2005

The results of the inversions performed using the gravity data collected between 1996 and 2005 are summarized in Table 4.2. The thickness of the density anomaly and the total mass are inversely related to the assumed density. Figure 4.32 displays profiles of the recovered surfaces. The shapes of the surfaces

recovered with each density value are very similar. Figure 4.33 shows the incremental mass changes recovered using this larger data set. The results recovered using these data are similar to those recovered using the sparser data stations collected between 1991 and 2005.

Table 4.2: Results of all surface inversions from 1996 to 2005, using results from 1991 to 1996 as starting surface. Thicknesses and masses shown are calculated from 1991.

Assumed Density Contrast (g/cm^3)	Assumed Top Surface (ft above sea level)	Maximum Thickness	Total Change in Mass (kg)
-0.05	2500, using 1991to1996 as start	918	-1.30E+11
-0.10	2500, using 1991to1996 as start	431	-6.15E+10
-0.20	2500, using 1991to1996 as start	209	-2.97E+10

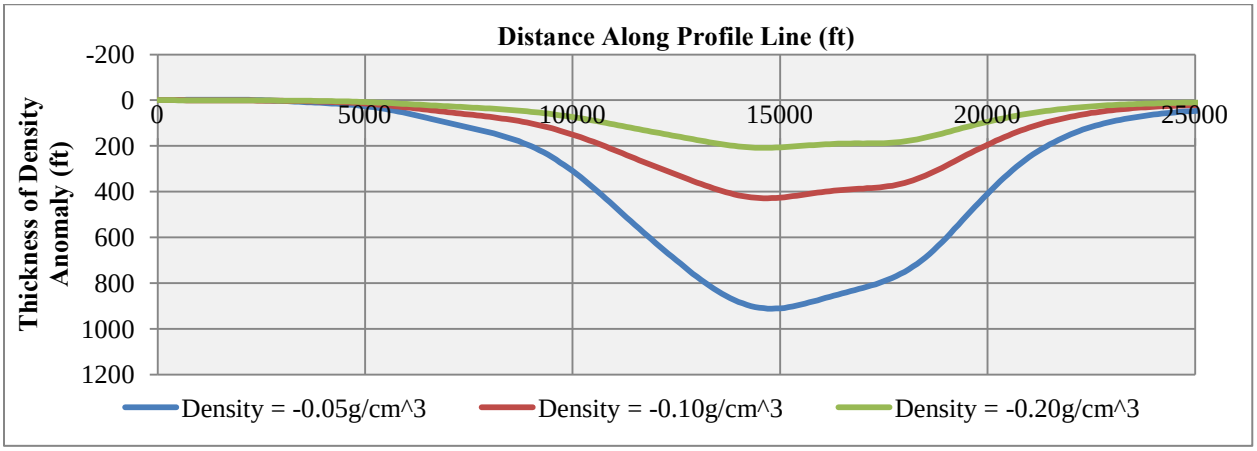

Figure 4.32: Thickness of density anomaly recovered using the surface inversion algorithm, the time lapse gravity data collected between 1996 and 2005, density contrast values of -0.05g/cm^3, -0.10g/cm^3 and -0.20g/cm^3 and the results of the inversion from 1991 to 1996 as starting surface.

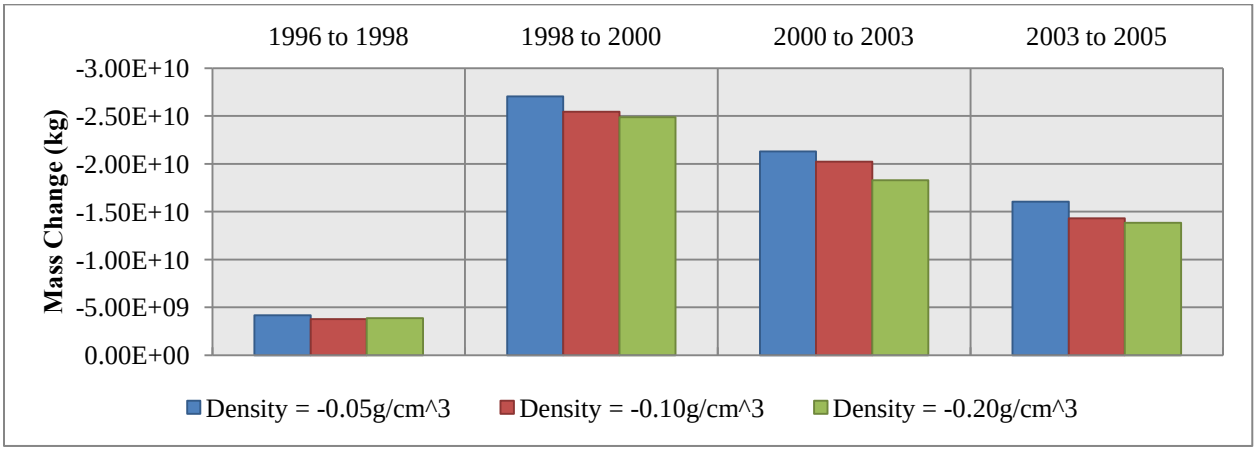

Figure 4.33: Mass change produced by surface inversion in kg for each time period between 1996 and 2005 using density values of -0.05g/cm^3, -0.10g/cm^3, and -0.20g/cm^3 and the results of the inversion from 1991 to 1996 as the starting surface.

4.3 Interpretations of Inversion Results

The time lapse gravity data and the inversion results both show a decrease in gravity and the top surface of the reservoir in the area of the field around CSE2 and CER15. Figure 4.34 shows the surface inversion results and the roads, well pads and geothermal plants of the field. There are wells pads in the southern part of the field where little change in gravity or reservoir top surface are observed. The reason for this difference in behavior is unknown but it could indicate differing reservoir porosity or permeability, a geologic separation between the two areas, or differences in reinjection procedures.

Also, the recovered thicknesses and mass changes are relatively similar between the two data sets inverted. Figure 4.35 shows the mass per 500 square foot surface area lost using the density value of -0.05g/cm^3 and the data set collected between 1991 and 2005. The thirty blue squares in the north central area around station CSE1 show a loss of -3.58x10^{10} kg in just that 7.5x10^6 ft^2 area. Figure 4.36 shows the same figure using the time lapse gravity data collected between 1996 and 2005.

Table 4.3: Summery of the results of the surface inversions performed.

Assumed Density Contrast (g/cm^3)	Assumed Top Surface (ft above sea level)	Maximum Thickness of Density Anomaly(ft)	Total Change in Mass (kg)
-0.05	2500	998	-1.39E+11
-0.05	3000	885	-1.11E+11
-0.10	2500	480	-1.30E+11
-0.20	2500	236	-1.26E+11
-0.05	2500, using 1991to1996 as start	918	-1.30E+11
-0.10	2500, using 1991to1996 as start	431	-1.23E+11
-0.20	2500, using 1991to1996 as start	209	-1.19E+11

Production data from the geothermal plant at Coso was obtained from the State of California (State of California Department of Conservation, 2013), shown in Table 4.4. The mass loss reported by this production data was 3.0x10^{11}kg. This reported loss is on the same order of magnitude as the total mass loss recovered by inversion but differs by 1.89 to 1.61 x10^{11} kg. The production losses were divided into the time periods corresponding to those used for the time lapse gravity inversions and are compared to the inversion results in Figure 4.37.

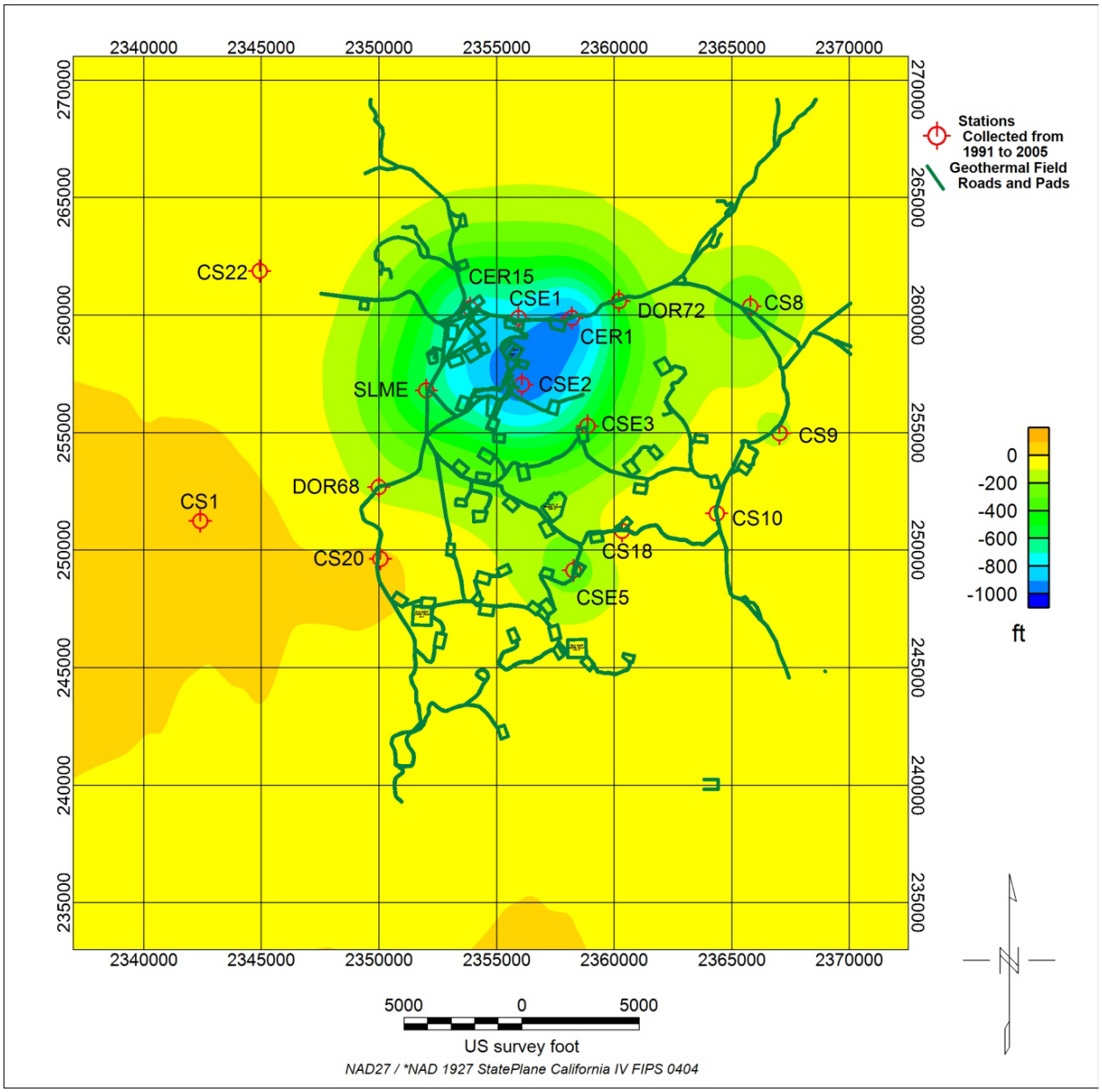

Figure 4.34: Difference between starting top surface and bottom surface produced by the surface inversion using gravity data between spring 1991 and spring 2005, an assumed density contrast of -0.05g/cm^3 and a top surface of 2500ft above sea level. Shown are the roads, well pads and geothermal plants of the field.

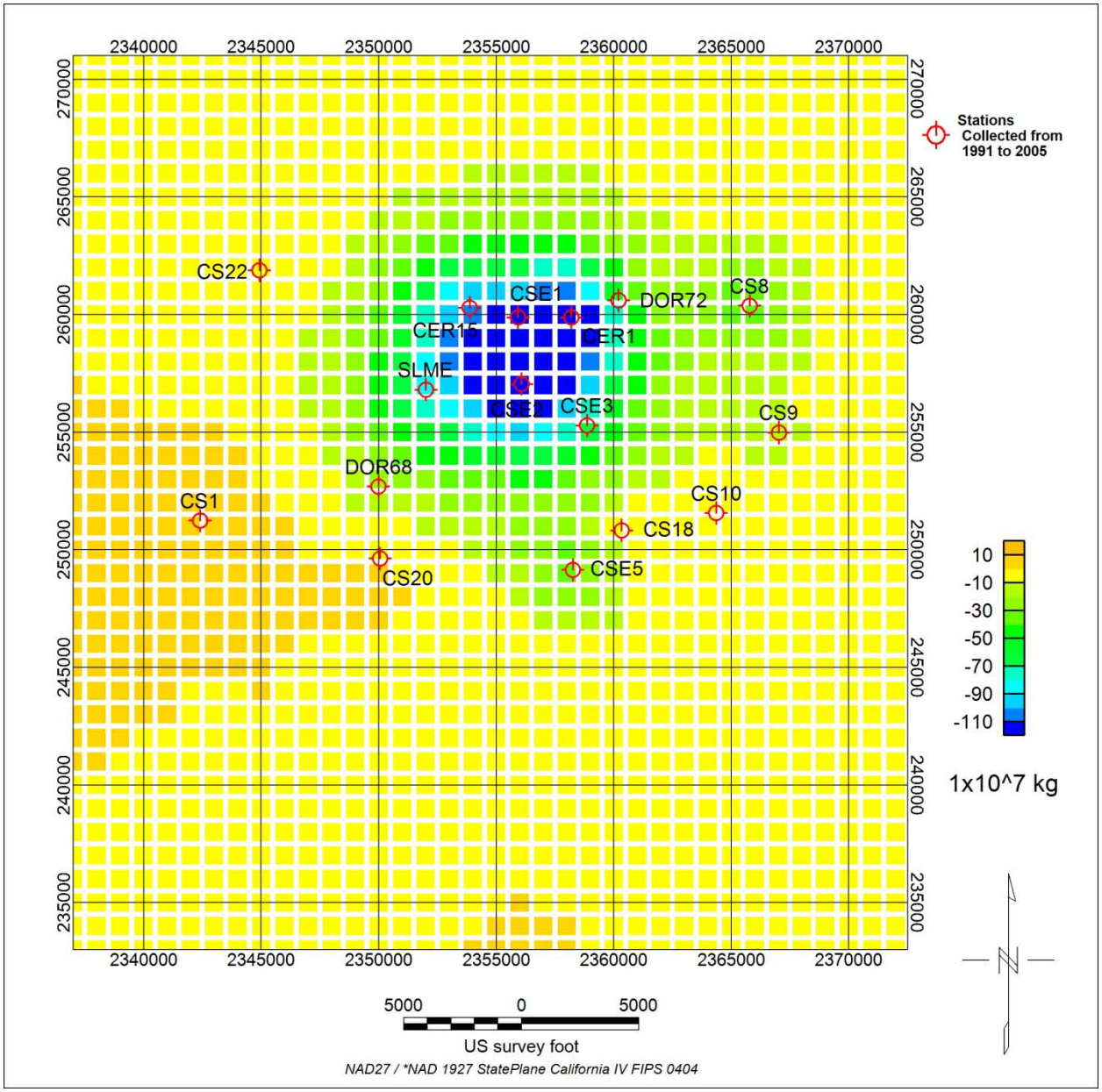

Figure 4.35: Mass change between 1991 and 2005, per 500ft^2 surface area produced by surface inversion using a density values of -0.05g/cm^3, a starting surface of 2500ft above survey level, and the time lapse gravity data set collected between 1991 and 2005.

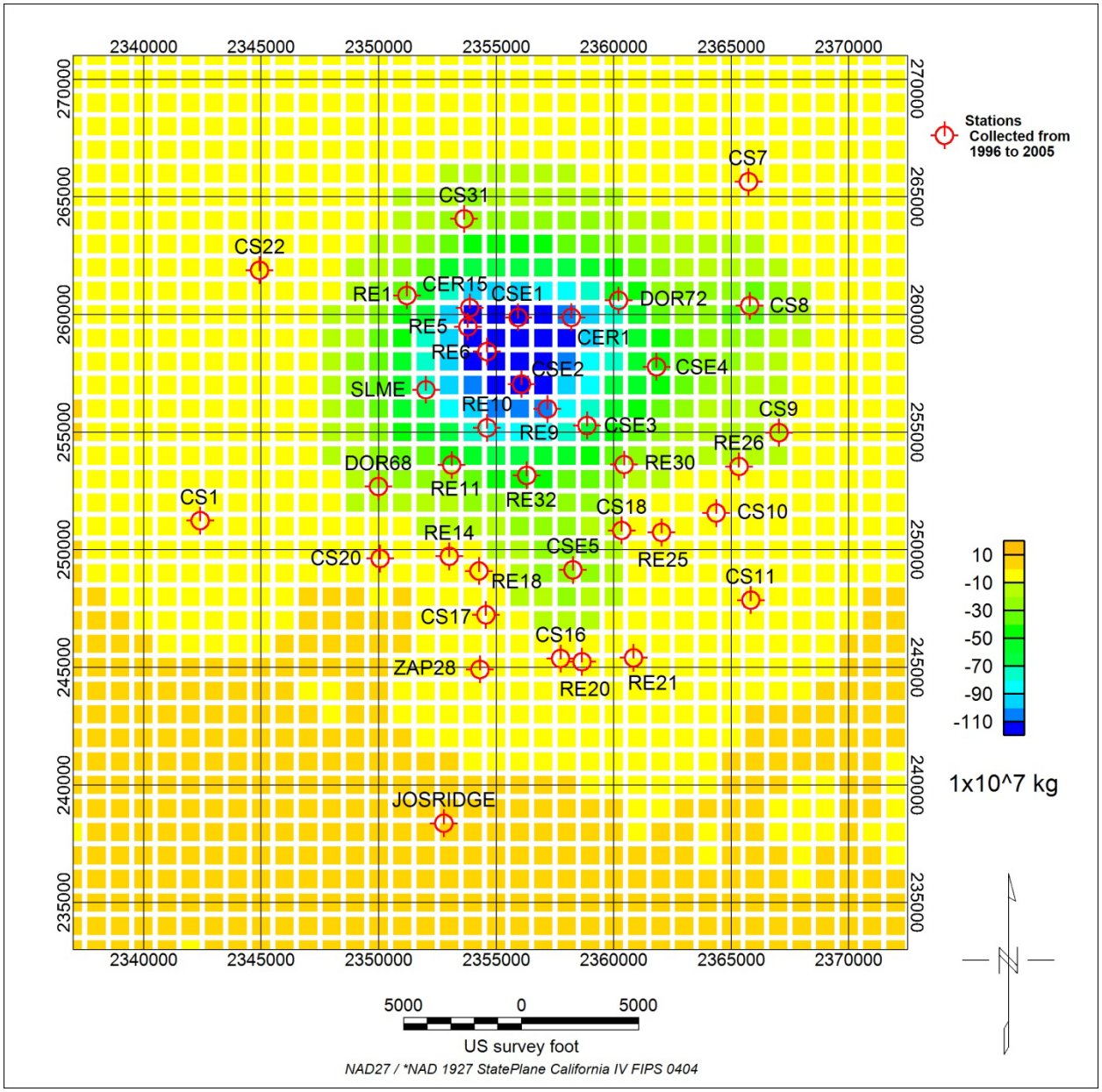

Figure 4.36: Mass change between 1991 and 2005 per 500ft^2 surface area produced by surface inversion using a density values of -0.05g/cm^3, a starting surface of the results of the inversion from 1991 to 1996, and the time lapse gravity data set collected between 1996 and 2005.

Table 4.4: Production and Injection data from the Coso Geothermal Plant for the years covered by the time lapse gravity survey. Obtained from the State of California Department of Conservation. http://www.conservation.ca.gov/dog/geothermal/manual/Pages/production.aspx

Year	Production (kg)	Injection (kg)	Net Removed (kg)
1991	4.8E+10	2.6E+10	2.2E+10
1992	4.4E+10	2.5E+10	1.9E+10
1993	5.1E+10	2.5E+10	2.6E+10
1994	4.6E+10	2.4E+10	2.2E+10
1995	4.3E+10	2.4E+10	1.9E+10
1996	4.2E+10	2.2E+10	2.0E+10
1997	3.8E+10	1.9E+10	1.9E+10
1998	3.9E+10	1.7E+10	2.2E+10
1999	3.9E+10	1.9E+10	2.0E+10
2000	3.9E+10	1.8E+10	2.1E+10
2001	3.9E+10	1.8E+10	2.2E+10
2002	3.5E+10	1.7E+10	1.8E+10
2003	3.5E+10	1.7E+10	1.8E+10
2004	3.5E+10	1.6E+10	1.9E+10
2005	3.4E+10	1.5E+10	1.8E+10
		Total:	3.0E+11

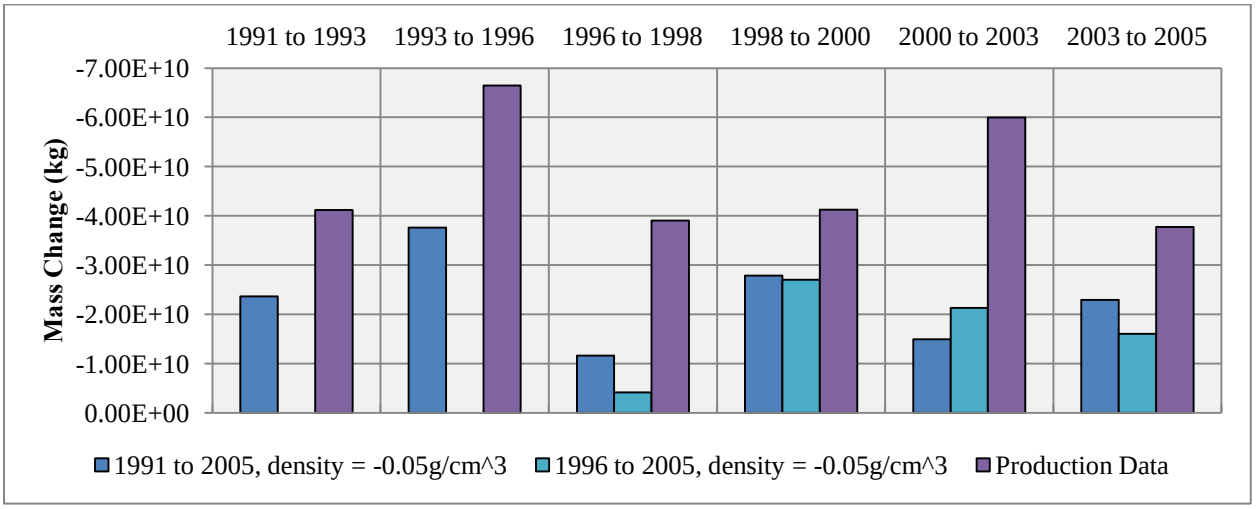

Figure 4.37: Mass change produced by surface inversion in kg for each time period between 1996 and 2005 using density values of -0.05g/cm^3 and data from both data sets, compared to the production data published by the state of California.

4.4 Summary

In this chapter I presented numerous inversion results using different density contrasts values and utilizing the data sets collected between 1991 and 2005 and 1996 and 2005. The density contrast values used were -0.05g/cm^3, -0.10g/cm^3 and -0.20g/cm^3. The inversion algorithm inverts for a density contrast body produced over time at the top of the reservoir, the difference between the top of the reservoir at time one and the top of the reservoir at time two. The thickest density contrast recovered was 998ft using the density contrast of -0.05g/cm^3 and the data spanning from 1991 to 2005. The thickest contrast was located at the station CSE2. The inverted changes in the top of the reservoir recovered were converted to mass loss. The greatest total mass loss produced, from the above mentioned inversion (1991 to 2005 data set, density -0.05g/cm3) was -1.39x10^{11} kg. When the location of the gravity anomaly and corresponding large change in the top of the reservoir is examined along with the locations of the power plants and well-pads, it is apparent that one area of the field is experiencing a decrease in gravity and reservoir where the other is not. One reason for this is that the gravity anomaly is not completely characterized by the gravity stations. Another possible reason could be that outside mass (ground water) is entering the system from areas not covered by the gravity.

.

CHAPTER 5:
DISCUSSIONS AND CONCLUSIONS

For this thesis I organized, processed and inverted fourteen years of time lapse gravity data collected at the Coso Geothermal field near Ridgecrest, California. Additionally, I participated in the collection of new data in January of 2013.

5.1 Discussions

The data collected from 1987 to 2005 were obtained from the Navy Geothermal Program office and were in various states of processing. They required a certain amount of organization, continued processing and in some cases, complete processing. The gravity data acquired in 1987 were only available in scanned hand written notes. These data required complete processing including drift, reference station leveling and elevation corrections. The gravity data from 1991 to 2003 had been processed; however these data used inconsistent reference stations which needed to be corrected. The data could not be differenced without being leveled to the same reference station. The data from 1991 until 2003 also had not been corrected for elevation changes. Without elevation corrections, a subsidence of one foot would result in a gravity signal of 92μGal, one third the total gravity anomaly observed. The data from 2004 and 2005 have been processed completely, including drift correction, reference station leveling and elevation corrections.

Additionally, little information was available on the error levels within the data. In order to estimate these error levels I first examined gravity stations that had been repeated within the 2004 data collection. I next examined two gravity stations located outside the geothermal field and observe the change in gravity seen there over the entire 14 year period. Lastly I forward modeled the expected gravity response due to surface construction near a gravity station. The resulting estimated standard deviation was 17μGal.

Only once this extensive processing effort and error analysis were complete could the data be inverted for further interpretations. The data from 1991 to 2005 were inverted in order to quantify the results of the gravity survey and to infer physical properties such as mass and change in the surface of the reservoir. The surface inversion algorithm, which inverts for the height of a density contrast, was used. This density contrast is formed between the top surface of the reservoir at time one and the top surface of the reservoir at time two. The assumptions of the inversion included a known starting top surface of the

reservoir and the density contrast. Due to uncertainty three density contrasts were used, -0.05g/cm^3, -0.10g/cm^3 and -0.20g/cm^3. The data were inverted in two groups, the stations collected continuously from 1991 to 2005, which for the most part used a starting reservoir surface of 2500ft above sea level, and the data stations collected from 1996 to 2005, which used the result of the inversion of the pervious data group between 1991 and 1996. An additional inversion was performed using a shallower starting surface of 3000ft above sea level for the 1991 to 2005 data group. The changes in surfaces were converted to mass loss using the assumed density contrasts. The total recovered mass change by the inversions ranged from -1.11 to -1.39x10^{11} kg.

Both the time lapse gravity data and the inversion results show differences in the behavior of the field between the area around station CSE2 and the southern area of the field. The CSE2 area shows the greatest decrease in gravity, the greatest change in top reservoir surface and the most mass lost. The stations in the southern area of the field show little to no change. This could indicate variations of the reservoir properties between that area and the southern area.

The results of the inversions are of the same order of magnitude as the mass loss reported in the production data, which are 3.0x10^{11} kg for the time period covered. The differences between the recovered losses and the reported mass loss range from 1.89 to 1.61 x10^{11} kg. The first reason for this discrepancy is that the gravity coverage is sparse and the entire gravity anomaly has not been captured. Additional loss might have been recorded with more stations. Lastly, it is possible that mass could be entering the system from outside the coverage of the gravity stations. Ground water from outside the field could be naturally recharging the reservoir, contributing mass to the system.

5.2 Future Work

The data acquired in January, 2013 need to be processed and included in the inversions. Additionally, this monitoring program has provided quality information on the behavior of the dynamic system of the Coso Geothermal field and should be continued into the future with new data collections occurring yearly. It is essential to collect elevation surveys on a regular basis as well, covering all gravity stations of interest. Newly collected data should be included in inversions to obtain information on mass and surface change from the gravity. The obtained mass losses and surface changes might be useful in ground water models as well as in planning of injection around the field.

Also, if more accurate prior information on the reservoir can be obtained, such as the top surface of the reservoir in 1991, a model of porosity and permeability, and the location of faults and fluid flow pathways, the existing data should be inverted again, possibly producing better results.

With the information learned during this project at the Coso Geothermal field it is possible to issue recommendations on the planning and procedures for a new similar time lapse gravity survey. First, a reference station should be established well outside the field. Forward modeling should be done to help ensure that it is a quiet point. Ideally this station should also be located in an area free from traffic and construction. Additional, back-up, reference stations should be established as well. Gravity collection should begin prior to drilling and water production to provide a true baseline and starting point. Gravity stations should be located away from drill pads in order to limit the possible error added by construction and drilling activities. Elevation data need to be collected at every gravity station. Gravity data should be collected yearly. Twice yearly data collection is not necessary. During data collection, note should be made of any above surface construction activity or mass changes. Data should be processed, well archived and inverted as collected. Gravity data could be used to regulate injection and production strategies to keep performance and possibly water levels of the field consistent.

The time lapse gravity data collected at Coso Geothermal field has produced valuable information on the behavior of the geothermal field. This monitoring program should be continued and similar programs would be beneficial on new or existing geothermal fields.

REFERENCES

Adams, M. C., Moore, J. N., Bjornstad, S., & Norman, D. I. (2000). Geologic History of the Coso Geothermal System. *Proceedings World Geothermal Congress.* Kyushu-Tohoku, Japan.

Arnet, F., Hans-Gert, K., Klingele, E., Smith, R. B., & Meertens, C. M. (1997). Temporal Gravity and Height Changes of the Yellowstone Caldera, 1977-1994. *Geophysical Research Letters Vol. 24, No. 22*, 2741-2744.

Biegert, E., Fergunson, J., & Li, X. (2008). Special Section 4D Gravity Monitoring -- Introduction. *Geophysics Vol. 73, No. 6*.

Blakely, R. (1995). *Potential Theory in Gravity & Magnetic Applications.* New York, NY: Cambridge University Press.

Davis, K., Li, Y., & Batzle, M. (2008, November). Time-Lapse Gravity Monitoring: A Systematic 4D Approach with Application to Aquifer Storage and Recovery. *Geophysics*, pp. WA61-WA69.

Duffield, W. A., & Bacon, R. C. (1981). Geologic Map of the Coso Volcanic Field and Adjacent Areas, Inyo County California. Department of Interior, United States Geological Survey.

Ehresman, T. (2002, April 12). *Idaho National Engineering and Environmental Laboratory*. Retrieved from What Is Geothermal Energy?: http://www.scs.sk.ca/vol-old/HTT/rr7/geothermal.id.doe.gov/what-is.html

Fergunson, J. F., Klopping, F. J., Chen, T., Seibert, J. E., Hare, J. L., & Brady, J. L. (2008). The 4D Microgravity Method for Waterflood Surveillance: Part 3 -- 4D absolute microgravity surveys at Prudhoe Bay, Alaska. *Geophysics Vol. 73 No.6*, WA163-WA171.

Grannell, R. B., Tarman, D. W., Clover, R. C., Leggewie, R. M., Goldstein, N. E., Chase, D. S., & Eppink, J. (1980). Precision Gravity Studies at Cerro Prieto. *Geothermics Vol. 9*, 89-99.

Hunt, T. M. (1995). Microgravity Measurements at Wairakei Geothermal Field, New Zealand; a rewview of 30 years of data (1961-1991). *Proceedings World Geothermal Congress 1995*, 863-868.

Hunt, T., & Bowyer, D. (2007). Reinjection and Gravity Changes at Rotokawa Geothermal Field, New Zealand. *Geothermics*, 421-435.

Lazaro, M. (2013, Feb 2). Personal Coorespondance. Ridgecreast, CA.

Monastero, F. C. (2002). Model for Success, An Overview of Industry-Military Cooperation in the Development of Power Operations at the Coso Geothermal Field in Southern California. *GRC Bulletin*, 188-194.

Monastero, F. C., Katzenstein, A. M., Miller, J. S., Unruh, J. R., Adams, M. C., & Richards-Dinger, K. (2005, Nov). The Coso geothermal field: A nascent metamorphic core complex. *GSA Bulletin*, pp. 1534-1553.

Nordquist, G., Protacio, J. A., & Acuna, J. A. (2004). Precision Gravity Monitoring of the Bulalo Geothermal Field, Philippines: independent checks and constraints on numerical simulation. *Geothermics,* 37-56.

Sarkowi, M., Wawan, K. G., & Santoso, D. (2005). Strategy of 4D Microgravity Survey for the Monitoring of Fluid Dynamics in the Subsurface. *Proceedings World Geothermal Congress.* Antalya, Turkey.

Spielman, P. (2002). *Coso Operating Company LLC Internal Memorandum: Coso Water Levels.* Unpublished.

State of California Department of Conservation. (2013). Retrieved from Oil, Gas & Geothermal Maps: http://www.conservation.ca.gov/dog/geothermal/manual/Pages/production.aspx

Weaver, C. S., & Hill, D. P. (1978). Earthquake Swarms and Local Crustal Spreading Along Major Strike-slip Faults in California. *Pageoph Voll. 117*, 52-64.